Università degli Studi di Udine
Dottorato di Ricerca in
Tecnologie Chimiche ed Energetiche
Sede Consorziata:
Università degli Studi di Trieste

SMALL SCALE COGENERATION SYSTEMS BASED ON ORGANIC RANKINE CYCLE TECHNOLOGY

Stefano CLEMENTE

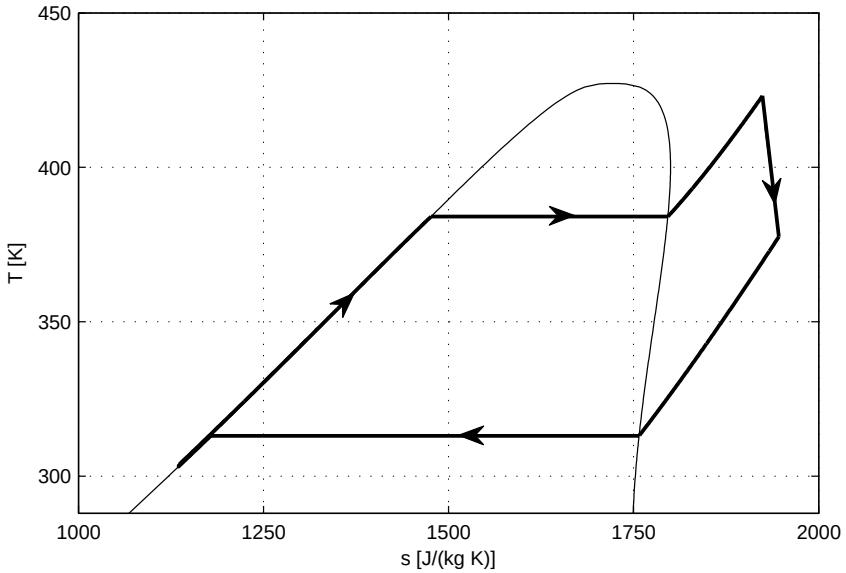

COMMISSIONE

Prof. Agostino GAMBAROTTA	Revisore
Prof. Giampaolo MANFRIDA	Revisore
Prof. Carlo NONINO	Commissario
Prof. Andrea LAZZARETTO	Commissario
Prof. Martino MARINI	Commissario
Prof. Diego MICHELI	Supervisore
Prof. Alfredo SOLDATI	Coordinatore di Dottorato

Ciclo XXV

Author's e-mail: sclemente@units.com – ing.stefano.clemente@gmail.com

Author's address:

Dipartimento di Ingegneria e Architettura
Università degli Studi di Trieste
Via A. Valerio, 10
34127 Trieste – Italia
tel.: +39 040 5583051
fax: +39 040 5583812
web: `http://www.units.it`

A note for the readers:
This work is optimized for both screen and paper use. In the digital version each reference to Chapters, Sections, Figures, Table, Equations and Bibliography contains a hyperlink for convenient navigation.

To Monica,
'cause tramps like us,
baby we were born to run.

Abstract

The Organic Rankine Cycle (ORC) technology represents one of the most studied solutions for the heat recovery from low temperature thermal sources, due to its peculiar features, such as the notable efficiencies, the possibility of operating at low pressures and its intrinsic suitability for cogeneration. The present thesis is aimed to contribute to the knowledge on ORCs, in particular on the domestic size applications, today the less commercially exploited. The research is based on the analysis of the state of the art, on the development of numerical models and on experimental activities on prototypes properly designed and built. The literature review conducted during the whole PhD program and reported in the present document highlighted the great potential of an ORC system in the range of power of few kWe and allowed to compare the results achieved by different researches on this topic. The numerical models focused first on the expander, one of the most critical components of the system: in particular, dedicated codes have been implemented for a scroll expander, a solution widely adopted on systems of such a low scale, and for a reciprocating machine, studied as a possible alternative. The analyses revealed very good performances for the devices, with overall isentropic efficiencies exceeding 0.60. These numerical codes have been then included in the global models of the cogenerator, implemented with different commercial software packages: these tools allowed the prediction of the system behavior in a wide range of working conditions and with several operating fluids. The values for the achievable electrical efficiency have been estimated between 0.08 and 0.12, meaning very interesting performances, in consideration of the low operating temperatures and of the small scale. The study has been completed by two experimental activities. First, a pump test bench has been developed, with the aim of verifying the suitability of a gear pump, originally designed for light oils, for the installation in small scale ORC systems. The measurement of the pump performances revealed that this can be a valid option, thanks to its efficient operations coupled with low costs, even if more tests are needed in order to confirm the results and to analyze some functioning problems before a final assessment could be drawn. Finally, a first prototype of cogenerator has been tested: the experimental activity confirmed the performances expected from the literature review and predicted by the numerical studies, but highlighted also the need for some improvements in order to achieve better performances and to reduce the costs. These represent the future developments of the work described in the present thesis, with the final aim of defining a technically and economically feasible design of a small scale ORC cogenerator.

Sommario

La tecnologia dei cicli Rankine a fluido organico (Organic Rankine Cycle, ORC) rappresenta una delle soluzioni più studiate per il recupero termico a partire da fonti di calore a bassa temperatura, grazie alle sue caratteristiche peculiari, come gli interessanti valori di rendimento, la possibilità di operare a basse pressioni e la sua intrinseca compatibilità con la cogenerazione. Lo scopo della presente tesi è quello di contribuire alla conoscenza sugli ORC, in particolare sulle applicazioni di taglia domestica, ad oggi quelle meno sfruttate commercialmente. La ricerca si basa sull'analisi dello stato dell'arte, sullo sviluppo di modelli numerici e sull'attività sperimentale su prototipi progettati e costruiti per lo scopo. L'analisi bibliografica, condotta durante l'intero svolgimento del Dottorato di Ricerca e riportata nel presente documento, ha evidenziato le grandi potenzialità di un sistema ORC nel range di potenza di pochi kWe e ha permesso di confrontare i risultati ottenuti dai diversi gruppi di ricerca focalizzati sull'argomento. I modelli numerici sono stati dapprima incentrati sull'espansore, uno dei componenti più critici del sistema: in particolare, sono stati implementati codici dedicati per un espansore scroll, soluzione frequentemente adottata sui sistemi di piccola scala, e per una macchina a pistone, studiata come possibile alternativa. Le analisi hanno evidenziato prestazioni decisamente buone per entrambi gli espansori, con valori del rendimento globale isentropico superiori a 0.60. Questi codici numerici sono stati successivamente inseriti in dei modelli globali del cogeneratore, implementati con diversi software commerciali: questi strumenti hanno permesso di simulare il comportamento del sistema in un ampio spettro di condizioni operative e con vari fluidi di lavoro. Il rendimento elettrico raggiungibile è stato stimato su valori compresi tra 0.08 e 0.12, rappresentando questi delle prestazioni molto interessanti, in considerazione delle basse temperature operative e della piccola taglia dei dispositivi. Lo studio è stato completato da due distinte attività sperimentali. Per primo è stato sviluppato un banco prova pompe, con lo scopo di verificare la compatibilità di una pompa, originariamente progettata per oli leggeri, con l'installazione in sistemi ORC di piccola taglia. La misura delle prestazioni della pompa ha evidenziato come questa possa essere un'opzione valida, grazie al suo alto rendimento accoppiato ai bassi costi, anche se sono necessari ulteriori test per confermare i risultati ed analizzare alcuni problemi operativi prima di poter trarre delle conclusioni definitive. Infine, è stato testato un primo prototipo di cogeneratore completo: questa attività sperimentale ha confermato le prestazioni attese dall'analisi bibliografica e previste dagli studi numerici, ma ha evidenziato anche la necessità di alcuni miglioramenti sul sistema, per poter raggiungere prestazioni migliori e ridurre i costi. Questi rappresentano gli sviluppi futuri del lavoro descritto nella presente tesi, con lo scopo finale di realizzare un prototipo tecnicamente ed economicamente vantaggioso.

Acknowledgments

First and foremost, I would like to express my deep and sincere gratitude to my supervisor, Professor Diego Micheli, not only for his competent guidance and inspiration, but also for his warm support and his friendship. It has been a real pleasure to work with him for these three years, and this work would not have been possible without him.

I wish to thank Professor Mauro Reini and Professor Rodolfo Taccani for their presence and their advice along all this period. We shared great professional and funny moments, and I think their help has been fundamental for the present thesis .

I sincerely acknowledge the reviewers of this dissertation, Professor Agostino Gambarotta and Professor Giampaolo Manfrida, for their constructive comments, an essential contribution for the quality improvement of this document.

I owe my gratitude to all the partners involved in the research project "PIACE", which has been funded by the Italian Ministry of Economic Development and has constituted the framework of most of the activities conducted during my PhD program, and in particular to Giuseppe Toniato, PhD, business consultant for Riello Group, and Roberto Bracco, MSc, project manager at Centro Ricerche FIAT in Orbassano (Turin), Italy.

I would also like to acknowledge Professor Daniel Favrat for having accepted me as a guest PhD student at the Laboratoire d'Energétique Industrielle - LENI, École Polytechnique Fédérale de Lausanne - EPFL, Switzerland, for a four-months period in 2011. I thank also Jonathan Demierre, PhD, for the fruitful collaboration in those months.

I am very grateful to all my colleagues and friends at the Energy System Laboratory, University of Trieste, for their priceless advice and the wonderful moments we shared in these years. Among the others, special thanks go to Robert, Nicola, Fabio and Marco. Beside them, I wish to express my gratitude to all my friends, former colleagues and mates not cited here, for their support during all my doctoral period.

I obviously owe my most warm and sincere gratitude to all my family, and in particular to my parents, Licio and Maria Rosa, for their love and their help in each moment, and to my sister, Monica, for being the best sister that one can desire.

Finally, I reserve my most special thanks to the most special person I have ever known, Monica. Her example guided me in the choice of starting my PhD program, her support allowed me to overcome all the difficulties arisen in these years, her knowledge and her advice helped me countless times, in my job and in my life, and her love has become quickly my driving force. She is simply the best there is. To her I dedicate this thesis.

Contents

List of figures

List of tables

1 Introduction

The challenge of energy sustainability represents one of the most important goals to be achieved by humanity in 21st century. Three main facts, useful to understand the present situation related to energy production in the world, can be highlighted.

First, the global energy demand is expected to grow up dramatically in the next 25 years, due to both the life-style evolution in developed countries and the new demands from emerging ones: according to the U.S. Energy Information Administration, the world energy consumption is foreseen to increase by 53% between 2008 and 2035, from 533×10^{24} J/year to 812×10^{24} J/year [1].

Second, the energy-related Greenhouse Gas (GHG) emissions, in particular carbon dioxide, have increased constantly over the past decades, and further growth is foreseen in the near future: for example, world energy-linked CO_2 emissions were equal to 21.6×10^9 t/year in 1990 and to 30.2×10^9 t/year in 2008, with an increment of 40%, while projections show a level of 35.2×10^9 t/year in 2020 and of 43.2×10^9 t/year in 2035, respectively 39% and 43% above the 2008 value. It's interesting to note that the developing countries are expected to give the main contribution in GHG emission growth in the next 25 years, since their energy demand is increasing with a very fast pace and they heavily rely on fossil fuels to meet this need: the CO_2 emissions of emerging nations are foreseen to raise by 73% between 2008 and 2035, while industrialized countries are expected to hold down this value to 6% in the same period [1].

Third, fossil fuels reserves are sufficient only for few decades, at the present exploitation rate. Total recoverable coal reserves in the world have been estimated in 948×10^9 t in 2009, while they were evaluated equal to 1145×10^9 t in 1991. If the global coal production in 2008, equal to 7.5×10^9 t/year, is taken into account, the reserves will be completely depleted in 126 years [1]. Even shorter durations are foreseen for oil and gas fields. In 2011 the total amount of known oil reserves has been calculated at 1.479×10^{12} barrels, while the 1995 estimation was 1.146×10^{12} barrels, with the growth due to the discovery of new exploitable fields. According to 2010 data on crude oil production, the reserves depletion will occur in 46 years. It's also interesting to note that 84% of the world oil reserves are in just ten countries, with the political implications which can be easily imagined [2]. The estimations on natural gas global reserves have grown from

$142.134 \times 10^{12}\,m^3$ in 1995 to $190.878 \times 10^{12}\,m^3$ in 2011, thanks to new discovered fields: even in this case, a very large share (77%) of the world gas amount is located in just ten countries. If the annual extraction rate will be kept equal on 2010 level, the world natural gas reserves will be depleted in 59 years [2].

Energy sustainability could be reached only if world energy demand is satisfied, but at the same time both GHG emissions and dependence on fossil fuels are reduced. One of the main strategies considered and studied to move towards this goal is represented by Combined Heat and Power (CHP) production, also known as cogeneration. CHP is defined as the simultaneous utilization of heat and power from a single fuel or energy source, at (or close to) the point of use [3]. Since part of the thermal energy rejected by the prime mover during the electricity production is recovered to provide heat on site, the overall efficiency of a cogenerator is high [4]: generally a CHP plant is capable to convert more than 75% of the fuel source into useful energy, while the most modern systems can reach levels of efficiency of 90% or more [3]. As stated in the previously reported definition, a cogenerator is usually located near the energy end user (an industrial plant, a District Heating and Cooling (DHC) network or a single commercial or residential building), in particular because of the high cost of transporting heat [4]. Thanks to these features of high efficiency and decentralized power production, cogeneration involves several advantages, such as reductions in operating costs, in GHG emissions and in transmission and distribution losses, or increasing in robustness and reliability of electrical grid [5]. Different systems could be used in a CHP unit to produce the electric power, such as an Internal Combustion Engine (ICE), a gas turbine, a Stirling engine, a fuel cell or a Rankine cycle. The latter is particularly interesting, since the thermal energy needed to evaporate the working fluid could be obtained, other than from a conventional combustion process, from a waste heat source or other low temperature thermal flows, while the energy rejected at the condenser can be exploited to warm up a heat carrier fluid.

Heat is a by-product always connected to an energy transformation process. Since there is a general lack of efficient recovery methods, this heat is usually rejected towards ambient, causing a low overall efficiency in the production of useful energy from fuel source. In particular, when industrial processes are taken into account, the huge discarded thermal flows represent not only a large fraction of unexploited resources, but also an environmental issue, since they create the so-called thermal pollution, resulting in an increase of the local temperature of air or a water body [6, 7]. For example, in 2006 it has been estimated that the total waste heat produced by the aluminum smelters in Canada is equal to 80×10^{15} J/year: the economic savings achievable recovering only 10% of this thermal energy have been evaluated in about 96 millions of dollars per year [8]. Other than from waste heat flows, it is relatively simple to collect thermal energy, most frequently at low temperature, from renewable sources, such as liquid-dominated geothermal fields, which are abundant in the world but scarcely exploited today, due to their low quality in comparison with vapor-dominated fields [9], or solar energy, which can be converted in low temperature heat using flat collectors, a technology characterized by limited costs, if compared with other solar systems like parabolic troughs or Concentrating Solar Power (CSP) plants [10].

Potentially, any heat flow could be exploited as thermal input for a Rankine cycle, however, if water is used as working fluid, an efficient conversion from heat to mechanical energy is not allowed when the source temperature is low, below a limit which in literature is reported to be in a range from 300 °C to 400 °C [6, 11]. For these applications, some typologies of organic fluids, such as refrigerants or hydrocarbons, are more suitable than water, due to their thermo-physical properties.

This thesis deals with CHP systems based on Organic Rankine Cycle (ORC), in particular in a range of power of few kWe, suitable for meeting the electricity and the heat demand of a single building. The main aim of the work is to achieve a better knowledge of this technology, by means of literature analyses, numerical simulations and experimental activities. The text is organized according to the following outline.

Chapter 2 contains a detailed introduction on ORCs, with a review of the abundant literature on this topic, an analysis of the state of the art of both experimental prototypes and commercial units, a discussion on the major ORC applications and a description of the main components of the system.

Chapter 3 focuses on the working fluids and on the criteria for their selection. As a case study, the choice of the most suitable working fluid for a biomass cogenerator is reported, using for the selection a procedure based on energy and exergy analysis.

Chapter 4 describes the different numerical models which have been developed to simulate an ORC and to predict the behavior of the expander, among the components with the largest influence on the system performances. In particular, both scroll and reciprocating expanders have been taken into account.

Chapter 5 gives detailed descriptions of the two test benches used for this research and reports the results of the experimental activities carried on them, aiming to achieve a better knowledge of the system, its dynamics and its components, and to get data useful to validate and calibrate the numerical models.

Chapter 6, finally, contains the conclusions of the research at the basis of the present thesis, with comments on the achieved results and suggestions on possible future developments of the project.

2

The organic Rankine cycle

2.1 General description

An ORC is based, except for the working fluid, on the same concepts of traditional steam Rankine cycles, one of the main technologies used for electricity production in power plants all over the world. A brief description of the different phases of the cycle is given, referring to Fig. 2.1, where a cycle with superheated steam (properly called Rankine-Hirn cycle) is reported on (T,s) diagram, and to Fig. 2.2, which represents a schematic view of the main components of the system:

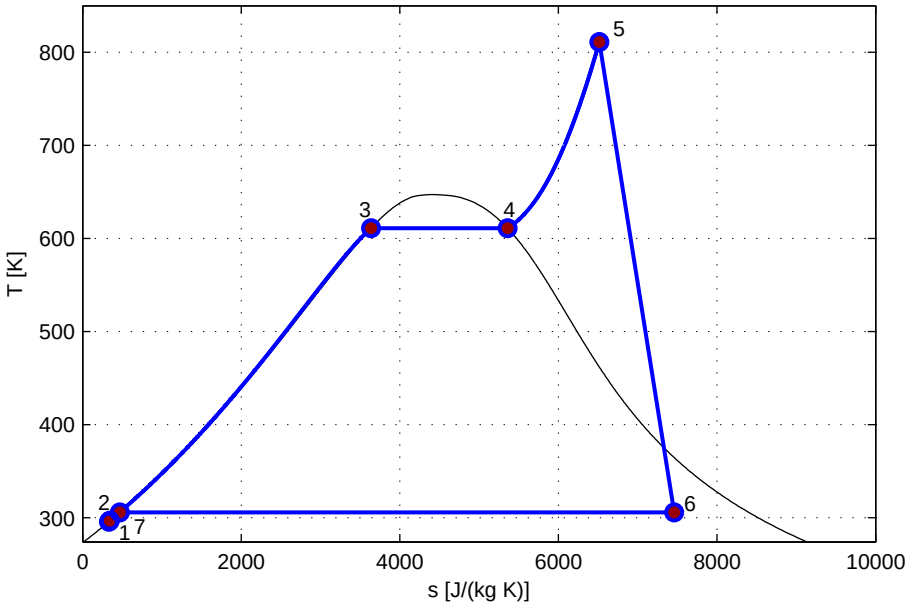

Fig. 2.1: A steam Rankine-Hirn cycle on (T,s) diagram

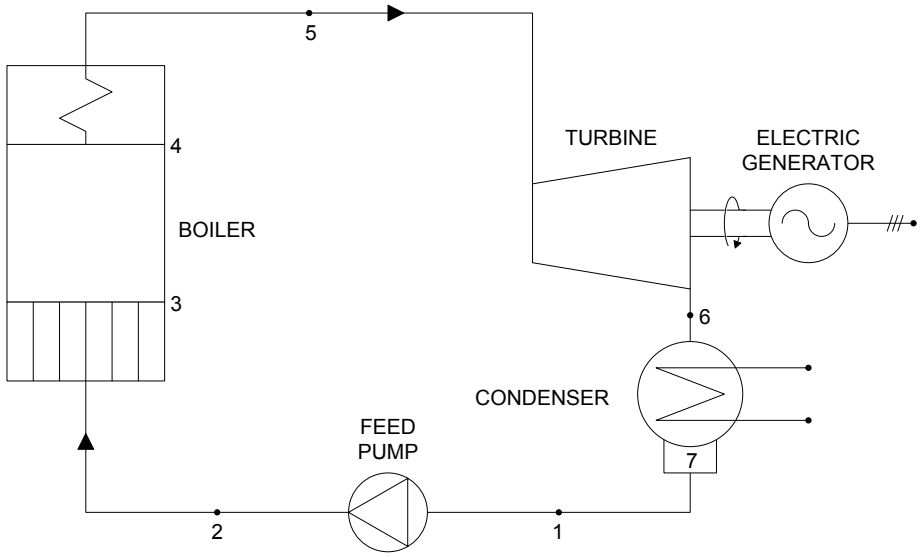

Fig. 2.2: Main components of a Rankine cycle installation

- the feed pump increases the pressure of the working fluid, here in a liquid state (phase 1→2);
- the liquid is heated up to the evaporation temperature in the first zone of the boiler, often called economizer (2→3);
- the vaporization of the fluid is achieved in the evaporative section of the boiler (3→4);
- the vapor is superheated in the last zone of the boiler, in order to reach the desired temperature at turbine inlet (4→5);
- an expansion takes place in the turbine, where the fluid energy is converted to mechanical work, exploited to move an alternator and thus to produce electricity (5→6);
- a condenser brings the expanded vapor back in a liquid state (6→7);
- a slight sub-cooling of the liquid takes place at the condenser outlet, in order to avoid cavitation problems at pump suction, where the cycle begins again (7→1).

Water is the natural choice as working fluid in large power plants, since it presents a large number of favorable features [12]:

- very good thermal and chemical stability, which avoids the risk of decomposition of the fluid in the system;
- very low viscosity, in particular in liquid state, resulting in a low work required from the feed pump;
- high specific latent heat of vaporization and specific sensible heat, which make water a very good energy carrier;
- non-toxicity and non-flammability, which reduce chemical and fire hazards related with a steam power plant;
- Ozone Depletion Potential (ODP) and Global Warming Potential (GWP) equal to zero, meaning that water does not represent any threat to the environment;
- abundance and relatively low cost.

On the other hand, the use of steam in a power cycle involves also some drawbacks, which are briefly summarized in the following list [12, 13].

- To increase the mechanical output and, thus, to ensure a high cycle efficiency, the steam must be condensed at a temperature as close as possible to ambient temperature. The pressure and the density of water in saturated vapor conditions at these low temperatures are very low: consequently, large sections at turbine outlet and at condenser inlet are required.
- Since evaporation takes place at a high pressure, in order to ensure a high specific enthalpy of the steam at turbine inlet, the expansion to the just reported very low condensation pressure is very large and has to be exploited in a multi-stage turbine, making the required machinery relatively complex and expensive, suitable only for large-scale applications.
- Water is a so-called wet fluid, i.e. its saturated vapor curve presents a negative slope on (T,s) diagram, as shown in Fig. 2.1: for this reason, if saturated steam is directly expanded in the turbine, the condensation will start immediately, with the formation of liquid droplets, which will cause a high risk of erosion on the turbine blades and a significant increase in turbine disc stresses, considering also the machine high rotational speed. In order to avoid this problem, a certain degree of superheating in the steam production is mandatory: even if the amount of additional heat needed is small, in comparison with the thermal energy required in the economizer and the evaporator, a higher temperature is demanded from the heat source, and this can be unfeasible in some cases.
- Although a considerable superheating is provided by the boiler, the presence of wet steam in the latest stages of the turbine, even if with a high quality, is practically unavoidable, as noticeable in Fig. 2.1: this complicates the turbine bearings design and reduces their operating life.

The use of different working fluids with favorable features, such as particular organic compounds, can mitigate the problems of steam Rankine cycles: a comparison between the saturation curves of water and refrigerant R245fa, as an example, is reported in Fig. 2.3 on (T,s) diagram.

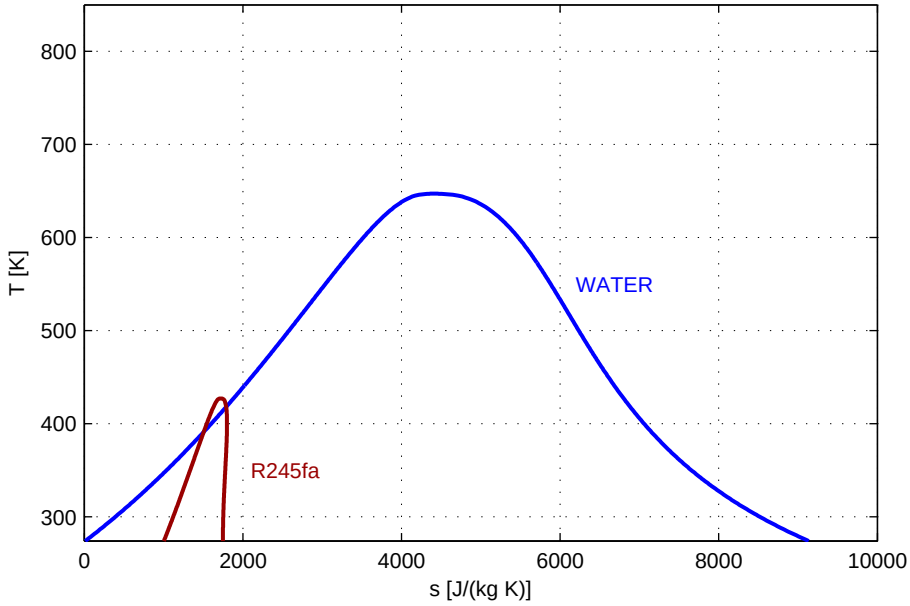

Fig. 2.3: Saturation curves of water and R245fa on (T,s) diagram

The analysis of Fig. 2.3 can facilitate the comprehension of the various advantages of an ORC over conventional steam installations [12]:

- since some organic fluids, called dry fluids, feature a saturated vapor curve with a positive slope on (T,s) diagram, the expansion ends in the superheated vapor region, so the risk of blades erosion is avoided and thus superheating is not needed;
- due to lower critical temperature, the fluid is evaporated at lower pressure and temperature, so less technological issues are involved in boiler and machinery construction;
- the lower difference between evaporation and condensation pressures allows the expansion exploitation in a simple single stage turbine;
- a low specific latent heat of vaporization is more suitable for some applications, e.g. when the thermal input is of small scale or at low temperature, even if, in general, the opposite feature makes a fluid a good energy carrier.

A detailed introduction on suitable working fluids and their main features is reported in Section 2.2.

As reported by Tchanche et al. [12], the opportunity of realizing Rankine cycles with working fluids different from water has been investigated since the 1880s, even if with little popularity in the first times. In 1926 Dow published a paper [14] in which a combined cycle for power production is taken into account, with a diphenyl oxide Rankine cycle superposed on a conventional steam cycle: the calculations presented by the author revealed that a gain of about 6 percentage points in the overall efficiency can be expected if this configuration is used instead of a traditional steam installation. The paper also highlights that "one of the thermodynamic properties of diphenyl oxide is that in an ordinary turbine where it expands adiabatically, instead of condensing like water, it superheats to a marked degree, even in a 100 per cent efficient turbine". Another article by Ray and Moss [15], printed in 1966, describes a growing interest around ORCs in those years, investigating some fluorochemicals as possible working fluids. Sawyer and Ichikawa [16] reported a detailed description of an ORC system placed in commercial operation in Mizushima, Japan in 1968 and still running in 1980, with an operational experience of more than 80 000 h. The installation used R11 as working fluid, exploiting a thermal source at 150 °C and featuring a condensation temperature of 40 °C. A rated power of about 3.8 MW was delivered by the system, with an overall efficiency equal to 0.123.

The interest around this technology was pushed up in the 1970s by the oil crisis and by the emerging environmental consciousness. In 1977 Davidson [17] realized an ORC prototype for a student competition. The heat sources of this system were low-temperature solar panels, the expander was a modified multi-vane air motor and the working fluid was the refrigerant R11. Although the maximum cycle temperature was below 100 °C, the expander efficiency was very low, between 0.20 and 0.30, and all the components were not optimized for the particular application, the system worked properly, delivering an electric power of about 1 kW, even if with an extremely low overall efficiency, between 0.01 and 0.03. A state-of-the-art description of ORC applications was presented in 1981 by Curran [18], with data provided on about 2150 operational Rankine engines. The analysis, reported and commented also by Badr et al. in 1984 [19], revealed that many of the installations at the end of the 1970s were experimental facilities, but a limited number of plants reached an operating time longer than 5 or even 10 years. The studied systems, covering a range of power of 0.1 kW to 1120 kW, were predominantly equipped with turbines as expanders and featured a long list of different working fluids, both refrigerants and hydrocarbons. One of the most recent historical reviews on ORC can be found in the paper published by Srinivasan et al. in 2010 [20]: a large number of studies on the application of Rankine bottoming cycles to Waste Heat Recovery (WHR) has been reported, referring to both the automotive field and the power generation industry and covering a time span from 1981 to 2010. It has been concluded that all these researches demonstrated that 10-15% improvements in fuel economy from status quo can be achieved applying the WHR ORC technology.

More and more researches on energy sustainability focused on ORC in the last years, as demonstrated by the increasing number of papers found in literature. Several works have been presented in the First International Seminar on ORC Power Systems, held in Delft, The Netherlands, in September 2011 [21], where all the peculiar features of this technology were introduced and discussed: both large and small scale systems were considered and studied with numerical or experimental approaches, and a large number of researches dealt with the components with the largest influence on the cycle performances, such as the expander, the pump, the heat exchangers and the working fluid.

2.2 The working fluids

The working fluid plays a key role in the definition of the thermodynamic performances, the economics and the technical feasibility of an ORC system, as already introduced in Section 2.1. A large amount of papers can be found on suitable working fluids and on criteria for their choice, and several literature reviews summarizing the results of these works are available [12, 16, 22–24]: the general relevant characteristics extracted from these studies are reported and discussed in the following paragraphs.

2.2.1 Thermodynamic performances

The fundamental skill of a direct thermodynamic cycle is obviously the capacity to produce the most mechanical power from a given heat source. In particular, a Rankine cycle should deliver from the turbine a power as high as possible, taking into account the temperatures of the heat source and the heat sink, the size of the thermal input and the cooling profile of the heat carrier, which has to be coupled properly with the heating profile of the working fluid, in consideration of a minimum differential temperature between the fluxes at the pinch point [24]. Hence, it appears natural that most researches indicate the maximization of the delivered power and/or of the system efficiency as the main criterion for the working fluid selection, even if this approach does not take into account directly the substance thermo-physical properties, the impact of which on cycle performances is often only estimated by interpreting the results of numerical simulations [24].

The choice of the most suitable index to evaluate the thermodynamic performances of an ORC has therefore a great importance for a proper selection of the working fluid, in particular because this technology is often exploited in CHP applications. In fact, when cogeneration is taken into account, the useful outputs of a system are both mechanical power and heat, but the quality of the energy content of the latter is very poor if compared with the first one, in particular when the heat is cogenerated at low temperatures. For this reason, many authors use the exergy efficiency to evaluate the performances of the cycle instead of a simple first law efficiency: the same exergetic approach is used in the present thesis in Chapter 3, where the fluid screening is performed.

2.2.2 Saturated vapor curve slope

As already reported in Section 2.1, some substances, like water, are called wet fluids and exhibit a saturated vapor curve with a negative slope on (T,s) diagram: for this reason, as shown in Fig. 2.1, a certain degree of superheating is needed in vapor production in order to avoid the start of fluid condensation inside the expander and the consequent formation of liquid droplets, requiring a higher temperature of the heat source. However, in particular applications, such as renewable energy or WHR systems, the thermal input is available only at a low grade, so the temperature of vapor production is limited: if the required evaporating pressure is high, this reduces the degree of superheating reachable by the fluid. Other fluids, for example the refrigerant R245fa reported in Fig. 2.3, do not exhibit the same behavior: the slope of their vapor saturation curve on (T,s) diagram is vertical (for isentropic substances) or positive (for dry fluids). Thanks to this feature, an expansion from saturated vapor conditions always ends in the superheated vapor region, avoiding the risk of premature condensation. Even if both isentropic and dry substances are suitable for ORCs exploiting low temperature heat sources, if the slope of the vapor saturation curve is excessive (i.e. the fluid is "too dry"), the vapor will leave the expander at a very high superheating degree, which represents an additional amount of waste energy and an increased cooling load at the condenser [23]. This energy can be conveniently recovered by using an internal heat exchanger to preheat the liquid after it leaves the feed pump and before it enters the boiler in order to increase the cycle efficiency, anyway quasi-isentropic fluids are among the most used for ORC applications. A comparison between two saturated vapor Rankine cycles with quasi-isentropic (the refrigerant R142b) and highly dry (the hydrocarbon isobutane) working fluids is reported in Fig. 2.4.

2.2.3 Density

A high fluid density is important in both liquid and vapor conditions to achieve better cycle performances. A lower specific volume in saturated (or slightly subcooled) liquid conditions would result in a lower work required to increase the fluid pressure from the condenser level to the boiler one, so a lower power would be absorbed by the pump [24]. A high density in vapor conditions is particularly important at low pressures, i.e. when the fluid leaves the expander and begins the condensation, otherwise very large equipments would be needed, especially for fluids showing very low condensing pressures [16, 22].

2.2.4 Working pressures

The working pressures of the cycle have a great influence on system complexity, technical feasibility and installation costs. Since a pure, phase-changing substance is an one-degree-of-freedom system, pressure and temperature are directly linked. For this reason, the condensing pressure of an ORC is highly dependent on the temperature of the heat sink: it can be at ambient level, but also at a higher one, when the system is used for CHP purposes. Each fluid assumes a different pressure during condensation at a certain temperature: in some cases this pressure can be very low, far below ambient pressure (for

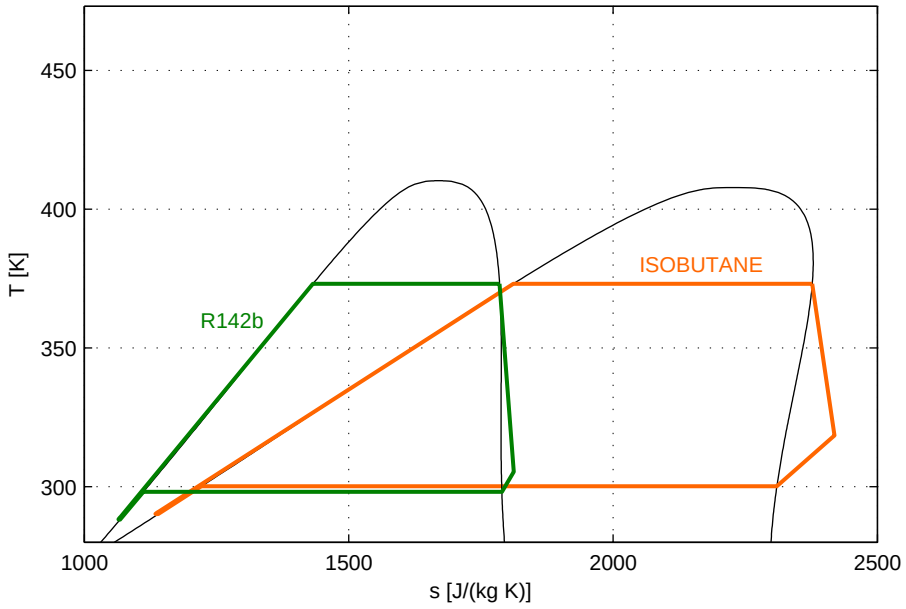

Fig. 2.4: Comparison between ORCs with quasi-isentropic (R142b) and highly dry (isobutane) working fluids on (T,s) diagram

example, pure water condenses at 30 °C at a pressure of 0.042 bar). Such low pressures involve several complications for the system, such as a more robust construction for the condenser, the need to realize and maintain the vacuum in the low-pressure side of the installation or the absorption of a higher power for liquid pumping. Moreover, as already reported in the previous Subsection 2.2.3, some substances exhibit very low densities at low pressures in vapor state, so some components, in particular the expander and the condenser, would need large volumes.

Once the condensing pressure is fixed, the efficiency of a Rankine cycle increases with the evaporating pressure, but the benefits become more and more limited above a certain pressure level, different from fluid to fluid. A similar curve can be drawn for the power delivered by the cycle as a function of the evaporating pressure in the case of refrigerants, while hydrocarbons are usually characterized by an optimal evaporating pressure which maximizes the delivered power [25]. These trends are calculated and analyzed for several substances in Chapter 3. If the pressure needed to reach acceptable performances is too high, all the equipments of the high-pressure side of the system are required to withstand strong stresses, so a larger thickness is needed for the structures, the manufacturing of all the components must be more accurate and the system has to be certificate to operate in more hazardous conditions: this results in an increased cost of the installation.

Therefore, a working fluid can be considered suitable for an ORC, and in particular for small scale installations, when good performances can be achieved even if the condensing pressure is not too low, better if above the atmospheric value, and if the evaporating pressure can be hold below acceptable limits, usually indicated around 25 bar [12].

2.2.5 Stability and compatibility with materials

Unlike water, organic fluids usually suffer chemical deterioration and decomposition at high temperatures [23]. For this reason, a substance is suitable for an ORC application only if its chemical stability temperature is higher than the maximum temperature the cycle can reach, with a certain safety margin, taking into account possible abnormal working conditions of the system and local hot spots in the boiler. Moreover, the fluid has to be compatible with the materials of all the wet parts along the circuit (for example, particular attention must be paid in the choice of the elastomer of the diaphragm pump, if this device is used in the system) and with the lubricating oil which is often mixed with the working fluid itself.

2.2.6 Safety

Each substance is characterized by a certain level of danger: ideally, a suitable candidate as an ORC working fluid should be, at the same time, non-corrosive, non-toxic and non-flammable, in particular for domestic installations. However, in practical situations, some of the above mentioned features are not critically necessary, so particular substances are used for their good performances, even if they are connected with slight flammability or toxicity hazards. For example, pentane is considered a flammable fluid, but this is not a problem if there is no ignition source around [23]. In any case, at high temperatures some organic substances can experience autoignition, so the maximum allowable concentration and the explosion limit should also be under consideration. Hence, contacts between working fluid and air should not be permitted, taking into account also the toxicity, even if at low levels, of most substances suitable for ORCs: for this reason, particular solutions must be adopted in order to realize a completely isolated circuit, such as hermetic machines or diaphragm pumps.

2.2.7 Environmental aspects

Even if ORCs operate in closed circuits, interactions between working fluid and environment are possible, during the installation, the expected long operative life (in particular the leakage through the sealings on the machines shafts is not a so uncommon phenomenon) and the dismantlement, so the possible ecological hazards must be taken into account in fluid selection. Three indexes are generally used to describe the environmental performances of a substance [26].

The Ozone Depletion Potential (ODP) is a ratio of ozone column destruction per unit mass of released gas. A value of 1 in ODP is assigned to the refrigerant R11, which is

considered the reference for all chemicals. Traditional refrigerants including Chlorofluorocarbons (CFCs) and Hydrochlorofluorocarbons (HCFCs) are characterized by ODP values between 0.1 and 1. Given the negative impact of chlorine on the atmosphere, modern refrigerants such as Hydrofluorocarbons (HFCs) and Hydrofluoroethers (HFEs) do not contain chlorine and have ODP values equal to 0.

The Global Warming Potential (GWP) estimates how much the mass of a chemical will add to global warming over a 100-year time period, and it depends on the radiative factor and on the decay rate of the substance. Carbon dioxide is the reference chemical, so it has a GWP value of 1.

The Atmospheric Lifetime (ALT) is an estimation of how long a gas will remain in the atmosphere after emission, on the basis of its decay rate and its likeliness to bond with other gases. This index is useful to determine the long-term effects of pollution: chemicals with a long ALT can potentially be harmful to the planet even if they are seen as not harmful now, due to unforeseen environmental impacts.

The environmental risks connected with chemicals have been gradually understood during the last century, and several substances have been banned in different phases: in 1987 the Montreal protocol was formulated, with the aim to rule the phase-out of the most harmful fluids [26]. On the basis of this protocol, CFCs, used as refrigerants since the 1930s due to their superior safety and performance features but characterized also by an extremely high impact as ozone depleters, were gradually phased out from 1991 to the definitive banishment in 2010, even if the levels of consumption and production of the refrigerants with the highest ODP values (according to the Montreal protocol, these particular hazardous substances are R11, R12, R113, R114 and R115) have been forced to zero by 1996 [27]. HCFCs are characterized by values of ODP much lower than CFCs: the inclusion of one or more hydrogen atoms in the molecule causes a large destruction of the latter in the lower atmosphere by natural occurring hydroxyl radical, ensuring that only a little part of the released fluid survives to enter the stratosphere [23]. For this reason, even if HCFCs represent anyway an environmental threat, they were seen as a temporary solution in the Montreal protocol, usable as replacing substances to CFCs in a transitional phase: the definitive banishment of them is scheduled in 2030 in developed countries and in 2040 in developing countries [26]. Hence, as reported above, today two categories of refrigerants are available for use in thermal systems, HFCs and HFEs: both of them do not contain chlorine and have ODP values equal to 0, even if HFCs are labeled as greenhouse gases, since they have a significant GWP.

2.2.8 Availability and cost

Even if no substance can rival with water in these features, the economic feasibility of an ORC system is largely dependent on the availability and on the cost of the working fluid. Generally, the refrigerants usable in thermal systems are expensive and they are produced by a limited number of manufacturers in the world, but they ensure superior performances and their cost can potentially be reduced by more massive productions [23].

On the other hand, even low cost hydrocarbons are suitable for ORC applications, although often involving lower global efficiencies: the identification of the best trade-off among different requirements is the object of the optimization of the system.

2.2.9 Final remarks

A literature review by Tchanche et al. [12] revealed that the potential substances identified as suitable working fluids for ORCs in the technology history are:

- hydrocarbons (HC);
- hydrofluorocarbons (HFC);
- hydrochlorofluorocarbons (HCFC);
- chlorofluorocarbons (CFC);
- perfluorocarbons (PFC);
- siloxanes;
- alcohols;
- aldehydes;
- ethers;
- hydrofluoroethers (HFE);
- amines;
- fluid mixtures (both zeotropic and azeotropic);
- inorganic fluids.

The selection among these fluid typologies, on the basis of the criteria described in the previous Subsections, leads to different conclusions, depending on the specific application and on the working conditions. For example, Mago et al. [28] studied a set of both wet and dry fluids, and concluded that the best choice varies for different maximum cycle temperatures.

In the present thesis, the selection of the working fluid has been carried out through an optimization of the ORC performances, given a list of boundary conditions such as the heat source and sink temperatures. The results of this work are reported in Chapter 3.

2.3 Applications

Due to its peculiar features, in particular the capability to exploit low-temperature and small scale heat sources, ORC technology is suitable for a large number of different applications, today already available on the market or just studied by the international scientific community. This section is dedicated to a general description of the various potential uses of the technology, focusing in particular on small and medium scale systems, but with some references also to larger installations. Interesting comprehensive reviews on ORC applications can be found in literature, for example in the papers by Tchanche et al. [12], Quoilin and Lemort [22] and Schuster et al. [29]: a similar task is carried out in the following Subsections, referring also to works more focused on single typologies of systems.

2.3.1 Geothermal energy

The interior of Earth contains a practically inexhaustible amount of energy, in thermal form, due to the internal structure of the planet and to the physical phenomena occurring under crustal plates. Thanks to this energy, an increase in rocks temperature with depth is notable, with an average geothermal gradient near the surface of about 30 K/km: in general usable heat could be found only at depths too great for industrial exploitation, but geothermal resources are unevenly distributed, and in some locations they are concentrated and relatively near to surface. The energy carrier necessary to the extraction of the heat is usually represented by rainwaters which, once penetrated into the Earth's crust, have been heated up, and in some cases evaporated too, due to contact with hot rocks, and then accumulated in aquifers, occasionally at high pressures and temperatures, up to 300 °C. This fluid can be extracted by drilling geothermal wells and then exploited for electric power production [30].

Geothermal systems are traditionally classified in vapor-dominated, where superheated steam is produced, and water-dominated, further divided into wet steam fields, producing mixtures of water and steam, and hot water fields. Vapor-dominated fields are the simplest and cheapest to be exploited for power generation, since the steam can be directly expanded in a turbine: however, the number of sites in the world where these high-enthalpy geothermal resources are available is low, and their operations are today limited by strict regulations for the reduction of gaseous pollutant emissions (generally geothermal steam contains large amounts of incondensable gases such as CO_2, H_2S, NH_3, CH_4, N_2 and H_2) [9, 30]. Wet steam fields can be exploited in flash power plants, which are based on the property that a certain mass of vapor can be separated from liquid at saturated conditions after a reduction of the system pressure: after the brine is flashed (even twice in series, in dual flash power plants), it is expanded directly in turbine [9]. For hot water fields, but also for low-temperature (below 150 °C) wet steam resources, it is difficult to realize cost-effective flash plants, so the only solution is represented by binary cycles, in which the energy of the geothermal fluid is transferred to a secondary working fluid in a closed Rankine cycle. Due to the low temperature of the heat source, the use of water as secondary working fluid is avoided, so the natural solution for geothermal binary

plants is represented by ORC [12]. In 2011, binary plants based on ORC technology constituted one third of the world total geothermal installations, with 162 operative units, but, due to the small size of these fields and to the low enthalpy of the extracted fluid, these plants generated only 4% of the global power from geothermal sources [12, 31].

ORC-based geothermal systems have been developed and commercialized since 1980s: equipped with conventional turbines, they are economically feasible in power ranges down to 1 MW, while smaller scale installations (down to 10 kW) can be cost-effective only if components with large production and market diffusion, such as devices derived from the Heating, Ventilation and Air Conditioning (HVAC) field, are used [12]. The typical first law efficiencies reported in literature for binary geothermal plants are in the range between 0.05 and 0.15, while the corresponding exergy efficiencies (defined as the ratio between the net delivered power and the exergy of the geothermal fluid flow rate entering the system [32]) are quoted between 0.20 and 0.54 [12]: a large number of researches has been conduced to improve these performances, inherently poor due to the low temperature of the thermal source, focusing in particular on new configurations and on the choice of the most suitable working fluid [12]: for example, interesting works on this topic are the papers by Borsukiewicz-Gozdur and Nowak [33] and by Heberle and Bruggemann [34].

2.3.2 Solar energy

The exploitation of solar irradiation for electric generation, in particular with small scale systems, can respond to several issues related to sustainable energy production: the need for distributed power systems in remote and isolated areas [22], the need for low-cost electric power in developing countries, the need for small and efficient CHP systems for grid connected applications in developed countries, the need (originated also by laws) to generate clean electricity through renewable energy sources, the deregulation and privatization of the electrical market [12].

One possibility to exploit solar energy is to collect it as heat in a hot fluid, and then to convert this heat into mechanical energy through a direct thermodynamic cycle. Normally, the temperature reachable by the energy carrier fluid at a collector outlet is limited (below 300 °C), even if higher temperatures can be obtained using complex and highly expansive technologies, such as a heliostat field with a central receiver or a dish concentrator: for this reason, the conversion from thermal to mechanical energy can be conveniently performed by an ORC.

The main advantages of a solar ORC system can be summarized in [12]:

- low temperature operation, which permits the usage of less sophisticated equipments, as collectors and ORC components, and allows to achieve good performances even in regions with low intensity in solar radiation;
- modularity, which involves the possibility to realize large scale plants simply with the combination of a certain number of ORC modules on the same site;

- reduced capital, operations and maintenance costs, since cheap machines, materials and substances (in particular the heat transfer fluid) are used, and remote control, with less operators, is possible.

Unlike photovoltaic modules, a solar ORC system offers some interesting possibilities:

- coupling with a thermal storage [35];
- direct utilization of the mechanical power delivered by the ORC expander, in the situations in which it is required (e.g. pumping stations or desalination plants [36]);
- installation of a single solar panel coupled with both the ORC generator and the heating system;
- coupling with a supplementary thermal source (e.g. a gas burner), with the aim of a time decoupling between the CHP production and the solar irradiation.

Both flat and concentrating solar panels are coupled with ORCs, depending on application and installation site: while flat plate collectors require a lower capital investment, concentrating systems, such as parabolic trough, ensure a higher total amount of produced energy throughout the panel operating life [26], especially if equipped with sun tracking systems. Abundant literature can be found on solar ORC technology, and systems equipped with both flat plate and concentrating collectors have been studied, developed and tested: some examples are reported hereunder.

Delgado-Torres and Garcia-Rodriguez [10] carried out a comparison between systems equipped with different collectors (flat panels, evacuated tube collectors and parabolic concentrators) and running with various working fluids, defining the configurations that lead to the minimization of the solar panels area. Wang et al. [37] built and tested an experimental low-scale (the rated power was in the range from 1.5 kW to 2.0 kW), low-temperature solar Rankine cycle system, featuring a direct evaporation of the working fluid, R245fa in this apparatus, in the solar panels: two typologies of collectors were chosen for this installation, i.e. flat plate and evacuated tube technologies. The average solar-to-electric conversion efficiency was equal to 0.032 in the tests with flat plate panels, which were able to heat the working fluid up to 100 °C, and to 0.042 when R245fa was evaporated in evacuated tube collectors, reaching a maximum temperature of 115 °C. Wang et al. [38] realized a very small ORC system (with a delivered power lower than 10 W), equipped with flat plate collectors, with the aim of comparing different working fluids, both pure substances and mixtures. The experimental tests confirmed the potential of zeotropic mixtures of achieving good performances in ORC applications, thanks to their typical non-isothermal phase changes, and revealed the importance of the optimization of the working fluid flow rate. Canada et al. [35] reported the description of a parabolic trough solar plant, in construction in 2004 in Arizona, which demonstrated the potential of ORC technology for large scale centralized power production: the main characteristics of the installation are the nominal power output of 1.0 MW, n-pentane as working fluid, the turbine inlet conditions of 22.3 bar and 204 °C, an ORC efficiency of 0.207 and a global (solar-to-electric) conversion efficiency of 0.121 at design point. The

work by Jing et al. [39] deals with the detailed simulation of a solar ORC installation, with dedicated submodels for solar irradiation, collectors behavior and thermodynamic cycle performances: the model, used for a global optimization of the system, revealed that the best configuration is different, depending on the geographical location, since the intensity and the distribution of the solar irradiation are the most influencing factors on the facility performances. Kane et al. [40] designed, built and optimized a mini-hybrid solar power system suitable for installation in remote areas of developing countries: the main components of the plant are a 100 m^2-field of solar concentrators, two superposed ORCs and a Diesel engine, the purpose of the latter being to guarantee a minimum level of both power and heat availability at night or during cloudy periods. The field tests confirmed the possibility to achieve acceptable performances with this prototype, even at partial loads, a fundamental feature for a system designed to operate in stand-alone mode, i.e. without grid connection.

The warming of water bodies exposed to solar irradiation is a well known phenomenon, which results in the natural thermal stratification occurring in particular in lakes, seas and oceans. In equatorial and tropical regions, the thermal gradient between surface seawater and the layers at a depth of 800 m to 1000 m can reach values around 20 K [12]. Different Ocean Thermal Energy Conversion (OTEC) systems have been suggested to exploit this low level heat, one of them being ORCs working with low boiling temperature fluids such as ammonia. Although the efficiencies expected from these installations are extremely low (in a range from 0.03 to 0.05), involving the need for huge seawater flow rates to generate even limited electric power, several potential markets have been identified for OTEC technology, in particular for integrated applications, aimed to power production but also to additional tasks such as desalination, HVAC purposes, cold water agriculture, aquaculture or hydrogen production [12].

The natural thermal stratification can be inverted by dividing artificially a water body into zones characterized by different salinities: this is the basic principle of solar pond power systems. A salt gradient solar pond is usually a large, uncovered reservoir of water, which is split in 3 vertical layers, in order to avoid internal convection and heat losses through the surface [41]:

- a narrow (between 0.15 m and 0.30 m) convective top layer with low salinity water, acting as transparent cover and thermal insulator;
- a middle layer, with a thickness between 1 m and 1.5 m and a downwards increasing salt concentration, which avoids the rising of lower, warmer mass of water;
- a bottom layer, of depth between 2 m and 7 m, with very high, in some case saturated, salinity, acting as heat absorber and store.

The lower zone of the pond can reach a temperature between 90 °C and 100 °C, making it suitable as heat source for an ORC running with a low boiling point fluid, while the top layer can serve as refrigerating source for the condenser. Although the solar-to-electric conversion efficiency is very low (in a range from 0.008 to 0.020), this technology has a good potential market, especially in areas with high intensity in solar irradiation, thanks to its inherent, unique heat storage capacity [12, 41].

2.3.3 Desalination systems

Desalination of seawater represents one of the most promising solutions to face the increasing world demand of fresh water for drinking, agricultural and industrial uses [42]. According to the separation mechanism, the available technologies can be classified in thermal-based and membrane-based systems. The first ones separate salt from water by evaporation and condensation, in serial processes such as Multiple Effect Distillation (MED) or Multiple Stage Flash (MSF) desalination, while in the second ones, based on the Reverse Osmosis (RO) phenomenon, water diffuses through a membrane, while the salts are almost completely retained, thanks to a property of certain polymers called semi-permeability [12, 29, 42]. Although the pressures required to overcome the osmotic pressure are high (in the range from 60 bar to 80 bar [12]), and even if the filtration is not perfect (an average fraction of about 1% of sea salts passes through the membrane, but this is acceptable for potable and agricultural uses and for most of the industrial applications [42]), RO desalination has a great potential market, since its specific energy consumption is 5–6 times lower than thermal technologies [42]. In order to reduce the environmental impact of a RO desalination system, the power needed for water pumping should be provided from renewable sources: in particular, since mechanical energy is directly required instead of electric, the direct coupling of the expander of an ORC with the seawater pump represents a very interesting opportunity, making possible to exploit low-temperature heat sources, such as the solar energy from non-concentrating collectors, for desalination purposes. The solar ORC-RO desalination technology is widely studied today, aiming to reach the economic competitiveness and to design low-cost systems suitable for application in particular in developing countries with dry climates [43, 44].

2.3.4 Cooling systems and heat pumps

The opportunity of exploitation of solar energy for air conditioning purposes involves a unique advantage: the maximum required cooling load, during days in summer period, is synchronized with the highest values in solar irradiation, resulting in the possibility of reduction of summer electricity peak load. For this reason, the solar cooling has been intensely studied in the 1970s, during the oil crisis, but the researches have been abandoned soon after the crisis, being resumed in recent years. The technical options available to convert the solar energy into cooling effect are three: sorption, photo-voltaic electricity and thermo-mechanical systems [12]. Among the lasts, one solution is represented by the Duplex-Rankine cooling system, in which the mechanical energy produced by a solar ORC is used to drive the compressor of a vapor compression refrigerating machine: this technology appeared to be very promising in the last years, but only few examples of this application can be found in literature up to now, since sorption systems are characterized by a long series of advantages, such as the need for a simpler control strategy, the use of non-harmful fluids and lower costs [12], and since several researches are now focused on an alternative way to exploit thermal energy for refrigeration purposes, i.e. the vapor ejection cycles [45].

In literature examples are reported of ORCs coupled not to cooling systems but to

heat pumps: since the condensation of both the cycles can take place at the same thermal level, i.e. at the temperature of the heated ambient, a unique condenser can be utilized for the installation. In this way, high values in Coefficient of Performance (COP) can be reached by the system, because almost all the heat rejected by the direct Rankine cycle is transferred to the heated room, representing useful energy. A low-power prototype presented by Demierre et al. [46, 47] features a micro radial turbine (for the power cycle) and a micro radial compressor (for the refrigerating cycle) directly coupled on the same shaft, rotating on refrigerant gas bearings: a such designed system presents a series of advantages, like being oil-free and fully hermetic and absorbing only a little electric power, in particular for the ORC feed pump.

2.3.5 Biomass power plants

Unlike other renewable energy resources, such as wind or solar energy, biomass is not limited by an inherent intermittent nature, so it is suitable to substitute fossil fuels also for base-load power production. Today biomass is the 4^{th} largest energy source in the world, contributing to nearly 14% of the global energy demand, and this share is even higher, from 20% to over 90%, in many developing countries [48]. The environmental impact of biomass combustion is almost null, if compared with fossil fuels:

- the amount of released carbon dioxide is the same absorbed by the plant during its life, so a nearly neutral effect on the atmospheric concentration of this GHG can be highlighted after a life cycle analysis;
- the emissions of products of incomplete combustion, such as carbon monoxide and particulates, are moderate, in comparison, for example, with an average coal-fired boiler;
- the sulfur dioxide is not a major problem, due to the sulfur content of biomass (between 0.1% and 1.0%), lower than the case of coal and fuel oil (between 1.0% and 5.0%) [48].

Biomass is most conveniently used locally, in distributed CHP production with systems of small or micro scale, due to two main reasons [22, 48]. First of all, the energy density of biomass is low, this meaning high transportation costs of the fuel. Second, biomass is widely available also as a waste product in a number of agricultural or industrial processes, which can represent an available on-site demand of heat and power: on the contrary, it is normally difficult to find an end-user for the energy (in particular the heat) produced in larger CHP systems. The only proven technology for decentralized applications producing electric power up to 1.5 MW from solid fuels is represented by ORC systems [29]: the most reliable competitor is gasification, i.e. the transformation of the biomass into a synthetic gas, composed mainly by H_2, CO, CO_2 and CH_4, which can be burned in an ICE or in a gas turbine, after further processes of purification and filtration. Gasification systems exhibit higher power-to-heat ratios, and then higher profitability, than ORCs, but on the other hand they need higher investment, operational and maintenance costs: today this technology appears to be far from maturity (almost

all the plants actually in operation are prototypes for demonstration purpose), while the number of biomass ORC systems available on the market and installed in the world is rapidly increasing [22, 48].

A typical small scale biomass power plant is made up of a boiler capable to burn solid fuels and an ORC module, normally coupled by means of a thermal oil loop: the usage of an intermediate heat transfer medium, which is gradually cooled down in the vapor generator, provides a number of advantages, such as pressures in the boiler near to atmospheric value, larger thermal inertia and lower sensitivity to load changes, simpler and safer control and operation [12]. Concerning the working parameters, they are different from other ORC applications: in particular, the maximum cycle temperature could be close to flame temperature, compatibly with the chemical stability of the working fluid (normally temperatures of about 900 °C are not exceeded), allowing also higher condensation temperatures (around 100 °C), then a higher quality of the cogenerated heat, without excessive penalizations in the power cycle efficiency [49].

While micro scale plants are still under development (today the installation of a domestic system is not convenient due to high investment costs and long pay-back periods [48]), the economic profitability of biomass ORC CHP facilities at medium scale (in the range of power from 0.1 MW to 1.5 MW) was demonstrated already in the 1990s: a commercial system, featuring a dynamic expander and a siloxane as working fluid, is described for example in a paper by Bini and Manciana dated 1996 [50]. The number of installations of these ORC plants is rapidly growing, making the technology mature and cost effective: in a recent review by Tchanche et al. [12], some installations in Italy (Dobbiaco, 1.1 MW), Austria (Lienz, 1.0 MW and Fussach, 1.5 MW) and Germany (Sauerlach, 0.7 MW) are reported as examples.

2.3.6 Energy recovery from internal combustion engines

Due to the inherent overall efficiency of ICEs, which only seldom, in the biggest units, approaches values higher than 0.50, a large amount of waste heat is always connected with their operations. For this reason, efforts to find solutions to recover a part of this thermal energy (available in particular from the exhaust gases and from the cooling water) and to produce mechanical work from it have been done since the oil crisis in the 1970s. Among other technologies, such as thermo-electricity or absorption cycle air conditioning, ORCs appeared to be the best suitable solution for this application since the first studies [22]. The features and the problems connected with the use of an ORC as bottomer cycle for an ICE are different for stationary and mobile applications, in particular if the latter ones are small scale engines.

Stationary ICEs are suitable for electricity production in a wide field of applications, such as generators in remote areas, backup and emergency units, power plants capable to follow rapid load fluctuations, CHP units or prime movers capable to burn particular fuels such as biogas or bio-Diesel. The sizes of the engines used in these cases are often in the medium range (from 50 kW to 3000 kW), and they usually operate at their rated

power for the most part of their working hours during a year. For these reasons, the available waste heat has features (in particular power rate, temperature, cooling profile and absence of excessive fluctuations) similar to the thermal sources already described in the previous Subsections, so the most suitable ORC modules for integration with a heavy-duty ICE are similar to the one analyzed for other applications. In particular, the high thermal level of the exhaust gases requires a system (and a working fluid) similar to the one suitable for coupling with a biomass boiler (see Subsection 2.3.6), while the heat obtained from the ICE cooling water circuit can be successfully exploited by an ORC comparable with the ones studied for solar applications (see Subsection 2.3.2). In recent years several studies have been published on the coupling of an ORC unit with a stationary ICE, with some examples reported here, useful to have an idea on the problems and on the solutions proposed for this application. Lombardi et al. [51] described a system designed for the exploitation of the biogas which is produced from biodegradable wastes in landfill sites: this gas, thanks to their reliability, low specific costs and relatively high efficiency. However, the waste heat originated by these engines is only seldom exploited for cogenerative purposes, since the waste treatment plants are normally located far from any potential heat user. Therefore the authors suggested to use the engine exhaust gases as the thermal source for a bottoming ORC, with the aim to increase the power production and then the overall efficiency of the system: in the paper different engine models and several ORC configurations have been analyzed, concluding that the power output can be increased by 13 percentage points and the overall efficiency by 4.7 percentage points with respect to the case of stand-alone ICE, when a bottoming ORC in regenerative configuration is coupled to the prime mover. Gewald et al. [11] proposed an exergetic and economic analysis on systems capable to recover heat from a number of heavy-duty Diesel engines of large scale (the rated power of the considered units varied from 9 MW to 18 MW) for stationary operations, in particular with a comparison between a traditional steam Rankine cycle and an ORC. The study, considering only bottoming cycles capable to recover energy from both the exhaust gases and the cooling water, concluded that the use of an organic fluid instead of water as working media involves advantages (in particular in terms of reduced cost of the produced electricity) when the size of the thermal source (and then the rated power of the recuperated ICE) falls below a certain threshold. Ast et al. [52] conducted an experimental investigation on an ORC prototype designed to recover the waste heat only from the cooling water of a stationary gas-fueled engine, concluding that the feed pump and the expander are the most critical components of the system, their working parameters being the most influencing on the overall performances of the unit. Vaja and Gambarotta [53], finally, presented a thermodynamic analysis of different solutions of bottoming ORC for a stationary ICE, the latter featuring a rated power of about 3 MW and a calculated electrical efficiency of 0.418. The authors compared a number of working fluids and three different configurations for the bottoming cycle: a simple cycle recovering heat only from the ICE exhaust gases, a simple cycle with both the exhaust gases and the cooling water as thermal input (the latter used to preheat the working fluid before evaporation) and a regenerative cycle, capable to recover only the thermal energy of the exhaust gases. The analysis concluded that the most significant enhancements in the performances of the system can be achieved by both the preheated and the regenerated ORCs, with an increase of the overall efficiency

of the system of about 5 percentage points. It is interesting to note that both these solutions are equivalent in terms of efficiency, since regeneration, while allowing a higher ORC efficiency, does not permit the exploitation of the cooling water as a thermal source (due to its low temperature), causing an incomplete heat recovery from the ICE. This confirms that the internal regeneration in a heat recovery ORC does not always involve significant benefits in terms of performances, hence the opportunity to install an internal heat exchanger has to be discussed in each case.

Unlike stationary applications, the regime of the ICEs used in transports is often transient, with rapid and continue fluctuations of both load and shaft speed. Obviously, this entails non-stationary conditions in flow rates, temperatures and cooling profiles for both the exhaust gases and the cooling water, so the exploitation of these thermal sources involves larger difficulties in comparison with heavy-duty engines. Nevertheless, the significant potential savings in fuel and emissions justified a large number of researches on the exploitation of waste heat of mobile ICEs through ORCs in the last decades, from the larger units (installed on ships) to the smaller ones, involved in ground transportation. The typical sizes of the terrestrial vehicles (trucks, coaches but also private cars) and of their engines require further features for the ORC components, such as compact dimensions and limited weight. Few examples of the papers available in literature on ICEs with bottoming ORCs for mobile applications are reported hereafter. Bonafin et al. [54] studied a marine engine with a rated power of 5.7 MW and an efficiency equal to 0.49, first of all taking into account the effective load distribution of the ICE, which often operates in off-design conditions: the analysis showed that, considering the average operation duty of the engine, equal to 6960 hours per year, it is run at full load, for maximum speed operations, for only 1.5% of the time, while an 85% load is used for the 85% of the time (to obtain the cruise speed), a 75% load is used for the 5% of the time, a 50% load is used for the 7% of the time (for ancillary services when the ship stops in port) and a 25% load is used for the remaining 1.5% of the time (in port operations). Starting from these values, the authors compared four different configurations of bottoming cycles: a simple ORC, recovering energy only from the exhaust gases, a preheated ORC, exploiting also the cooling water waste heat, a regenerative cycle, which does not allow to use the cooling water as a thermal source, and a combination of two ORCs in cascade, which recuperate energy from both the exhaust gases and the water and exchange energy also each other (the condensation heat of the upper cycle is used to start the evaporation of the fluid of the lower cycle). Considering only the design conditions, the authors showed that the regenerated cycle and the combination of two ORCs gave more or less the same performances, but after an off-design analysis, they recognized the regenerated ORC as the best to be installed as bottoming cycle for the studied engine, since the large decrease in the cooling water temperature at partial loads affects significantly the performances of the combined cycle. Durmusoglu et al. [55] conducted an analysis similar to the previous one on a two-stroke engine installed on a container vessel: taking into account also the ICE operation at partial load, the authors calculated that the installation, on a single ship, of a bottoming ORC would save approximately 1230 t/year of fuel and would reduce the CO_2 emissions of about 54 t/year. An application of ORCs on ground vehicles is described by Aumann et al. [56], who calculated the potential savings connected with

the use of a combined ICE-ORC propulsion system on a truck. The authors concluded that, while with the original engine (a 12.1 l Diesel ICE with a rated power of 279 kW) the mean fuel consumption of the truck was 34.0 l/100 km, the installation of a heat recovery ORC would reduce this data to 32.1 l/100 km, meaning a fuel saving of 5.6%. The application of the ORC technology on heavy vehicles such as trucks or coaches is very attractive due to high power of engines, high number of working hours during a year (meaning high amount of fuel that can be saved) and large available spaces in comparison with cars, making the weight and dimension issues less restrictive. For this reason, researches on this vehicles began already in the 1970s during the oil crisis: for instance, a prototype powered by an ICE-ORC system was designed and tested in 1976 by Mack Trucks, achieving an improvement of 12.5% of the fuel consumption [22]. In recent years, due to the always more restrictive laws on emissions, a number of manufacturers studied also the possible installation of a recuperative ORC on private cars: for example, the system proposed by Honda achieved a global thermal efficiency of 0.327, coupling the cycle to an engine with a rated efficiency equal to 0.289 [12].

2.3.7 Energy recovery from other sources

Even if the applications described in the previous Subsections are the most common, ORCs can be coupled also to other, less diffused thermal sources, allowing large potential savings in primary energy consumption and pollutant emissions, in particular in large industrial processes. In the already cited paper by Tchanche et al. [12] the case of cement manufacturing is reported: during the process, an intermediate product called clinker has to be cooled down from the kiln temperature (at about 1000 °C) to around 100 °C using ambient air, which is heated up to about 300 °C. If the thermal energy of this hot air stream could be recovered by means of a low-temperature ORC, a not negligible amount of electric power can be generated (up to few tens of MW, depending on the plant size), covering 10-20% of the installation electricity demand.

Yari and Mahmoudi [57] analyzed the case of the gas turbine modular helium reactor, a new generation nuclear reactor currently being developed by an international consortium: these installations consist in a graphite-moderated reactor core cooled down by gaseous helium which flows in a closed-loop Brayton cycle [58]. After the expansion, the helium exits from the turbine at a temperature of about 150 °C and has to be cooled down to about 25 °C before being compressed. Normally the compression process is split in two stages, with an intercooler aimed to cool the gas from about 100 °C again to about 25 °C: the two heat exchangers (precooler and intercooler) dissipate a significant amount of thermal power in form of hot water (approximately 300 MW in a plant capable to generate a net electric power of about 280 MW). This low temperature heat source can be exploited through an ORC and the authors of the study calculated that this would improve the global first law efficiency of the plant of about 3 percentage points, corresponding to an increase of more or less 15 MW in the net generated power for an installation of the analyzed size.

An ORC can operate also at very low thermal levels, for example evaporating the

working fluid at ambient conditions and exploiting an available low temperature heat sink for condensation: in these cases it is usually called cryogenic Rankine cycle. For instance, a generally unexploited cold potential is represented by Liquefied Natural Gas (LNG): in order to allow maritime transportation, the gas is condensed at atmospheric pressure and stored in special tankers at a temperature of −162 °C. Once unloaded, the fuel needs to be heated and re-vaporized before utilization: this task can be obtained burning a little amount of the gas itself or, more frequently, using seawater in a particular heat exchanger called Open Rack Vaporizer (ORV). Even if this process requires only a little amount of energy (essentially that absorbed by the water circulating pumps), it implies the waste of all the LNG cold energy, which is rejected to the sea [59]. Maertens, in his study dated 1986 [60], reported that in the 1980s there was already 14 cryogenic Rankine cycle installations coupled with LNG terminals, all located in Japan, for an overall generating capacity of 46 MW. These plants utilized particular mixtures of refrigerants as working fluids, in order to allow condensation at very low temperatures (without risks of solidification) and evaporation at ambient conditions, exchanging heat with seawater. The recovery of cold energy potential achievable by these systems is significant: while the electricity demand connected to the liquefaction of 1 t of natural gas can be estimated in about 850 kWh, the exploitation of the regasification of the same amount of LNG by means of a cryogenic Rankine cycle could produce up to 240 kWh, i.e. 28% of the original consumption [59]. Hisazumi et al. [61] proposed an enhanced system, capable to recover even a higher share of the electricity involved in the liquefaction process: they studied the integration of the LNG vaporizers with a combined cycle power plant by means of an ORC which exploits the waste heat of the power cycle (from the exhaust gases of the heat recovery steam generator and from the condenser of the steam turbine) as thermal source and rejects its condensation heat, at very low temperatures, to the vaporizing natural gas. Other than not requiring seawater (and then saving the concerning pumping work), the power produced by the ORC interposed between the combined cycle and the vaporizers is higher than the previous case, since the heat source is at a higher temperature: the authors estimated that the ORC can generate by itself 400 kWh of electric energy when vaporizing 1 t of gas, i.e. 45% of the electricity related to the LNG production.

One last example of ORC application can be represented by the bottoming of a micro gas turbine. Even if the heat rejected with the exhaust gases is normally used to produce hot water at high temperature, in one of the most classical configuration of cogenerator, in some cases the available heat can not be conveniently exploited: for instance, this happens when the turbine is used as emergency generator or Uninterruptible Power Supply (UPS), or when the heat is required at low temperatures, for example for a floor heating system, and then the cooling of the high temperature exhaust gases in this way would represent an unacceptable exergy destruction. In this cases, the implementation of a bottoming ORC appears to be one of the most natural solution to enhance the fuel exploitation, increasing the overall efficiency. Invernizzi et al. [62] completed a study on the feasibility of a system of this typology, considering a 100 kW commercial micro gas turbine as starting point. After the choice of the most suitable working fluid and the preliminary design of the main components of the bottoming cycle, the authors concluded that the installation of the ORC would allow to produce an additional electric power of 45 kW, increasing the

electrical efficiency from 30% to about 40%. Yari [63] conducted a parametric study on a micro turbine-ORC combined cycle of the same size: the results confirmed the possibility to enhance the overall electrical efficiency to around 40%, but also underlined that the performances achievable with a simple and a regenerated bottoming cycle are very similar, confirming that the opportunity of installing an internal regenerator in a recuperative bottoming cycle must be carefully evaluated in each case, as already explained in the previous Subsection 2.3.6.

2.4 An important component: the expander

When a low temperature heat source is involved, as in the applications studied in the present thesis, the thermal efficiency of a Rankine cycle is inherently low due to thermodynamic reasons (for instance, the efficiency of a Carnot cycle evolving between 150 °C and 30 °C is equal to 0.284), so the effectiveness of all the components involved in the system has to be as high as possible, in order to obtain a generator with an acceptable global efficiency. Nevertheless, these small scale installations should not be too expensive in order to reach an economic competitiveness, so the cost is another important selection criteria for all the components of the circuit. The expander, which function is to convert the thermal energy of the fluid in mechanical work, is one of the elements most influencing the global performances of the system, so its choice represents a critical step in the design process of an ORC-based generator. For this reason, a large number of works can be found in literature concerning expanders and their possible applications on small scale ORCs.

In 1984 Badr et al. [19] presented an interesting analysis aimed to find a prime mover suitable for solar power generators to be installed in developing countries: the authors indicated low cost and mechanical simplicity as the main required features for the machine. On the basis of technical data, available for over 2000 ORC plants in the range of power from 0.1 kW to 1120 kW [18], it was shown that both positive displacement expanders and radial inflow turbines were used in these small scale applications. The shaft speeds in the first case varied in a range from 1000 rpm to 4000 rpm, while in the second they were in the typical range of small turbomachinery, from 35 000 rpm to 60 000 rpm. Only multi-vane and reciprocating expanders were installed in the smaller systems, with an electric power lower than 3 kW, while also screw expanders were used beyond this threshold. A classical similitude approach, based on the definitions of specific speed and specific diameter, showed that, at low specific speeds, positive displacement expanders can reach efficiencies higher than radial or axial turbines. After the analysis, the authors concluded that multi-vane expanders are the best suitable units to be installed in the small scale, low-temperature ORC systems, due to their simple construction, their low noise and vibration, their high efficiency (up to 0.80-0.85) in a wide power range, their high torque at low or zero speed, their relatively high volumetric expansion ratio (up to 10 with a single stage expansion) and their capability to work also with low quality (highly wet) vapors. In the paper, however, several problems still to be resolved also have been highlighted, such as the reduction of breathing losses, internal leakages, heat

transfer losses and frictional dissipations in the machine.

In a successive work by Badr et al. [64], the authors conducted a research program on multi-vane expanders working with steam and several organic fluids, finding very promising performances for these machines, in particular an achievable isentropic efficiency higher than 0.73, at rotational speeds up to 3000 rpm. Besides, in the same paper a Wankel-type expander has been designated as another possible choice for a steam Rankine cycle with a rated output power of 10 kW.

Wang et al. [37] described a low-temperature solar Rankine plant featuring R245fa as working fluid and a rolling piston machine, designed and assembled specifically for this experimental facility. The mean delivered power of the system was 1.73 kW, with an average isentropic efficiency of 0.452 at a maximum shaft speed of 3600 rpm, but a significant deterioration in the performances was observed during the experiment, due to the progressive rising of frictional and leakage losses.

Haiqing et al. [65] studied another machine called swing expander, which features a mechanical structure very similar to a rolling piston type, but involves less problems of leakage and inefficient lubrication, since the swing blade and the piston are integrated together. The authors described the application of this expander in a CO_2 heat pump to replace the throttling valve. The efficiency was in the range from 0.28 to 0.44, with shaft speeds varying from 700 rpm to 1900 rpm and with a maximum delivered power of about 1 kW.

Recently the already cited Wankel expander [64] has been proposed again by Manfrida and Padula [66] for a steam CHP application, considering that the main problems which always affected this engine, in particular those related with materials and lubrication, can be now overcome thanks to the present technology: the simulation model developed by the authors confirmed the potentiality of this machine for use in the distributed generation field.

In the last 20 years another possible alternative has been taken into account and deeply studied by several authors: a modified scroll compressor used as an expander. The scroll machine has been invented at the beginning of the 20^{th} century by Léon Creux, a French engineer who obtained the U.S. patent on it in 1905 [67]. The working principle, probably derived from some projects by Archimedes and Leonardo da Vinci related to water handling, is based on the interaction between two spirals, generally called scrolls, which define different variable-volume chambers filled by the fluid thanks to their coupling and their relative motion. Due to the extremely low tolerances needed to obtain an acceptable scrolls coupling, the exploitation of the invention by Creux has not been possible until the mid-1970s, when, given the improvements in machining processes, the American physicist Neils Young saw the opportunity of construction and practical utilization of this machine; therefore a development program was launched at Arthur D. Little Enterprises, which led to a new patent in 1975 (in particular on the use of the scroll machine as pump and compressor) [68] and to the following commercialization of

the first scroll compressors at the beginning of the 1980s [69]. The peculiar features of this typology of compressors - the high efficiency, the limited number of moving parts, the low levels of noise and vibrations and, therefore, the high reliability - led the machine to a rapid diffusion on the market, in different fields: the main applications are for HVAC (the first commercial model is dated 1987 [70]) and refrigeration (for example in supermarket rails, in land transportation and in maritime containers), but this technology is used also in natural gas compression stations and for the pressurization of cryogenic gases [71]. Thanks to its working principle, a scroll compressor can be used as an expander, reversing its rotation wise and after only minor modifications to the machine: in some applications, such as a small scale ORC, this option is very interesting, due to a series of factors:

- scroll compressors have a high-series low-cost production;
- they are designed to operate on refrigerants which are very similar, in physical and thermodynamic properties, to the organic fluids suitable for ORCs;
- the expander typically required by a low-scale ORC should feature a rated power which is included in the range offered by the scroll compressor market;
- the natural behavior of a scroll compressor to reverse its rotation wise can be often observed in air conditioning and refrigeration systems if appropriate countermeasures are not adopted, in particular just after the shut down of the apparatus, when the pressure at the machine outlet is higher than the one imposed at the suction but no driving torque is applied to the shaft [72].

Referring to an isentropic expansion, efficiencies values in the range from 0.60 to 0.65 [73–76], with peaks between 0.68 and 0.70 [40, 75, 77, 78], are reported in literature for scroll expanders derived from commercial compressors, but lower values can also be found. Lemort et al. [75] conducted a series of tests on three different scroll expanders fed with air and water steam, in some cases mixed with propylene glycol, and running at different operating conditions, detecting an efficiency variable in the range from 0.30 to 0.70, depending mainly on the fluid used. In the papers by Kim et al. [79] and Peterson et al. [80] the authors reported very low efficiencies for the scroll expanders they studied, in the range from 0.30 to 0.40, due mainly to an excessive clearance between the scrolls and to the poor interaction with lubricating oil, causing a large fluid leakage from the high pressure chambers to the lower pressure one. This phenomenon has one of the highest influences on the scroll machine performances, together with the mechanical losses, the heat transfers and the matching between the imposed pressure ratio and the one defined by the scroll geometry.

Finally, a number of works can be found in literature on the installation of reciprocating expanders in small scale ORC systems: for example, Badr et al. [19], in their paper dated 1984, indicated piston machines as the most common expanding devices for these applications. In the last 30 years, however, different types of expanders (in particular the just described scroll machine) have been studied and intensely developed, so the the use of reciprocating devices for ORC applications has been only seldom considered.

Nevertheless, today the piston-type expanders can be rediscovered, thanks to the innovations achieved in materials, machining processes and engine control systems, derived from the ICE sector, as reported by Manfrida and Marraccini in a recent paper [81]. Badami et al. studied a steam Rankine cycle capable to generate an electric power in the range from 10 kW to 25 kW, featuring two different reciprocating expanders, a three-cylinders unit [82] and a two-cylinders one [83]. Baek et al. [84, 85], finally, developed a refrigeration system based on a CO_2 trans-critical cycle with the throttle valve replaced by a small two-piston expander derived, after deep modifications, from a commercial four-stroke ICE, using fast-acting solenoid valves to control the expansion process. The authors adopted this engine in order to enhance the performances of a refrigeration cycle, but this can also be considered another example of the feasibility of Rankine power cycles featuring reciprocating expanders.

2.5 An important component: the pump

The choice of the feed pump has a key role in the design process of an ORC-based cogenerator. Even if the most important selection criteria for a pump are the delivered flow rate and the achievable differential pressure between suction and discharge, the choice of the best-suited technology for particular applications like the ORCs depends also on other factors such as operating temperatures and pressures, compatibility of the fluid with materials or fluid viscosity [86]. In particular, this last parameter is one of the most critical, since organic fluids feature, in most cases, a very low viscosity, causing important leakages from the machine seals and from the pumping mechanisms and limiting the lubricating properties of the fluid itself. While the current technology in large and medium scale ORC installations is represented by centrifugal feed pumps [50], this solution is not suitable for smaller systems: in fact, the concurrent requirements of low flow rates and high differential pressures can be satisfied by a centrifugal machine only if multi-stage architectures are considered, but this option entails excessive cost and bulk [86]. Positive displacement pumps appear then a more suitable alternative for small scale ORCs, but they involve some drawbacks such as a relatively low efficiency. For this reason, unlike in a traditional steam cycle, the electric power absorbed by the feed pump is not negligible, so the optimization of this component is essential to achieve an acceptable global electrical efficiency for the system.

Despite this, only few works can be found in literature related to the feed pumps of small scale ORC systems. In 1985 Bala et al. [87] presented a paper in which they described the tests carried on a sliding-vane pump operating with two different organic fluids, the CFCs R11 and R113, now banned. The authors found that some enhancements in the pump performances can be achieved adding a small percentage (around 10%) of oil in the refrigerants, but in any case the machine cannot reach global efficiencies higher than 0.21, which means that the electrical absorption of the device is almost 5 times higher than the needed pumping power.

In his PhD thesis, Aoun [86] conducted an interesting analysis on the different pumps potentially adoptable in a small scale ORC, evaluating the main features of a large

number of commercially available positive displacement units. The first machines taken into account by the author were the gear pumps: according to him, the main problem related with their usage in an ORC is the fluid low viscosity, which decreases dramatically the pressures and the flow rates achievable by these pumps. Nevertheless, a model capable to achieve the requested performances was found on the market. Aoun studied also the sliding-vane pumps: a commercial unit suitable to deliver the needed flow rate at a sufficient pressure was found, but the expected performances, in terms of overall efficiency, were relatively low, confirming the results of the already cited paper by Bala et al. [87].

As an alternative, the author indicated the diaphragm pumps: in these machines a reciprocating piston moves, by means of an interposed amount of oil, an elastic membrane, in order to vary the volume of a chamber enclosed between two check valves and filled by the fluid, which is pumped by this mechanism. In this way the diaphragm provide a physical sealing towards ambient, so every leakage problem is avoided and the maximum achievable pressures are independent from the fluid viscosity [88]. Therefore, according to Aoun, diaphragm pumps represent the best suited option for small scale ORC applications, even if also this technology presents a number of drawbacks. In fact they are generally heavier and bulkier than gear or sliding-vane pumps and they are extremely sensitive to cavitation, which may cause the membrane perforation [86]. Moreover, these devices are characterized also by very low efficiencies: for example, Declaye [88] and Quoilin [89] described the experimental prototype of an ORC cogenerator designed and installed at the University of Liège, Belgium, in which the diaphragm feed pump was not capable to reach global efficiencies higher than 0.15-0.20 at the best working conditions.

The last typology of pump analyzed by Aoun in his dissertation was the reciprocating piston machine. Even in this case special solutions are needed in order to ensure good performances with low-viscosity working fluids, so the author was able to find only few examples of suitable devices on the market: however, the working temperatures of these pumps are limited (in particular at 50 °C), so they can be adopted only for systems which are not required to cogenerate heat at high temperatures. On the other hand, the overall efficiency of these special reciprocating pumps is estimated by Aoun to be very high, up to 0.78 at the best working conditions [86]. In any case, these values are only hypothetical, calculated starting from literature data, since the author chose to adopt a diaphragm pump in his test facility. A little information on a piston-type pump actually installed on a small scale ORC system can be found in the Bachelor's thesis by Davidson, dated 1977 [17]: he used a small brass reciprocating pump (delivering a rated volumetric flow rate of about 0.2 l/s), which exhibited a maximum global efficiency variable in the range from 0.174 to 0.204.

2.6 Final remarks

The literature review conducted in this Chapter 2 highlighted the great potential and the several possible applications of small scale ORC-based systems. On the other hand,

the analysis showed also many aspects which need further studies and experimentations, before this technology can achieve the technical and economic feasibility. The present dissertation is developed in this context: the next Chapters include the descriptions and the results of a series of numerical and experimental analyses on different ORC systems, aimed to give a certain contribution to the enhancement of the general knowledge in this field and to allow the design and the construction of a fully functional prototype of micro-ORC cogenerator.

3

The working fluid

The choice of the working fluid holds a key role in the design process of an ORC. As already described in detail in Section 2.2, a fluid is suitable for these applications only if it satisfies a series of thermodynamic, compatibility, safety, environmental and economic requirements. According to literature, several substances have been identified as possible ORC working fluids in the past years: they have been listed in Subsection 2.2.9. Starting from a such defined group of potential operative substances, the final identification of the best suited fluid for a particular application should be conducted with a detailed study of the specific case. In this Chapter, the procedure of selection of the fluid for a domestic-scale ORC cogenerator is reported: a method based on the integration of the thermal streams has been adopted, which leaded to a multi-objective optimization of the system. In order to define a realistic set of boundary conditions, a specific case has been considered, in particular an ORC system coupled with a biomass boiler sized to satisfy the heat demand of a residential building. The results of the optimization constitute a valid decision criterion and are at the basis of the final choice of the working fluids considered in the simulation models and adopted in the experimental facilities described in the next Chapters.

3.1 Description of the selection process

The Process Integration is a widely used approach in several industrial sectors (e.g. chemical, petrochemical or steel) that allows to increase the profitability of a process through reductions in energy consumption and in waste heat generation. Among all the integration methodologies, the Pinch Analysis is the most common, due to its simplicity, associated with the results obtained in several projects worldwide in the last decades [90].

In general, an energy transformation process requires high temperature heat as input and generates waste heat at a lower temperature. If several processes are integrated, in some cases the quality of the outlet stream of one of them is sufficient to satisfy the demand of another one: the fundamental principle of the Pinch Analysis is the matching of the individual requirements of heat with the available sources. The maximization of these matches will result in a minimization both in the requirements of heat at the highest

temperature from an external utility and in the generation of useless low-temperature waste heat [91].

Even if the main applications of the methodology are in the large industrial plants, the Pinch Analysis can be useful also in smaller processes. In this thesis, a micro cogenerator for domestic application has been chosen as case study. A biomass boiler has been sized in order to satisfy the thermal demands of a 200 m^2 house occupied by 4 persons: a 4 kW floor heating system and a hot water production utility of 30 kW have been considered, taking into account also the heat demand fluctuations on yearly (for the first one) and daily (for the second) basis. Since the flue gases produced by biomass combustion can reach high temperatures, while the heat is required at relatively low levels, an ORC can conveniently be added to the boiler, in order to produce electricity burning only a minimum amount of additional fuel. The Process Integration allows to optimize the combination between all the streams of the system (including a possible regeneration in the power cycle), in order to produce the maximum possible electric power. To achieve a realistic prediction of the heat exchanges involving the flue gases, a complete analysis of a given biomass has been conducted, in order to obtain the cooling profile (temperature-enthalpy) of the combustion products. The aim of the study is to find the best ORC parameters, including the working fluid, the expander size, the maximum temperature and the working pressures, in order to produce the maximum annual amount of electricity running the cogenerator only when the produced heat can be exploited. Since the cogenerator has to follow the needed heat profile, the task corresponds to maximize the exergy efficiency of the system, maintaining always the first law effectiveness at its best value. Due to safety and construction issues in a domestic device, the maximum working pressure has to be limited, so a two-objective optimization has been carried out, with the aim to reach a good trade-off between the maximum exergy efficiency and a low evaporating pressure.

The final calculations have permitted to determine the fraction of the annual electricity demand covered with the cogenerator, and also the additional biomass needed to produce all the needed electric energy, using the system in dissipation mode, which is feasible adding a simple air condenser in the cycle.

3.2 Problem input parameters

A biomass boiler has been sized to satisfy the heat demand by a 200 m^2 house occupied by a 4 persons family. The boiler has to feed a floor heating system and produce the needed hot water.

The maximum thermal power of the heating system has been set to 4 kW, with a nominal water flow rate of 0.064 kg/s. A typical yearly-based working profile for the town of Lausanne, Switzerland has been considered for the system, taking the needed data from the European Commission Joint Research Centre [92]. A functioning at the maximum power for 14 h/d has been supposed in December and January, while a partial load proportional to the heating degree days has been considered in the other months.

The hot water production system maximum power has been set to about 30 kW, with a rated flow rate of 0.2 kg/s. Since the typical hot water consumption can be estimated in about 70 l/d per capita, a total of 280 l/d has to be warmed up in the considered house, so the system is running for about 30 min/d.

Finally, an electricity demand of 4.8 kWh/d per capita has been taken into account, since this is the average data reported by the International Energy Agency for European Union: a total consumption of 19 kWh/d has been considered for the studied house [93].

The synthesis of heat and power demands has been reported in Tab. 3.1, on a monthly basis.

Tab. 3.1: Heat and electric power demands

Month	Degree days	Heating system working period	Hot water system working period	Heat produced when all systems are active	Heat produced when only the floor heating system is active	Heat produced when only the hot water production system is active	Electric demand
	[DD]	[h/d]	[h/d]	[kWh/d]	[kWh/d]	[kWh/d]	[kWh/d]
Jan	492	14.0	0.5	1.961	7.193	0.000	19.000
Feb	405	11.5	0.5	1.961	5.861	0.000	19.000
Mar	304	9.0	0.5	1.961	4.529	0.000	19.000
Apr	181	5.0	0.5	1.961	2.398	0.000	19.000
May	60	0.0	0.5	0.000	0.000	1.725	19.000
Jun	19	0.0	0.5	0.000	0.000	1.725	19.000
Jul	3	0.0	0.5	0.000	0.000	1.725	19.000
Aug	25	0.0	0.5	0.000	0.000	1.725	19.000
Sep	126	3.5	0.5	1.961	1.599	0.000	19.000
Oct	270	8.0	0.5	1.961	3.996	0.000	19.000
Nov	447	13.0	0.5	1.961	6.661	0.000	19.000
Dec	495	14.0	0.5	1.961	7.193	0.000	19.000

3.3 Biomass analysis

To achieve a realistic representation of the problem, a specific woody biomass has been considered to feed the boiler; its composition is reported in Tab. 3.2 [94, 95].

The combustion of this biomass with an air index equal to 2 has been simulated in Belsim VALI environment [96]: in this way it has been possible to calculate the enthalpy-temperature cooling profile of the flue gases, reported in Fig. 3.1, where the larger enthalpy variations (due to condensation of the water contained in the combustion products) can be noticed at the lowest temperatures. Here it is assumed that the flue

Tab. 3.2: Biomass analysis [94, 95]

Proximate analysis		
Humidity	[%wt]	20.00
Ash content	[%wt]	0.00

Ultimate analysis (organic fraction)		
Carbon	[%wt]	51.09
Hydrogen	[%wt]	5.75
Oxygen	[%wt]	42.97
Nitrogen	[%wt]	0.19
Sulfur	[%wt]	0.00

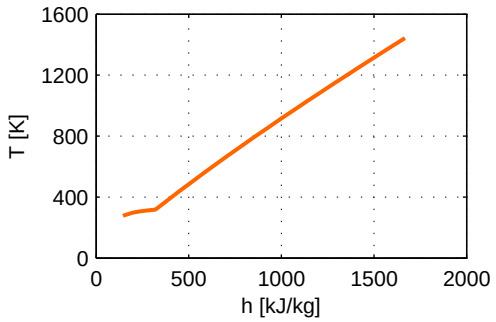

Fig. 3.1: Enthalpy-temperature cooling profile of the flue gases

gases are cooled down from the adiabatic flame temperature. Actually, at high temperatures the heat transfer is highly radiative and the temperatures at which the heat is transferred are lower. However, this affects the flue gases cooling profile only at high temperatures, and since the temperatures of the other streams of the system are much lower, this simplification has no impact on the Process Integration.

Moreover, a lower heating value of 14 354.40 kJ/kg has been determined for the fuel after the simulation; according to a set of semi-empirical formulas found in literature [97, 98], starting from this value and considering the composition of the fuel, a chemical exergy of 16 650.20 kJ/kg has been calculated for the specified biomass.

3.4 Cycle design, Process Integration and optimization

A simple ORC has been designed, fixing its main points: pump inlet (1), pump outlet (2), expander inlet (5) and expander outlet (6): for example, a possible cycle is reported on (T,s) diagram for R245fa as working fluid in Fig. 3.2. In this first step of the analysis a generic expander has been considered, with an isentropic efficiency equal to 0.65. Note that no hypothesis has been made on recuperative heat exchange inside the cycle: the only inputs are that the fluid has to be heated up from point 2 to point 5 and to be cooled

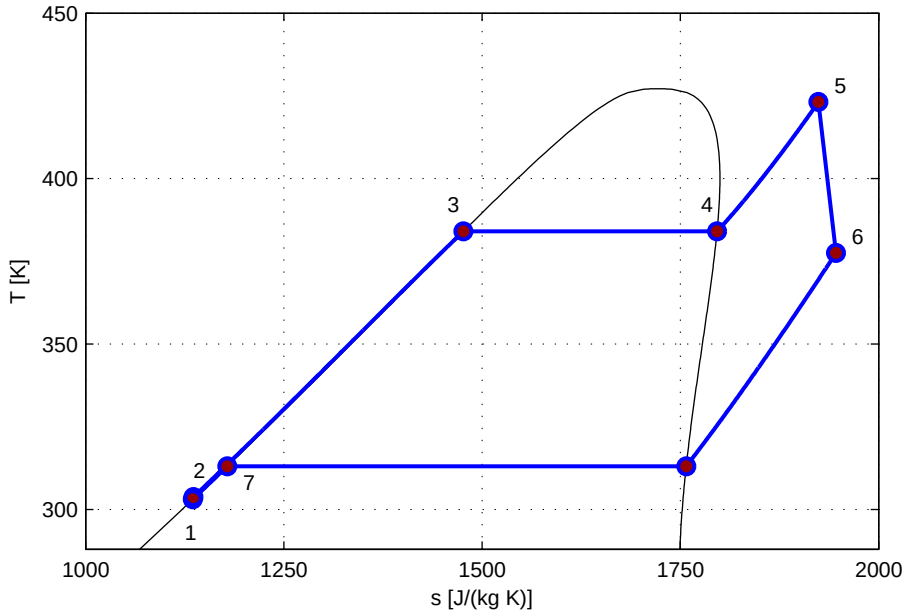

Fig. 3.2: A R245fa ORC on (T,s) diagram

down from point 6 to point 1, while the way these heat exchanges are conducted is decided after the Process Integration. Other than in the vapor generator, heat is required as an input for both the floor heating system and the hot water production, so these are the so-called cold streams, while the desuperheating - condensation - subcooling process is treated as a hot stream. In the Process Integration the hot utility is the heat source from outside the system, and in this case it is represented by the flue gases, while the cold utility is the external sink where the heat is rejected: an air condenser has been added to the system to carry out this task. Once the working fluid, the main thermodynamic parameters and the size of the power cycle have been fixed, the Process Integration is performed using a MATLAB® platform called OSMOSE (developed at the Laboratoire d'Energétique Industrielle - LENI, École Polytechnique Fédérale de Lausanne - EPFL, Switzerland), with the aim to minimize the use of both the hot and the cold utility, i.e. to minimize the biomass consumption and the heat rejected towards ambient respectively, and therefore to find the best stream configuration for the given system parameters. In these calculations it has been assumed that, when a partial load is required from the boiler, a reduced biomass flow rate is burned, keeping unchanged the combustion air-to-fuel ratio: for this reason, on first approximation the flue gases chemical composition and their cooling profile, reported in Fig. 3.1, are supposed to be invariant. Besides, it has been hypothesized that the ORC system can operate at partial load with the reduction of the working fluid flow rate (obtained by the pump running at lower speeds), but keeping

the same optimal values for the working pressures and temperatures. Such a decrease in the flow rate will result in a slowing down of the expander-generator machine, since the rotational speed of the latter is assumed to be free: on first approximation, finally, the overall efficiency of the expansion device is supposed to be constant with the speed.

The performances of the micro-cogenerator have been evaluated with two different indexes. The first one is the energy (or first law) efficiency η_I, defined by Eq. 3.1:

$$\eta_I = \frac{\dot{Q}_{hs} + \dot{Q}_{hw} + P_{exp} - P_{pmp}}{\dot{m}_{bm} LHV_{bm}} \tag{3.1}$$

where $\dot{Q}_{hs}$ is the heat required by the floor heating system, $\dot{Q}_{hw}$ is the thermal power needed for the hot water production, P_{exp} is the mechanical power delivered by the expander, P_{pmp} is the power absorbed by the pump, $\dot{m}_{bm}$ is the biomass flow rate and LHV_{bm} is the biomass lower heating value.

The second index adopted in the present analysis is the exergy efficiency η_{II}, defined by Eq. 3.2:

$$\eta_{II} = \frac{\dot{m}_{hs}(b_{hs,out} - b_{hs,in}) + \dot{m}_{hw}(b_{hw,out} - b_{hw,in}) + P_{exp} - P_{pmp}}{\dot{m}_{bm} \varepsilon_{ch,bm}} \tag{3.2}$$

where $\dot{m}_{hs}$ is the water flow rate in the heating system, $\dot{m}_{hw}$ is the produced flow rate of hot water and b is a state function called specific availability [99, 100], which allows to take into account the quality of the heat entering and exiting from the system, with respect to its temperature, and which is defined by Eq. 3.3:

$$b = h - T_{amb} s \tag{3.3}$$

where all the properties (specific availability, b, specific enthalpy, h and specific entropy, s) are referred to the considered thermodynamic state, while T_{amb} is the ambient temperature (here assumed equal to 298 K). In Eq. 3.2, in particular, $b_{hs,in}$ and $b_{hs,out}$ are the specific availability values of the heating system water at the heat exchanger inlet and outlet, respectively, $b_{hw,in}$ is the specific availability of fresh water and $b_{hw,out}$ is the specific availability of the produced hot water.

It can be noted that while in the definition of η_I all the product streams of the cogenerator (heat and power) are treated in the same way, in η_{II} the mechanical power is weighted more than the heat flow rates: this is particularly important in the performances evaluation of a combined production of power and heat at low temperatures, since the quality of the energy content of the latter is very poor if compared with the first one.

For every possible working scenario (both of hot water and heating required, only one of the two systems active, only electric power needed), several multi-objective optimizations (with different working fluids) have been conducted, in order to find the best suited cycle in each situation. The variables of the optimization are five: the expander inlet

temperature, the evaporation pressure, the condensing pressure, the degree of subcooling of the fluid at condenser outlet and the size of the cycle, i.e. the delivered mechanical power. The chosen objectives are three. First of all, the maximization of the energy efficiency η_I, defined by Eq. 3.1; the second of them is the maximization of the exergy efficiency η_{II}, defined by Eq. 3.2; finally, the third one is the minimization of the vaporization pressure of the cycle. This last task has been introduced due to technical and safety issues, since the studied micro-cogenerator has been supposed to have a domestic utilization.

3.5 Fluid screening

The aim of the first set of simulations was to compare the cogenerator performances with different working fluids; in particular, 13 substances have been considered: R245fa, R134a, isobutane, R143a, isopentane, ammonia, R407c, R125, R227ea, R404a, R507a, R1234yf and R1234ze. In each case, an optimization has been conducted in the hypothesis of full power required from both the heating system and the hot water production: since the energy efficiency is independent from the fluid and from the other cycle parameters (and equal to $\eta_I = 1.097$ when both the heat systems are activated), a set of Pareto curves on a plane with the vaporization pressure, p_{evap} on the horizontal axis and the exergy efficiency, η_{II} on the vertical axis has been considered to compare the fluids and is reported in Fig. 3.3. The optimization algorithm does not eliminate systematically all the points that are not near the Pareto front. Nevertheless, those points are clearly not optimal solutions and as such can be ignored.

As it can be seen from Fig. 3.3, the exergy efficiency η_{II} increases with the evaporation pressure, but the slope of the curves decreases at higher pressures, so for each fluid there is an optimal evaporation pressure. In Fig. 3.4, a histogram with the achievable exergy efficiency and the corresponding optimal evaporation pressure is reported.

From both Figs. 3.3 and 3.4 it can be noted that six fluids allow to reach an exergy efficiency higher than $\eta_{II} = 0.15$, but for three of these (R143a, ammonia and R227ea) the evaporation pressure p_{evap} has to be very high. Vice versa, a cycle running with R245fa and isopentane reaches reasonably good performances at an evaporation pressure of about 20 bar. Finally, using isobutane the performances are so good that a high exergy efficiency could be achieved even if the pressure is maintained low, far from the curve flattening. These values of exergy efficiency have to be compared with the one of a high efficiency condensing gas boiler, which is around 0.11.

For these reasons, further calculations have been conduced considering only R245fa, isopentane and isobutane as working fluids, with a maximum allowed evaporation pressure of 20 bar. Since the flue from biomass combustion is available at high temperatures, the only limitation in the cycle maximum temperature is represented by the chemical stability of the fluids, so the expander inlet temperature is fixed to $T_{exp,in} = 440\,\mathrm{K}$ for R245fa, $T_{exp,in} = 500\,\mathrm{K}$ for isopentane and $T_{exp,in} = 575\,\mathrm{K}$ for isobutane respectively.

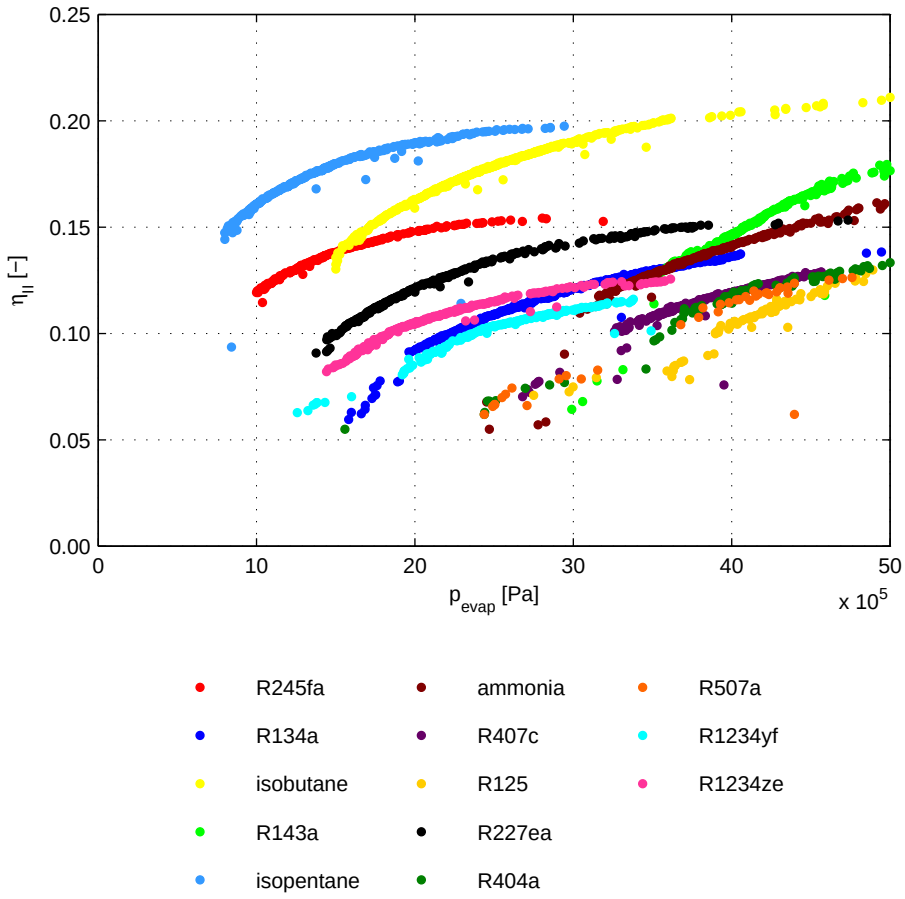

Fig. 3.3: Pareto curves for different working fluids

3.6 Overall performances calculation

The working parameters of the micro-cogenerator have been optimized, for each selected fluid (R245fa, isopentane and isobutane), in 4 different working scenarios: heat produced for both floor heating system and hot water production (1), for only one of the two systems (2 and 3) and produced heat totally rejected to air condenser (4). The working periods of the systems are reported in Tab. 3.1 for each month. In this analysis, the condensation pressure, the subcooling degree and the ratio between the mechanical power and the heat produced by the cogenerator are the variables, while the exergy efficiency η_{II} is the objective of the maximization. Note that in scenario (4) the power-to-heat ratio has no meaning, so the cycle is sized to deliver the same mechanical power

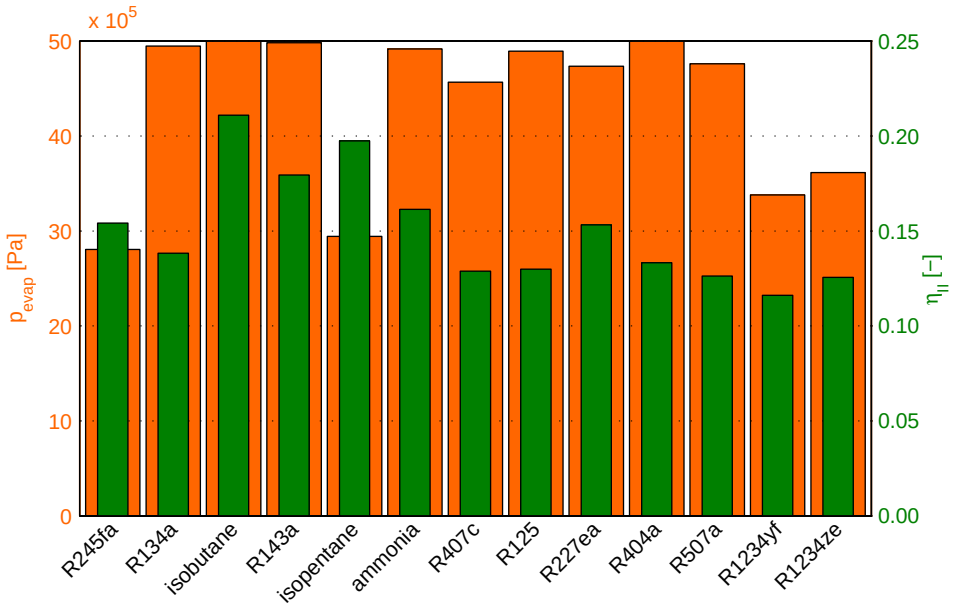

Fig. 3.4: Optimal evaporation pressure and exergy efficiency for different fluids

of scenario (1). In Tab. 3.3 the main working parameters of the optimized cycles are reported for each scenario and each selected fluid.

Every month the micro-cogenerator has to produce thermal power for heating and hot water production purposes for a certain number of hours, so the system can be run in the thermal following operating strategy: in this way, a quote of electricity demand of the house can be produced by the ORC system without rejecting any heat towards ambient. It has to be noted that electric energy is not produced when it is required by the users, so a grid-connection is needed: if this is not possible (but an energy storage system is available), the micro-cogenerator can be run in dissipation mode (using an air condenser) for a certain number of hours, in order to cover all the electricity demand. The summary of the calculations on electric energy production and biomass consumption is reported in Tabs. 3.4, 3.5 and 3.6, for systems using R245fa, isopentane and isobutane respectively.

When heat is needed, the concurrent electricity production is very convenient, since only a little additional amount of biomass is burned in the cogenerator, and almost all the extra energy introduced in the system is converted into mechanical work: in fact the condensation heat is not rejected towards ambient but exploited to warm up the water.

Tab. 3.3: Optimized cycles

Fluid	Floor heating system	Hot water production system	Evaporation to condensation pressure ratio	Total thermal power	Power to heat ratio	Net mechanical power	Working fluid flow rate	Energy efficiency (η_I)	Exergy efficiency (η_{II})
			[-]	[W]	[-]	[W]	[kg/s]	[-]	[-]
R245fa	ON	ON	5.636	33 278	0.118	3923	0.166	1.097	0.149
R245fa	ON	OFF	6.580	4012	0.133	533	0.020	1.056	0.165
R245fa	OFF	ON	5.636	29 266	0.118	3450	0.146	1.097	0.147
R245fa	OFF	OFF	7.251	0	-	3923	0.144	0.128	0.110
Isopentane	ON	ON	9.450	33 278	0.180	6000	0.088	1.097	0.191
Isopentane	ON	OFF	10.966	4012	0.200	803	0.011	1.056	0.207
Isopentane	OFF	ON	9.450	29 266	0.180	5277	0.078	1.097	0.189
Isopentane	OFF	OFF	12.039	0	-	6000	0.079	0.180	0.155
Isobutane	ON	ON	2.849	33 278	0.139	4633	0.096	1.097	0.164
Isobutane	ON	OFF	3.226	4012	0.160	643	0.012	1.056	0.182
Isobutane	OFF	ON	2.849	29 266	0.139	4074	0.084	1.097	0.162
Isobutane	OFF	OFF	3.487	0	-	4633	0.080	0.152	0.131

Tab. 3.4: Electric production and biomass consumption (fluid: R245fa)

Month	Electric consumption	Electric energy produced when all systems are active	Electric energy produced when only the floor heating system is active	Electric energy produced when only the hot water system is active	Total electric production	Electric demand covered by the the μ-CHP (NOT used in dissipation mode)	Biomass consumed by the μ-CHP (NOT used in dissipation mode)	Dissipation mode time needed to cover the entire electric demand	Biomass consumed by the μ-CHP (when used in dissipation mode)
	[kWh]	[kWh]	[kWh]	[kWh]	[kWh]	[%]	[kg]	[h]	[kg]
Jan	589	61	223	0	284	48.18	584	78	597
Feb	532	55	164	0	219	41.17	452	80	613
Mar	589	61	140	0	201	34.16	416	99	759
Apr	570	59	72	0	131	22.94	273	112	860
May	589	0	0	53	53	9.08	116	137	1048
Jun	570	0	0	52	52	9.08	112	132	1014
Jul	589	0	0	53	53	9.08	116	137	1048
Aug	589	0	0	53	53	9.08	116	137	1048
Sep	570	59	48	0	107	18.74	225	118	907
Oct	589	61	124	0	185	31.36	383	103	791
Nov	570	59	200	0	259	45.38	532	79	609
Dec	589	61	223	0	284	48.18	584	78	597
Year	6935	475	1194	212	1881	27.12	3908	1288	9892

Tab. 3.5: Electric production and biomass consumption (fluid: isopentane)

Month	Electric consumption	Electric energy produced when all systems are active	Electric energy produced when only the floor heating system is active	Electric energy produced when only the hot water system is active	Total electric production	Electric demand covered by the μ-CHP (NOT used in dissipation mode)	Biomass consumed by the μ-CHP (NOT used in dissipation mode)	Dissipation mode time needed to cover the entire electric demand	Biomass consumed by the μ-CHP (when used in dissipation mode)
	[kWh]	[kWh]	[kWh]	[kWh]	[kWh]	[%]	[kg]	[h]	[kg]
Jan	589	93	336	0	429	72.84	618	27	223
Feb	532	84	247	0	331	62.27	478	33	280
Mar	589	93	212	0	305	51.71	441	47	397
Apr	570	90	108	0	198	34.81	289	62	518
May	589	0	0	82	82	13.89	122	85	707
Jun	570	0	0	79	79	13.89	118	82	685
Jul	589	0	0	82	82	13.89	122	85	707
Aug	589	0	0	82	82	13.89	122	85	707
Sep	570	90	72	0	162	28.47	238	68	569
Oct	589	93	187	0	280	47.48	405	52	431
Nov	570	90	301	0	391	68.61	564	30	250
Dec	589	93	336	0	429	72.84	618	27	223
Year	6935	726	1799	325	2850	41.09	4135	681	5698

Tab. 3.6: Electric production and biomass consumption (fluid: isobutane)

Month	Electric consumption [kWh]	Electric energy produced when all systems are active [kWh]	Electric energy produced when only the floor heating system is active [kWh]	Electric energy produced when only the hot water system is active [kWh]	Total electric production [kWh]	Electric demand covered by the the μ-CHP (NOT used in dissipation mode) [%]	Biomass consumed by the μ-CHP (NOT used in dissipation mode) [kg]	Dissipation mode time needed to cover the entire electric demand [h]	Biomass consumed by the μ-CHP (when used in dissipation mode) [kg]
Jan	589	72	269	0	341	57.90	597	54	409
Feb	532	65	198	0	263	49.43	462	58	444
Mar	589	72	169	0	241	40.97	426	75	574
Apr	570	69	87	0	156	27.43	279	89	683
May	589	0	0	63	63	10.72	118	113	868
Jun	570	0	0	61	61	10.72	114	110	840
Jul	589	0	0	63	63	10.72	118	113	868
Aug	589	0	0	63	63	10.72	118	113	868
Sep	570	69	58	0	127	22.35	230	96	731
Oct	589	72	150	0	221	37.58	391	79	607
Nov	570	69	241	0	311	54.51	545	56	428
Dec	589	72	269	0	341	57.90	597	54	409
Year	6935	561	1442	251	2253	32.48	3995	1011	7731

If the cogenerator is used only when the condensation heat can be recovered, a quote of the annual electricity demand can be covered: as reported in Tabs. 3.4, 3.5 and 3.6, the calculations revealed that this percentage is equal to 27.1% in case of R245fa as working fluid, 41.1% for isopentane and 32.5% for isobutane.

In special cases, e.g. when the house is isolated from the grid, it can be interesting to cover all the electricity demand with the cogenerator, even if the system operates with a very low efficiency when heat is dissipated. In any case, it must be noted that the process can be considered fully-renewable, since the boiler is fed only with biomass. The calculations showed that the system burns more or less 4 t of biomass in a year when used only in cogeneration mode, for each of the three considered working fluids. The additional needs to complete the electricity demand coverage are around 10 t of biomass for a R245fa system, 6 t in the case of isopentane and 8 t for isobutane. The complete monthly-based analysis of these demands is reported in Tabs. 3.4, 3.5 and 3.6.

3.7 Final remarks and fluid selection

The work described in this Chapter allowed to find R245fa, isopentane and isobutane as the best working fluids for domestic ORC applications, considering the system maximum pressure, which is a cost and safety issue. In particular, the best results are achieved by an isopentane cycle system. Nevertheless, the slightly worse performances of a R245fa-based cogenerator are counterbalanced by the possibility to work satisfactorily at lower temperatures of the heat source, by its null ODP and by its very low toxicity levels. For these reasons, the choice of R245fa as working fluid for a small scale ORC system, reported in several works in literature, is confirmed here, and this substance has been selected for all the experimental facilities realized within this project and described in Chapter 5. However, the numerical analysis conducted in parallel to the field tests and reported in Chapter 4 considered, in some cases, even isopentane as working fluid, in particular for the applications linked to higher temperature thermal sources.

4 Numerical models

This Chapter reports the descriptions of the numerical models realized in the framework of the research on small scale ORC cogenerators, with the aim of simulating and predicting the behavior of the system and of its main components. In particular, in the first part the models of two different possible expanders (scroll in Section 4.1 and piston-type in Section 4.2) are illustrated, while the different simulation tools used to describe the behavior of the whole system are reported in Section 4.3

4.1 Scroll machine

As already reported in Section 2.4, an expander for ORC applications can be derived, without major revisions, from a commercial scroll compressor. For this reason, a numerical model has been implemented, aimed to the prediction of the performances of a scroll expander as well as of the scroll compressor from which it derives. The simulation code has been calibrated and checked comparing its results with measurements on a commercial hermetic scroll compressor, fed for simplicity with atmospheric air.

4.1.1 Description of the machine

The scroll is a positive displacement machine essentially formed by two identical spiral-shaped wraps fixed on back plates, as illustrated in Fig. 4.1. One wrap has a hole in the back plate and is held fixed, while the other can orbit. In compression mode, the working fluid enters the suction chambers through openings at the external endings of the wraps and exits from the central chamber through the fixed back-plate hole. If the machine is used as an expander, the working fluid moves from the central chamber towards the external ones and the orbiting wrap changes its rotation wise.

The major difference between the ideal behavior of a scroll machine and the real one is leakage: a certain quantity of working fluid flows from high-pressure chambers to low-pressure ones through gaps between the scroll wraps. There are two different kinds of leakage: the radial one has the path formed by a gap between a back-plate and a scroll, while the tangential (or flank) leakage has the path formed by a gap between the

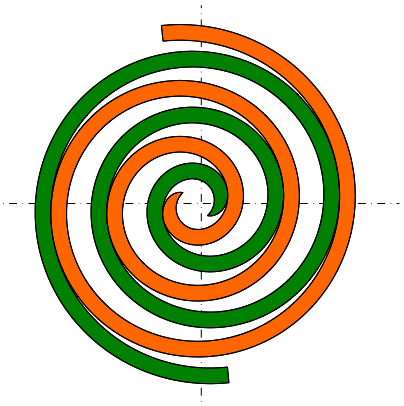

Fig. 4.1: Schematic view of a scroll machine

flanks of the two scrolls. The main consequence of leakage is a significant degradation of volumetric efficiency, defined by Eq. 4.1:

$$\eta_{vol} = \frac{\dot{m}_{wf}}{\rho V_{displ} n} \tag{4.1}$$

where $\dot{m}_{wf}$ is the mass flow rate of the working fluid, V_{displ} is the machine displacement, n is its shaft speed and ρ is the fluid density, always referred to the conditions at the machine inlet. Moreover, leakage raises the requested compression work (or reduces the delivered work, if in the case of an expander).

Another important difference between an ideal and a real scroll machine is the heat exchange involving the working fluid, leading to non-adiabatic processes.

4.1.2 Description of the model

There is a relatively abundant literature on scroll machine simulation models, which are classifiable in two main categories. Semi-empirical models, as the one proposed by Lemort et al. [78] for expanders or by Winandy et al. [101] for compressors, are made up by a limited number of equations, whose parameters are identified with the minimization of the errors between the model outputs and the results of laboratory measurements [102].

Vice versa, deterministic models are constituted by a larger series of equations, in order to describe exactly the geometry of the machine and all the actual phenomena taking place inside. While the first type of models requires shorter simulation times but needs the availability of experimental data, the second ones allow a more detailed

knowledge of how the machine works and can be used as design tools, so a deterministic model has been chosen for this project and is presented here. In Halm [103] and in Chen et al. [104, 105] there are detailed descriptions of a compressor model: starting from these works and referring also to Wang et al. [106], a new numerical code has been developed, applicable not only to compressors but also to expanders. For simplicity, this Subsection refers to the compressor case.

4.1.2.1 Volume of the chambers

The most diffused shape of the scrolls is an involute of a circle. Every wrap is defined by two involutes which develop from the same basic circumference and which are spaced by a constant distance, the wrap thickness, as shown in Fig. 4.2. The inner portion is usually defined by the cutter used to machine the scroll: here a circular arc connecting two involutes is assumed, as shown in Fig. 4.3. In these figures φ represents the generic involute angle, which defines the coordinates of each point of the inner and the outer profiles ((x_i, y_i) and (x_o, y_o) respectively), α_i and α_o are the starting position angles of the inner and the outer involutes, r_b is the radius of the basic circumference, r_c is the radius of the circular arc forming the inner portion of the scrolls and, finally, φ_{is} and φ_{os} are the initial angles of the inner and the outer spirals respectively. This accurate definition of geometry allows to calculate exactly the volume of all the machine chambers, at every orbiting angle, as the product of the scroll height and the area enclosed by the scrolls between two consecutive angles of wrap contact. These equations are only reported here, while they are derived and fully described in Halm [103] and in Chen et al. [104].

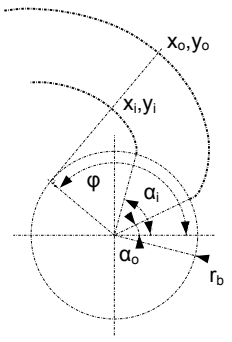

Fig. 4.2: Scroll general geometry

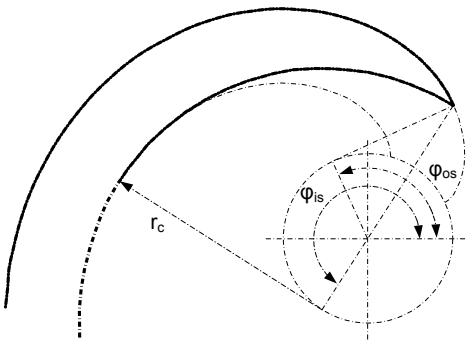

Fig. 4.3: Scroll internal geometry

In particular, the suction volume is expressed by Eq. 4.2 as a function of the shaft angle θ:

$$V_s(\theta) = \frac{1}{2} h_s r_b r_o \Big[2\varphi_e \theta - \theta^2 - \theta\left(\alpha_i + \alpha_o + \pi\right) + 2\left(1 - \cos\theta\right) - 2\left(\varphi_e - \pi\right)\sin\theta - \frac{\alpha_i + \alpha_o}{2}\sin\left(2\theta\right) \Big] \tag{4.2}$$

where the not previously defined symbols are h_s, the height of the chambers, r_o, the radius of the orbiting circular path and φ_e, the ending angle of the involutes.

Compression chambers are organized in K_{max} couples, where K_{max} depends on the wraps length. While the outer levels (until $K_{max}-1$) exist for the whole working cycle, the K_{max}-th one opens to discharge region at a defined orbiting angle θ_d. The volume of a K-th level compression chamber is defined in Eq. 4.3:

$$V_{c,K}(\theta) = \pi h_s r_b r_o \{2\varphi_e - 2\theta - [\alpha_i + \alpha_o + (4K-1)\,\pi]\} \tag{4.3}$$

The discharge region is formed by three different chambers: the lateral ones V_d (these were compression chambers before θ_d), and the inner zone V_{dd}, directly connected to the discharge hole. This volume reaches his minimum at θ_d: in this case it is called clearance volume V_{cl}. The discharge process begins at θ_d, when the two K_{max}-th level chambers open to discharge region. Initially, the gap between scrolls is too small to permit pressure equalization, so the three chambers have to be treated separately. When the pressure equalization is reached, a unique discharge zone V_{d-dd} must be considered. V_{cl} is defined by Eq. 4.4:

$$V_{cl} = h_s {r_c}^2 \left[\pi - \arcsin\left(2\,\frac{r_b}{r_c}\right) - 2\,\frac{r_b}{r_c}\right] \tag{4.4}$$

while V_{d-dd} is expressed by Eq. 4.5:

$$V_{d-dd}(\theta) = h_s r_b r_o \left[{\varphi_K}^2 - (\varphi_{os}+\pi)^2 - (\pi + \alpha_i + \alpha_o)\,(\varphi_K - \varphi_{os} - \pi)\right] + V_{cl} \tag{4.5}$$

where φ_K, the involute angle of the innermost contact point between scrolls, is defined by Eq. 4.6:

$$\varphi_K = \begin{cases} \varphi_e - 2\pi K_{max} - \theta, & \text{for } \theta \le \theta_d, \\ \varphi_e - 2\pi\,(K_{max}-1) - \theta, & \text{for } \theta_d < \theta \le 2\pi. \end{cases} \tag{4.6}$$

Eq. 4.7 is the expression of the volume of the inner discharge zone V_{dd}:

$$V_{dd}(\theta) = h_s r_c\,[r_c\beta - (r_c - w_{d-dd})\sin\beta] \tag{4.7}$$

where β is a coefficient introduced for practical purposes and defined by Eq. 4.8:

$$\beta(\theta) = \pi - \arccos\left[\frac{r_c - r_o + r_o\cos(\theta-\theta_d)}{r_c - w_{d-dd}}\right] - \arcsin\left(2\,\frac{r_b}{r_c}\right) \tag{4.8}$$

and w_{d-dd} is the width of the opening between the discharge regions, expressed by Eq. 4.9:

$$w_{d-dd}(\theta) = r_c - \sqrt{{r_o}^2 + (r_c - r_o)^2 + 2\,r_o\,(r_c - r_o)\cos(\theta - \theta_d)} \tag{4.9}$$

Finally, the volume of lateral discharge chambers is defined by Eq. 4.10:

$$V_d(\theta) = \frac{1}{2}\,[V_{d-dd}(\theta) - V_{dd}(\theta)] \tag{4.10}$$

4.1.2.2 Suction and discharge sections

The flow area through the openings at external endings of wraps can be simply expressed by Eq. 4.11:

$$A_{suct}(\theta) = h_s r_o (1 - \cos\theta) \tag{4.11}$$

The discharge ports are represented by the openings between scrolls in the inner portion of the wraps. Their flow area is described by Eq. 4.12:

$$A_{d-dd}(\theta) = w_{d-dd} h_s \tag{4.12}$$

where w_{d-dd} is defined by Eq. 4.9. The flow rates of all porting processes are calculated using the isentropic flow equation for a compressible gas.

4.1.2.3 Thermodynamic process

The core of the model is represented by Eqs. 4.13 and 4.14, which represent the energy and the mass balances respectively, applied to each chamber, within the hypothesis of uniform thermodynamic properties in each volume:

$$\frac{dT}{d\theta} = \frac{1}{mc_v}\left\{\frac{\dot{Q}}{\omega} + \sum \frac{\dot{m}_{in}}{\omega}(h_{in} - h) - T\left(\frac{\partial p}{\partial T}\right)_v \left[\frac{dV}{d\theta} - \frac{v}{\omega}\left(\sum \dot{m}_{in} - \dot{m}_{out}\right)\right]\right\} \tag{4.13}$$

$$\frac{dm}{d\theta} = \sum \frac{\dot{m}_{in}}{\omega} - \sum \frac{\dot{m}_{out}}{\omega} \tag{4.14}$$

Eqs. 4.13 and 4.14 are derived in Halm [103] and in Chen et al. [104].

The simulation code requires a third equation to correlate the thermodynamic properties of the fluid. Air is modeled as a perfect gas, while the fundamental equations of state described by Lemmon and Span [107] are used for other real fluids such as R245fa, isopentane and toluene. The model is also equipped with correlations to calculate the needed values of fluid thermo-physical properties such as specific heat capacities, thermal conductivity and dynamic viscosity.

4.1.2.4 Internal leakage

A fixed value is assigned both to radial gap and to flank (or tangential) gap, so flow areas can be simply calculated considering wraps length and height. The flow model adopted for leakage is the isentropic one for a compressible gas through a constant area.

4.1.2.5 Heat transfer

The main problem in calculating heat flow rates in the machine is the choice of a suitable heat transfer coefficient, because no matching case in geometry and fluid motion can be found in literature. As suggested by Chen et al. [104], a correlation based on Dittus-Boelter equation, derived for a spiral plate heat exchanger [108], has been adopted. In this formula a hydraulic diameter is used, so the area enclosing each chamber at every orbiting angle has to be calculated. Moreover, the temperatures of the two wraps are needed to determine the heat fluxes involving working fluid in the scroll zone: the temperature is assumed to grow linearly along the scrolls, from outer end to inner zone. The mean value of this distribution is determined by summing up the intermediate temperature between suction and isentropic discharge conditions to a quantity increasing with shaft speed, defined according to experimental data. The total heat rate involving a fluid pocket in a chamber at a given orbiting angle can finally be calculated according to the method described by Halm [103]. Other than the heat transfers with the wraps, it is necessary to determine the fluid heating-up before it enters the scroll zone (this may be caused, for example, by the fluid passage in the motor zone in the case of hermetic compressor) and the cooling-down in the discharge volume after the compression end. These heat flow rates are calculated by a global energy balance of the compressor.

4.1.2.6 Discharge process

Although a scroll machine does not need valves, commercial compressors are often equipped with a check valve on the discharge duct, in order to prevent the fluid from going back after shut-off and therefore from causing backward rotations. This device has been modeled as a simply one-degree-of-freedom plate valve driven by a spring, so the flux area depends on the differential pressure between the central discharge chamber and the pipe. The isentropic flux theory is used to calculate also the mass flow rate through this valve.

4.1.3 Model validation

The performances of a hermetic commercial scroll compressor, whose main geometrical features are detailed in Tab. 4.1, have been measured in order to calibrate and validate the numerical code.

Tab. 4.1: Scroll compressor geometrical data

Displacement V_{displ} [cm^3]	34.31
Radius of the basic circumference r_b [mm]	2.1
Wrap thickness [mm]	3.7
Scroll height h_s [mm]	30.4
Starting angle of the outer involute α_o [°]	-80
Starting angle of the inner involute α_i [°]	-63
Ending angle of the involutes φ_e [°]	1086

4.1.3.1 Description of the tests

The tested machine was designed to operate at variable speed, by means of an inverter driven motor, in a refrigerating closed cycle with R410a as working fluid. However in this case the compressor has been used with air in an open cycle, in order to simplify the test bench. A digital thermal mass flow meter has been inserted in the suction tube, while a manual valve has been installed at the end of the exhaust pipe in order to control the discharge pressure. Thermocouples and a pressure transducers have been installed on both the suction and discharge pipes of the compressor. Finally, the inverter internal instrumentation has been used to measure the values of the needed electrical variables, i.e. the voltage, the current, the frequency and the absorbed power.

High temperatures were expected to be reached during the tests, since air has a lower heat capacity, in comparison with R410a, so the compressor oil had to be changed, with the selection of a lubricant more suitable to the new working fluid. Moreover, an oil separator has been installed at the compressor exit.

4.1.3.2 Detection of the gaps between scrolls

Since the compressor is a hermetic machine, the direct measurement of the gaps between wraps was impossible, so a preliminary set of numerical simulations has been conduced, in order to find the values of tangential and radial gaps that allow to reach the best matching between calculated and experimental volumetric efficiency. It was assumed that tangential gap δ_f depends on compressor speed, with the law reported in Fig. 4.4, since it is determined by the thickness of the oil film on the wraps, while radial gap depends on both compressor speed and pressure imposed in the discharge pipe. In fact the machine is equipped with a gasket seal on the top of the scrolls, which is kept in position by the difference of pressure between two contiguous chambers: so the sealing is more efficient when the machine works with a higher discharge pressure. The radial gap law utilized in the model is described by Eq. 4.15:

$$\delta_r = f(p_{discharge}/p_{suction})\,(1+\gamma_{speed}) \tag{4.15}$$

where γ_{speed} is a coefficient obtained by the interpolation of the data reported in Tab. 4.2 and the dependence from pressure ratio $p_{discharge}/p_{suction}$ is shown in Fig. 4.5 for the case in which the machine operates at 60 rev./s.

Tab. 4.2: Corrective factor for the radial gap size

n [rev./s]	γ_{speed} [-]
30	−0.460
60	0.000
90	0.675
120	2.000

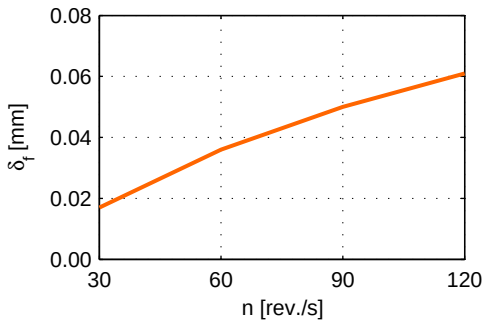

Fig. 4.4: Flank gap as a function of shaft speed

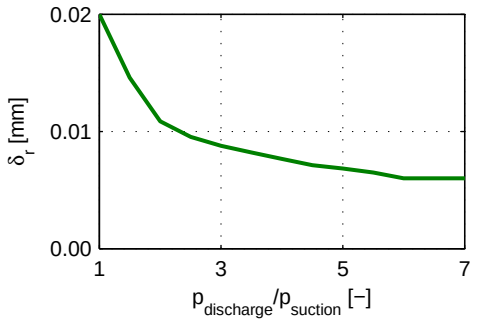

Fig. 4.5: Radial gap as a function of the compression ratio at 60 rev./s

After an analysis of Figs. 4.4 and 4.5, it can be concluded that the flank gap size is approximately 10 times greater than the radial one, since the latter is widely decreased by the seals; so the main leakage path in the tested machine is the tangential one. The values calculated for this gap, variable from 20 µm to 60 µm, are comparable with those found in literature [79, 103].

4.1.3.3 Comparison between numerical and experimental results

A first comparison between experimental and numerical data has been conducted considering the discharge mean temperature $T_{discharge}$ and the machine volumetric efficiency η_{vol}, defined by Eq. 4.1. The trends of these parameters are reported in Figs. 4.6 and 4.7 respectively, as functions of the discharge pressure at different various shaft speeds.

It can be seen that these trends are well predicted by the model, in particular at medium-to-high compression ratios (i.e. in the best working conditions for the machine): in this zone the maximum gaps between experimental and numerical data are lower than 5 K for $T_{discharge}$ and lower than 3 percentage points for η_{vol}. It is important to note that only few of the working points shown in Figs. 4.6 and 4.7 have been used to calibrate

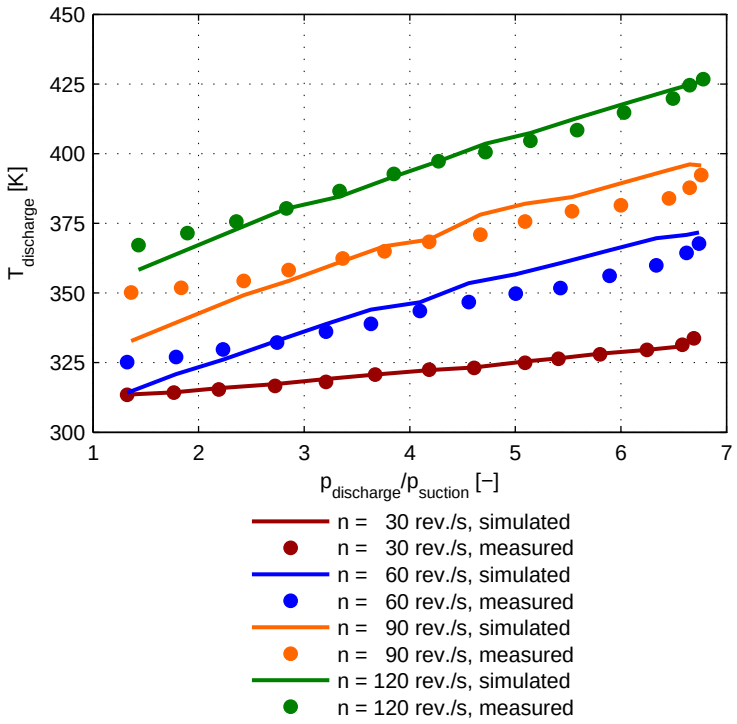

Fig. 4.6: Discharge mean temperature as a function of the compression ratio

the model, so the diagrams reveal an effective good agreement between experimental and numerical data. The values measured and calculated for the volumetric efficiency (always below 0.50) are very poor if compared with the best data found in literature (Cuevas et al. [102] reported values above 0.90 at every operating condition). This is realistically due to the fact that the compressor has been tested with a working fluid (air instead of refrigerant) and with a lubricating oil different from those it was designed to operate with.

The overall isentropic efficiency is defined by Eq. 4.16 as the ratio between the power needed to pressurize the fluid with an isentropic process and the shaft power absorbed by the device:

$$\eta_{is} = \frac{\dot{m}_{wf}(h_{dis,is} - h_{suction})}{\dot{Q} + \dot{W}_{loss} + \dot{W}_f} \tag{4.16}$$

The shaft power is calculated adding the net heat flow rate involving the fluid $\dot{Q}$ and a constant mechanical loss $\dot{W}_{loss}$ to the work rate of the fluid $\dot{W}_f$. The latter, as reported

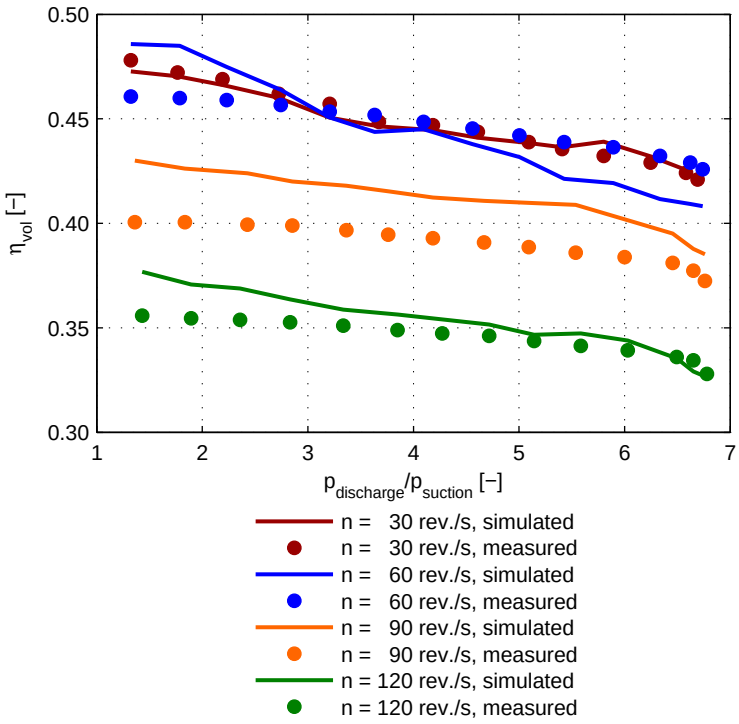

Fig. 4.7: Volumetric efficiency as a function of compression ratio

in Eq. 4.17, is the product of the actual mass flow rate $\dot{m}_{wf}$ and the sum of the fluid specific enthalpy variation in the scroll zone to the work made by the fluid during a quasi-isochoric expansion in the discharge chamber [101]:

$$\dot{W}_f = \dot{m}_{wf} \left[h_{scr,out} - h_{scr,in} + v_{scr,out}(p_{scr,out} - p_{discharge}) \right] \tag{4.17}$$

The mechanical losses are assumed to be invariant with respect to the discharge pressure and equal to a fixed fraction (0.10) of the power absorbed at the maximum compression ratio. This value has been fixed after a comparison between the results of a preliminary set of simulations and the experimental data. The overall isentropic efficiency predicted by the model has been reported in Fig. 4.8 as a function of the compression ratio, together with the values calculated starting from the data measured on the test bench. It can be seen that a maximum gap of 5 percentage points was found between experimental and numerical results. However, it must be noted that in Eq. 4.16 the electric motor losses are neglected: these are dependent on the compression

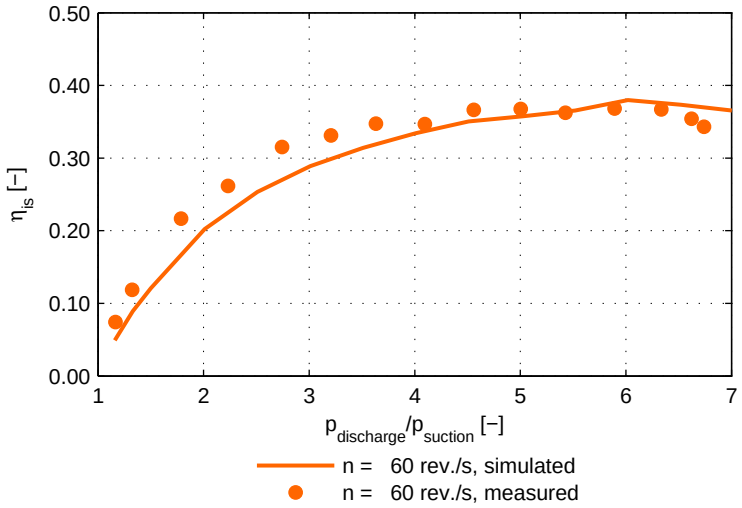

Fig. 4.8: Overall isentropic efficiency as a function of compression ratio at 60 rev./s

ratio, so they can affect significantly the trends shown in Fig. 4.8. Moreover, it must be considered that the isentropic efficiency expressed by Eq. 4.16 could be affected by the error introduced with the measurement of the discharge temperature in the pipe instead of directly in the discharge chamber, due to the difficulties connected with the opening of a hermetic machine.

4.1.4 Expander simulation results

Once the compressor model has been calibrated and verified, it has been adapted to predict the performances of the scroll machine working as an expander. All the code internal parameters were the same of the compressor case.

A first series of simulations has been conducted, considering R245fa as working fluid, in order to obtain the expander performances as functions of the expansion ratio imposed between inlet and discharge conditions. The overall isentropic efficiency is defined in this case as the ratio between the real power available at the shaft and the power obtained from an ideal isentropic expansion from supply to discharge pressure. In analogy to the compressor case, it is defined by Eqs. 4.18 and 4.19:

$$\eta_{is} = \frac{\dot{Q} - \dot{W}_{loss} + \dot{W}_f}{\dot{m}_{wf}(h_{inlet} - h_{dis,is})} \tag{4.18}$$

$$\dot{W}_f = \dot{m}_{wf}\left[h_{scr,in} - h_{scr,out} + v_{scr,out}(p_{scr,out} - p_{discharge})\right] \tag{4.19}$$

The submodels forming the code have been progressively de-activated in order to quantify the influence of the different phenomena involving the fluid on the expander efficiency, obtaining the series of curves shown in Fig. 4.9. The higher curve has been generated taking into account only the losses connected with an unadapted expansion ratio: it can be seen that a unity efficiency can be reached only if the machine built-in pressure ratio is imposed between inlet and discharge. Otherwise, for smaller expansion ratios the fluid is re-compressed at the discharge, while for higher ratios a part of the expansion is unexploited. Pressure evolutions with respect to the volume filled by the fluid for expansion ratios equal, lower or greater than the built-in one are shown in Figs. 4.10, 4.11 and 4.12 respectively. When heat transfers are considered (first only between the fluid and the wraps, then also with the inlet pipe and finally also from the machine towards ambient), the isentropic efficiency decreases: it can be noted that the most significant of these effects is related to ambient losses, so the scroll expander has to be thermally insulated in order to achieve better performances. Since the mechanical losses are approximately independent from the expansion ratio, they have a greater influence on the efficiency at lower ratios, when a lower work is extracted from the fluid. As last step, also the leakage model is activated in the code: this phenomenon causes a great reduction in the isentropic efficiency, as shown by the lowest curve in Fig. 4.9.

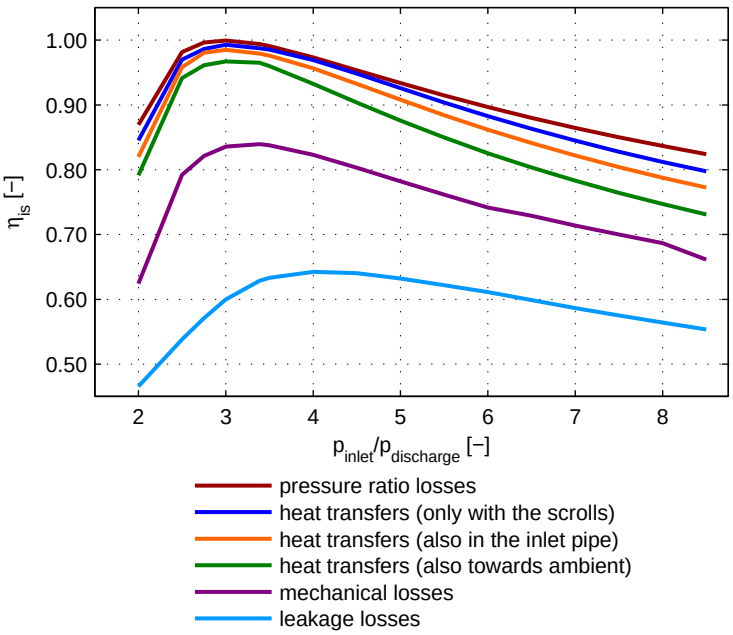

Fig. 4.9: Contribution of different phenomena on the expander overall isentropic efficiency

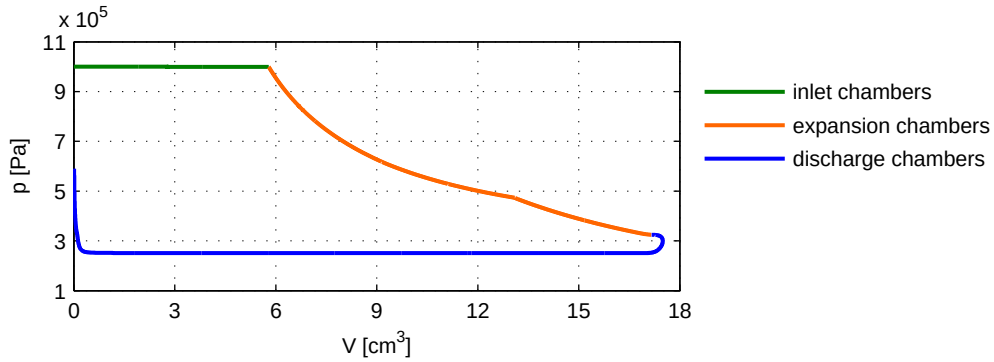

Fig. 4.10: Expansion on (p,V) diagram, pressure ratio equal to the built-in one

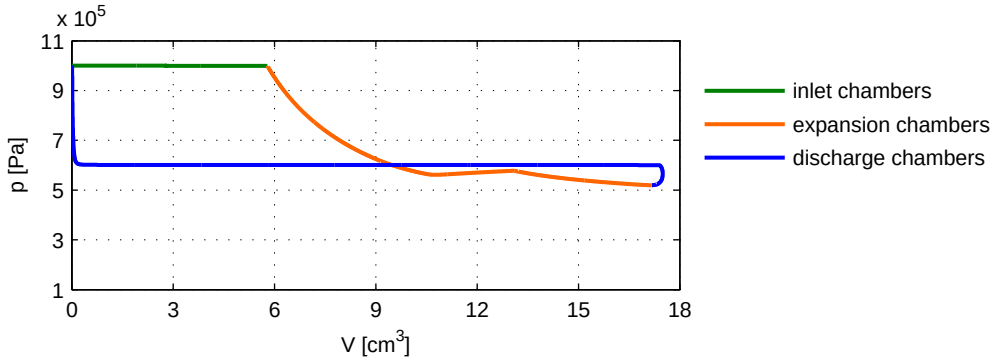

Fig. 4.11: Expansion on (p,V) diagram, pressure ratio lower than the built-in one

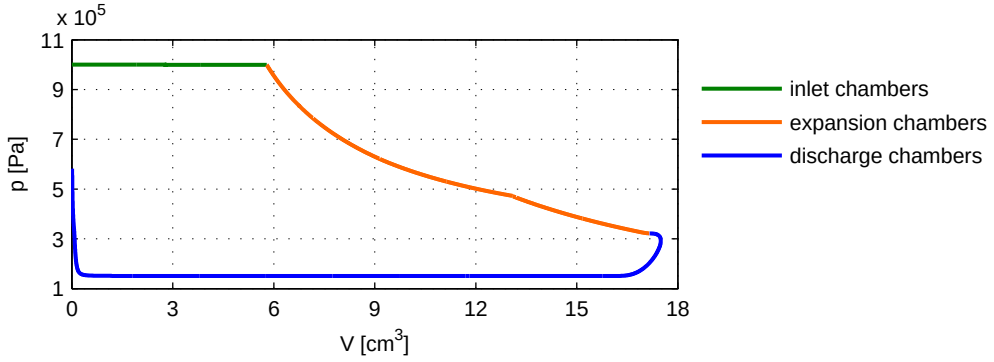

Fig. 4.12: Expansion on (p,V) diagram, pressure ratio higher than the built-in one

The maximum value reached with these simulations is about 0.65, comparable with the ones found in literature [73, 75, 78]. It is also interesting to note that the expansion ratio that ensures the best isentropic efficiency is greater than the one defined by the machine geometry (which leads the higher curve in Fig. 4.9 to reach a unity efficiency), as observed also by Lemort et al. [78].

The code can be used to compare the performances of a scroll expander with different working fluids: in particular, in this phase the substances taken into account have been R245fa, isopentane and air. In Fig. 4.13 a comparison in terms of isentropic efficiency has been carried out: the trends shown for R245fa and isopentane are quite similar, with the maximum reached for a pressure ratio slightly greater than the built-in one and with the best performances achieved with the first fluid. On the other hand, the behavior of the expander fed by air is very different, because of the different thermo-physical properties of this fluid.

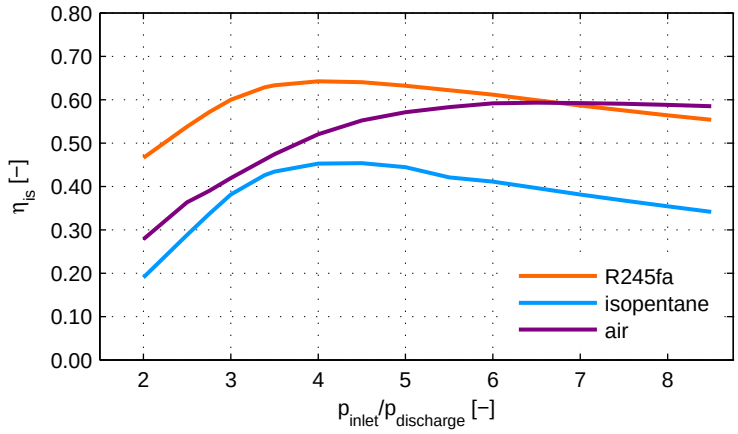

Fig. 4.13: Expander overall isentropic efficiency as a function of expansion ratio for three different fluids

The volumetric efficiency of the expander is defined by Eq. 4.1, already introduced for the compressor case. Since the main phenomenon affecting the volumetric performance of the machine is leakage, which consists in a flow through the gaps between scrolls from the inlet zone to the discharge chambers, the index defined by Eq. 4.1 assumes always values greater than unity for an expander (with better performances for lower values). The trends of the volumetric efficiency for the three fluids above mentioned are shown in Fig. 4.14. It can be seen that the performances achieved by R245fa and isopentane are quite similar, while the same machine fed by air is affected by larger leakage losses.

One of the best skills offered by a simulation code is the opportunity to determine the instantaneous conditions of the fluid evolving in the machine without placing a large

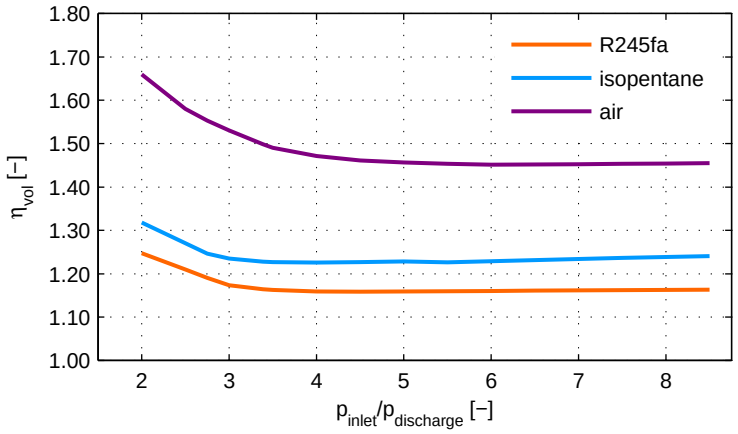

Fig. 4.14: Expander volumetric efficiency as a function of expansion ratio for three different fluids

number of sensors inside it: some trends of thermodynamic properties with respect to the orbiting angle have been obtained in order to test the effective prediction capacity of the model. As an example, the temperature assumed by R245fa inside the scroll machine, when the built-in pressure ratio is imposed, is reported in Fig. 4.15.

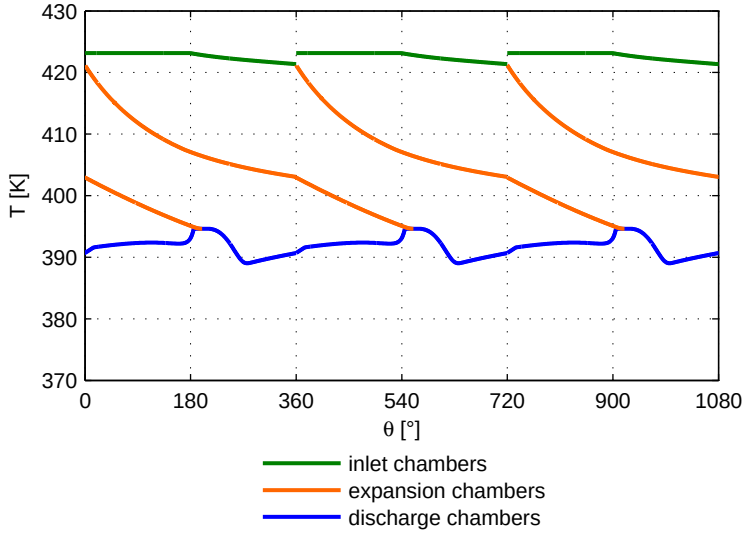

Fig. 4.15: Temperature assumed by R245fa during the expansion process

4.2 Piston-type expander

The utilization of a reciprocating machine as expander in an ORC system has been already cited in Section 2.4, where the simplicity and the wide diffusion have been underlined as the main advantages of this technology [81]. Since a comparison between the performances of piston-type and scroll expanders was required, in order to make possible the definitive choice for an ORC prototype which had to be realized, a reciprocating machine has been modeled following an approach similar to the one described in the previous Section 4.1.

4.2.1 Description of the model

Like in the case of scroll machine, a deterministic approach has been chosen: the model is composed by a large series of equations which describe exactly the geometry of the machine and all the actual phenomena which take place into it.

The ideal cycle of a single-stage single-acting reciprocating expander is reported on (p,V) diagram in Fig. 4.16: during the mechanical admission (phase 1→2), the inlet valve is open and the fluid at high pressure enters the cylinder as the piston moves towards the Bottom Dead Center (BDC); at a defined crank angle (point 2), often called cut-off, the inlet valve is closed and the isentropic expansion takes place (phase 2→3); when the piston reaches the BDC, the exhaust valve is opened and the fluid is thermodynamically discharged (phase 3→4); then the piston begins to move towards the Upper Dead Center (UDC) and drives the fluid out of the cylinder through the exhaust valve, during the mechanical discharge process (phase 4→5); finally, at the UDC the exhaust valve is closed and the inlet one is opened, so the thermodynamic admission takes place, in which the fluid instantaneously enters the expander chamber, until it reaches the upstream pressure (phase 5→1).

In the real machine, the isentropic transformations cannot take place and the real fluid cannot vary its pressure instantaneously, so the model has to describe the actual transformations of the fluid from its admission in the expander to its discharge. To describe the geometry of the expander and to define its volume with respect to the crank angle, some parameters have to be fixed. The shaft speed has been set to 1500 rpm, with the aim of maintaining a low value of the friction losses. Since the mass flow rate of the cycle is low, a quite small machine is required, so a mono-cylindrical architecture for the latter has been chosen.

As found in literature for steam piston expanders [82], the stroke has been considered equal to the bore: fixing the value to 60 mm, the displacement of the machine is 169 cm^3. The crank-to-rod ratio has been set to 0.2. The volumetric expansion ratio ε_v is one of the most important working parameters for a reciprocating expander, together with the cut-off ratio Φ [81–83], defined as the ratio between the cylinder volume at the moment in which the admission valve is closed (minus the dead volume) and the machine

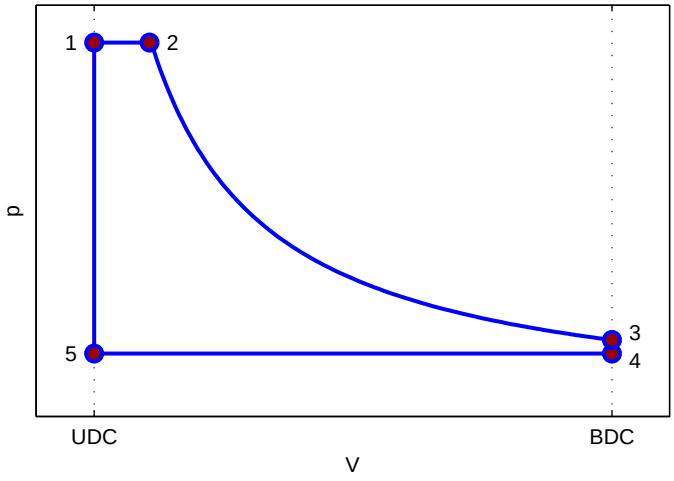

Fig. 4.16: Ideal cycle of a reciprocating expander

displacement, as indicated in Eq. 4.20:

$$\Phi = \frac{V_{cut-off} - V_{UDC}}{V_{displ}} \tag{4.20}$$

A small cut-off timing results in a smaller torque but also in a higher ideal cycle efficiency; vice versa, a high cut-off value causes a larger torque but also a lower ideal efficiency. To achieve a good trade-off, a value of Φ less than about 0.15 must be chosen [83]. Both volumetric expansion and cut-off ratios have been considered free design parameters as explained in the next Subsection 4.2.2.

The porting processes have a great influence on the functioning of the expander, so they are treated in detail by the model. The machine has been assumed to have only two poppet valves (one for admission and one for discharge), the latter being as large as possible, with respect to the cylinder diameter. Since at discharge the fluid specific volume is larger than at inlet, the outlet valve has to be larger than the other, in order to keep the same velocity for the two fluxes and to have similar pressure drops in the inlet and in the discharge ducts. In this first design of the machine, it has been assumed that the valves are driven by cams with constant-acceleration profiles and that the maximum valve lifts are as large as possible, with respect to the height of the dead space V_{UDC}. The instantaneous flux areas through the valves have been calculated as reported by Heywood in his work [109]. Finally, the timing for the opening and the closing of the valves has been set, according to literature [81], in order to make the real cycle as similar as possible to the ideal one, but avoiding the concurrent opening of the two valves.

The evolution of the fluid in the expander is modeled by the concurrent resolution of

the energy and mass balances, already introduced for the scroll case and expressed by Eqs. 4.13 and 4.14 respectively.

The heat transfer involving the fluid has been assumed to be equal to a fixed fraction (0.12) of the work-per-cycle [109]. In the same way, the fluid leakages through the piston rings have been considered equal to a fixed fraction (0.02) of the mass expanded per cycle [83]. Eqs. 4.13 and 4.14 have to be discretized and solved simultaneously. Moreover, an equation of state of the working fluid has to be implemented in order to correlate all the thermodynamic parameters: in the model, the equations described by Lemmon and Span [107] have been utilized.

The evolution of a real fluid (R245fa) in a machine with $\varepsilon_v = 5$ and $\Phi = 0.12$, as simulated by the code, is reported on (p,V) diagram in Fig. 4.17 with a green bold line, while the ideal cycle evolving between the same pressures is represented by the orange thin line. It can be seen that, setting the proper valve timing, the real cycle is quite similar to the ideal one, even if neither instantaneous nor isentropic transformations can take place.

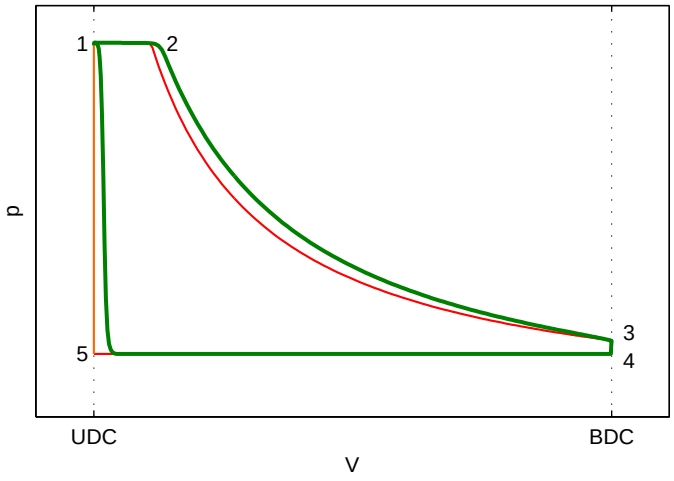

Fig. 4.17: Real cycle of a reciprocating expander

The model has been used to calculate the main working parameters of the expander, i.e. the net power output and the overall efficiency, as functions of the fluid conditions imposed upstream and of the pressure imposed downstream. To achieve these results, the mean specific enthalpy of the fluid discharged by the machine has been considered. The real enthalpy drop has finally been multiplied by the mechanical efficiency (a constant value equal to 0.88 has been set), in order to find the delivered specific work. The overall

efficiency is defined as the ratio between the latter and the enthalpy drop of an isentropic expansion from the actual inlet conditions to the imposed discharge pressure.

4.2.2 Design choices and expander performances

The main design choice is the selection of the operating fluid: for the simulations of the reciprocating expander, only R245fa and isopentane have been chosen.

The volumetric expansion ratio must be chosen according to the operating fluid and the ORC requirements, which depend on the fluid properties again and on the application constraints taken into account. Referring to the typical features needed from a heat recovery cycle, ε_v has been considered variable in a range from 5 to 7. As the volumetric expansion ratio rises, the optimal value of the cut-off ratio decreases slightly, and the gradient of the efficiency reduction when Φ leaves such optimal value becomes higher [81–83], therefore Φ has been considered a function of ε_v, with the aim of obtaining the best efficiency rather than improving the expansion work. The first sets of numerical results are presented in Figs. 4.18 and 4.19, where the expander efficiency and the net power are reported respectively as functions of the imposed cycle expansion ratio, ε_v, with R245fa as working fluid. Figs. 4.18 and 4.19 refer to a condensation temperature of 40 °C (corresponding to a discharge pressure of 2.518 bar), a superheating temperature of 150 °C and a shaft speed of 1500 rpm. It must be noted that that in the situations reported in the diagrams higher expansion ratios mean higher evaporating pressures and, for a given superheating temperature, also lower superheating degrees.

Three values of volumetric expansion ratio are considered (5, 6 and 7), these corresponding to optimal values of Φ equal to 0.12, 0.11 and 0.10 respectively. The related maximum efficiencies are always calculated equal or very near to 0.70, so this index can be considered practically constant with volumetric expansion ratio. These values are also comparable with the ones obtainable with other typologies of volumetric expanders, and in particular with scroll machines, as reported in the previous Section 4.1. If the imposed pressure ratio is lower than the optimal value (i.e. at the built-in volumetric ratio ε_v), the efficiency decreases rather quickly, while the slope of this trend at higher values of the pressure ratio, in a quite large range, is much lower. This asymmetry is due to the well known behavior of volumetric expanders of being more penalized by over expansion phenomena, occurring when the overall pressure ratio is lower than the built-in one and fluid is re-compressed at the discharge, than by under expansion phenomena implying that a part of the expansion is unexploited. The pressure evolutions with respect to the volume filled by the fluid for expansion ratios lower or greater than the built-in one are shown in Figs. 4.20 and 4.21 respectively, compared with the pressure evolutions in the built-in ratio case.

As observable in Fig. 4.19, the net power delivered by the expander decreases with ε_v, at a given pressure ratio. This is a combined effect of the different mass of operating fluid trapped in the cylinder at the UDC and of the previously discussed variation of the cut-off ratio Φ.

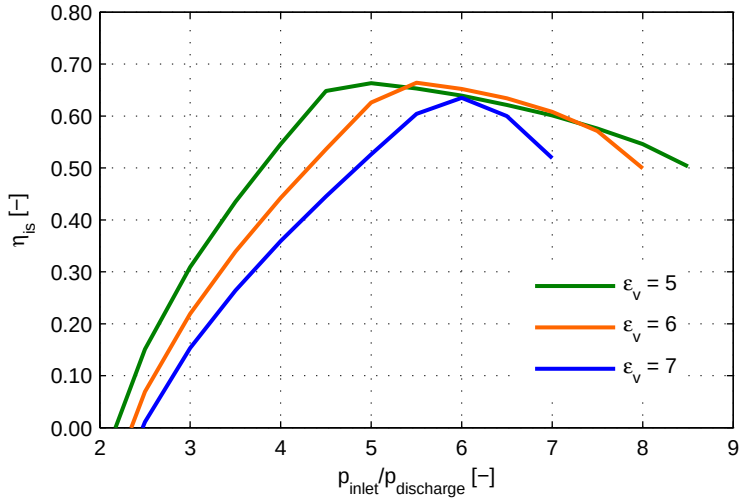

Fig. 4.18: Reciprocating expander efficiency at various ε_v - fluid: R245fa

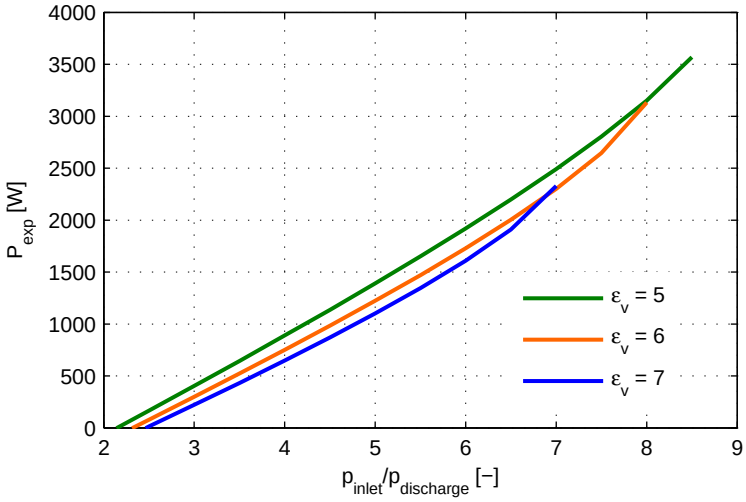

Fig. 4.19: Reciprocating expander net power at various ε_v - fluid: R245fa

With isopentane as working fluid the reciprocating expander exhibits the performances reported in Figs. 4.22 and 4.23, which show the trends of the efficiency and of the delivered power respectively and are derived under the hypotheses of condensation temperature equal to 40 °C (corresponding in this case to a discharge pressure of 1.515 bar), a superheating temperature of 200 °C and a shaft speed of 1500 rpm. In these

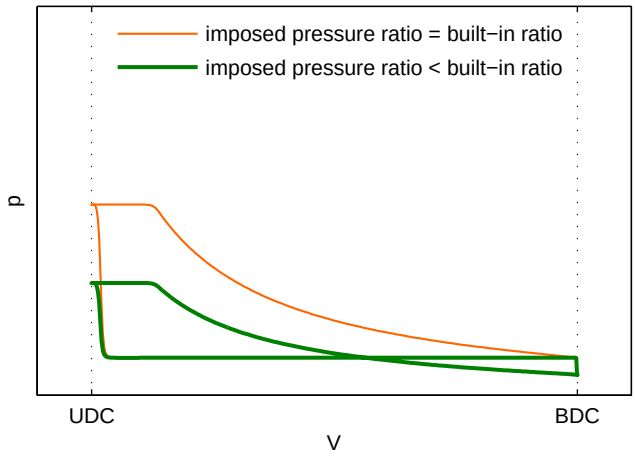

Fig. 4.20: Real cycle with the pressure ratio lower than the built-in one

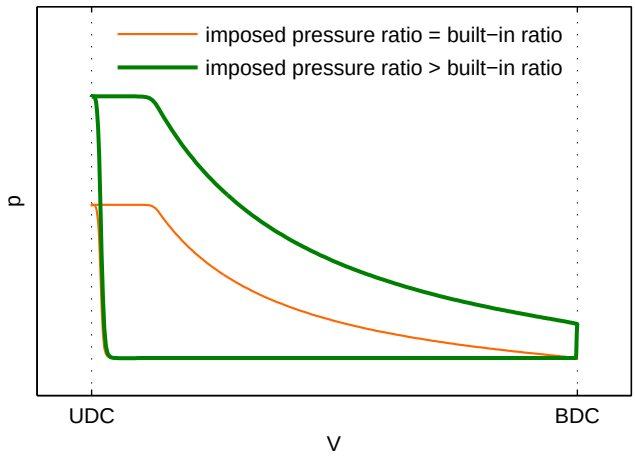

Fig. 4.21: Real cycle with the pressure ratio greater than the built-in one

conditions, the evaporation of isopentane occurs at a pressure and at a temperature always much lower than their critical values, also at the highest expansion ratios taken into account for the realization of these curves, so the variations in thermodynamic properties with both the imposed pressure ratio and the machine built-in volumetric ratio are more regular than in the case of R245fa. As a result, the maximum efficiency is reached with a cut-off ratio equal to 0.12 at all the considered values of ε_v and it increases with the

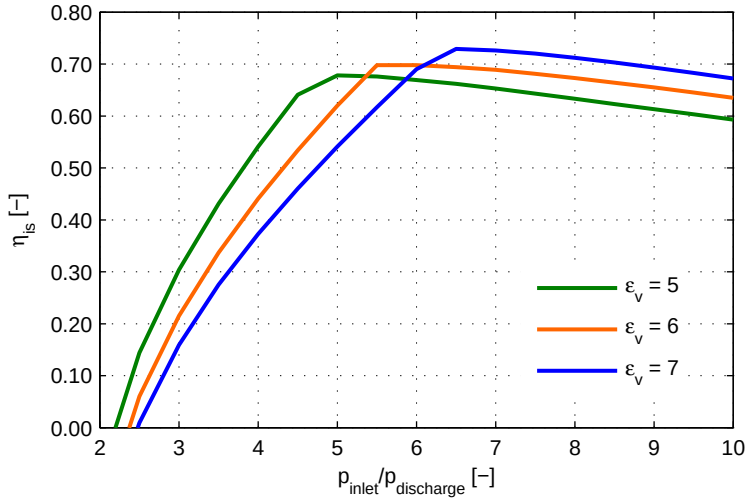

Fig. 4.22: Reciprocating expander efficiency at various ε_v - fluid: isopentane

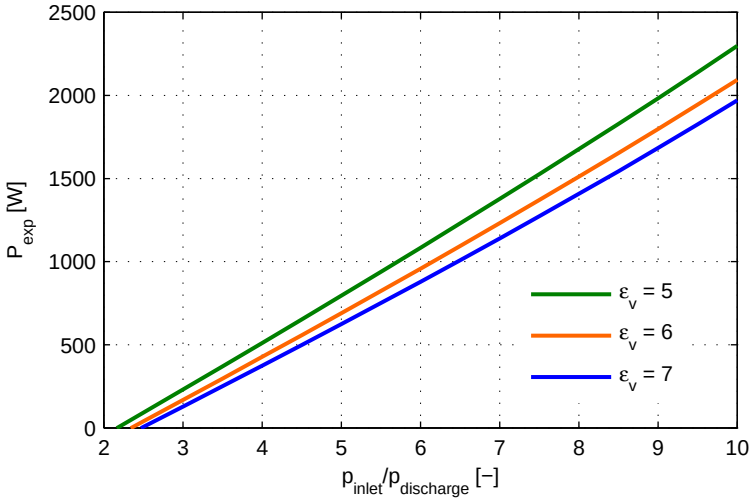

Fig. 4.23: Reciprocating expander net power at various ε_v - fluid: isopentane

volumetric expansion ratio from 0.72 for $\varepsilon_v = 5$ to 0.77 for $\varepsilon_v = 7$. Values higher than 0.60 can be reached by the expander efficiency at every pressure ratio higher than 3, for each considered volumetric expansion ratio. Also the reduction of P_{exp} with ε_v at a given value of the pressure ratio, as visible in Fig. 4.23, is more regular than in the case of R245fa, due to the invariance of Φ.

4.2.3 Final remarks

The analysis of the results obtained from the numerical model of reciprocating expander described in this Section 4.2 allows to take some general considerations on the possibility to use this technology in a small scale ORC system. Maximum efficiency values in the range around 0.70 are predicted for machines with cut-off ratios and valve timing properly chosen, in line with the typical efficiencies of scroll expanders. Nevertheless, these performances appear to be reachable only with machines newly and properly designed, this involving costs surely higher than the minor modifications needed by a commercial scroll compressor to work satisfactorily as expander for organic fluids. For this reason, even if a piston machine can be considered a viable option to be evaluated carefully in future works, in this phase the scroll machine appears to be the most suitable solution to be installed in a small scale ORC prototype.

4.3 Cycle simulation tools

The behavior of an ORC system in various conditions has been studied using different numerical tools, in order to realize models of increasing accuracy and complexity. Normally, the first step adopted for the analysis of a new system has been the calculation of the thermodynamic states of each cycle point by means of a simple flow sheet or a MATLAB® script, aimed to define quickly the performances potentially achievable in the specific case. Although very useful, these models are very simple and their description appears to be unnecessary in this thesis. Once the feasibility of a system had been verified thanks to these tools, more accurate models have been realized in order to predict more in detail its behavior. In particular two commercial products have been used for this purpose: AspenTech Aspen Plus®, with the comprehensive modeling of the heat exchangers through the dedicated tool AspenTech Aspen Exchanger Design and Rating (EDR), and LMS Imagine.Lab AMESim®. The results of the simulations conducted with these programs are reported in Subsections 4.3.1 and 4.3.2 respectively.

4.3.1 Aspen Plus® model

The simulation software Aspen Plus® by AspenTech has been used to realize the model of a small scale ORC experimental prototype, currently under construction in the Department of Engineering and Architecture at University of Trieste. This activity was aimed to achieve a preliminary knowledge of the behavior of the test bench in both design and off-design conditions.

4.3.1.1 Description of the model

The general flowchart of the Aspen Plus® model is reported in Fig. 4.24: as deducible from the scheme, in this typology of simulation codes each component of the circuit is treated by a specific submodel, which shares its inputs and outputs with the blocks directly linked with it. In particular, the main submodels taken into account in this project have been those related to the expander, to the pump and to the heat exchangers.

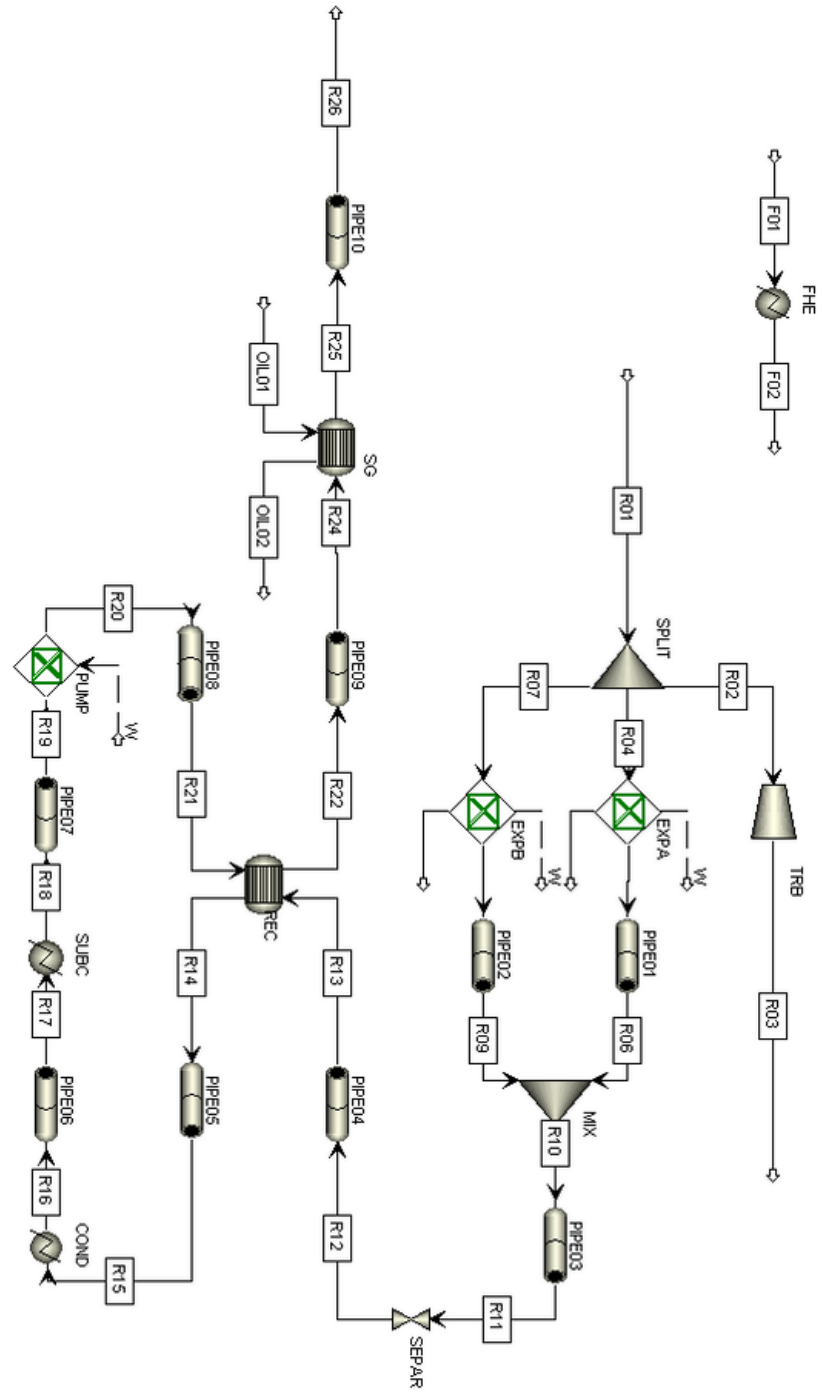

Fig. 4.24: Aspen Plus® flowchart

The considered expander - a scroll machine derived from a commercial compressor - has been modeled with the in-house developed tool described in Section 4.1. More specifically, a series of simulations has been conducted, with the aim of defining the performance maps of the selected expander at different working conditions. As an example, the trends of the expander isentropic efficiency (defined by Eq. 4.18) as functions of the expansion ratio and at different superheating degrees ΔT_{sh} are reported in Fig. 4.25. These curves have been recorded on tables used by the Aspen Plus® model as inputs to be interpolated to find the needed performances of the expander in a defined working condition.

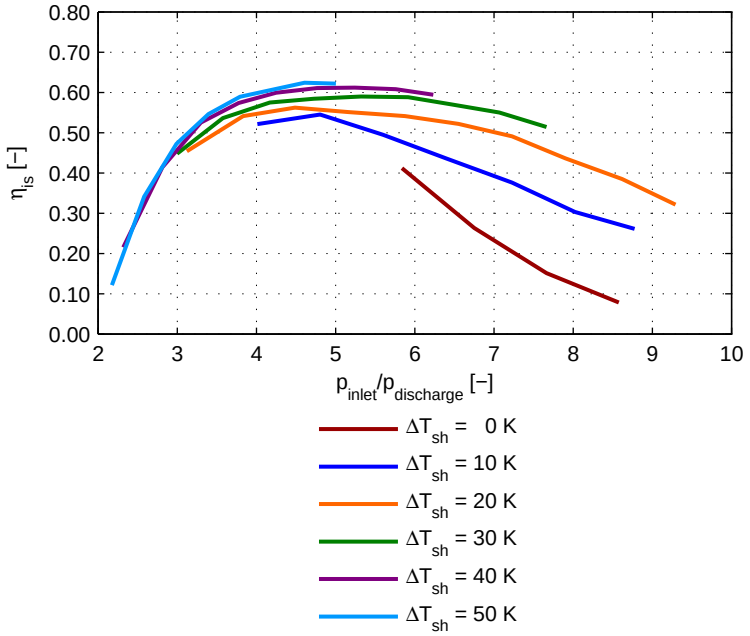

Fig. 4.25: Expander overall isentropic efficiency at different superheating degrees

Also the performances of the diaphragm pump to be installed on the test bench have been inserted in the global model through a table built starting from the data gathered from the manufacturer. Among the other curves, Fig. 4.26 shows the specific energy and the efficiency as functions of the R245fa mass flow rate delivered by the selected model of diaphragm pump.

All the plate heat exchangers planned for the system (a vapor generator feed by thermal oil, an internal recuperator, a condenser and a liquid sub-cooler) have been modeled

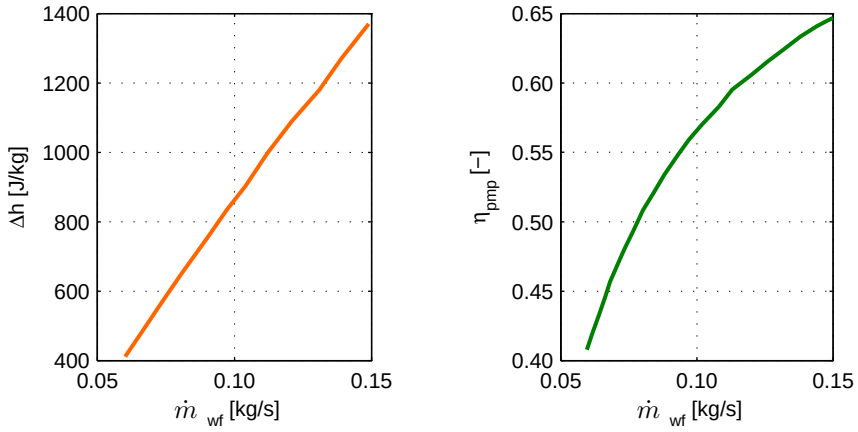

Fig. 4.26: Diaphragm pump main performances

starting from the data available in the technical sheet provided by the manufacturer: the main features of each exchanger have been reported in Tab. 4.3. The modelization has been conducted with a dedicated tool, the commercial software AspenTech Aspen Exchanger Design and Rating (EDR): this software allows a real-time communication with Aspen Plus®, so the real behavior of the heat exchangers can be calculated, even in off-design conditions.

Tab. 4.3: Main features of the heat exchangers

Exchanger	Rated heat load [kW]	Heat transfer area [m^2]	Number of plates [-]
Vapor generator	37.170	2.016	36
Recuperator	8.686	1.060	40
Condenser	35.180	2.800	50
Sub-cooler	1.942	0.336	14

4.3.1.2 Analysis of the results

The model realized in Aspen Plus® environment has been used to conduct a large number of simulations, aimed to predict the behavior of the test bench in a wide range of operating conditions. The most interesting results are reported in this paragraph, in graphical form.

In Fig. 4.27 the electrical efficiency of the system, η_{ORC}, is reported as a function of the imposed expansion ratio, for different values of the superheating degree ΔT_{sh} and

considering R245fa as working fluid, in both the cases of simple and regenerative cycles. First of all, it can be noted that larger superheating degrees involve remarkable benefits in the electrical efficiency, for values up to 30 K. Beyond this threshold, an increasing in ΔT_{sh} leads to negligible efficiency gains, while reduces the maximum achievable evaporation pressure, because of the limitations in maximum working temperatures, due to R245fa chemical stability. From the analysis of Fig. 4.27 it can be concluded also that the maximum values in the system efficiency are reached at high values of the imposed expansion ratio (i.e. at high evaporation pressures), because in these conditions the gains in the thermodynamic efficiency of the ideal cycle overcome the reduction in the expander isentropic efficiency reported in Fig. 4.25. Finally, the maximum values shown in Fig. 4.27 for the electrical efficiency of the simulated system can be underlined, i.e. 0.07 and 0.09 for the simple and the regenerative configurations respectively.

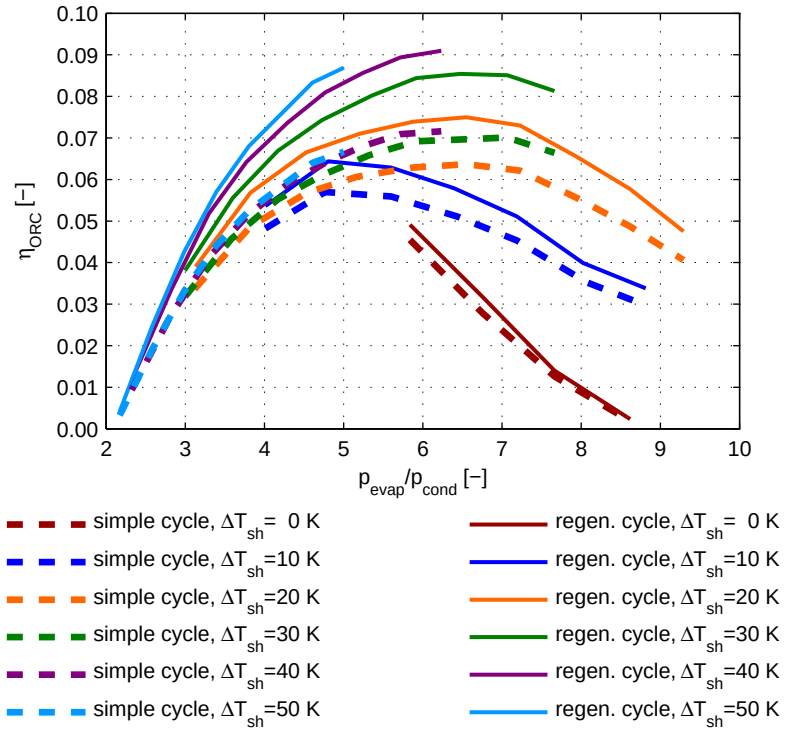

Fig. 4.27: Cycle electrical efficiency at different superheating degrees

On the basis of the considerations just exposed, a superheating degree equal to 30 K is chosen for a deeper analysis of the influences of the working pressures on the system performances. In particular, the electrical efficiency is reported as a function of both the condensation and the evaporation pressures in Figs. 4.28 and 4.29, in the cases of simple

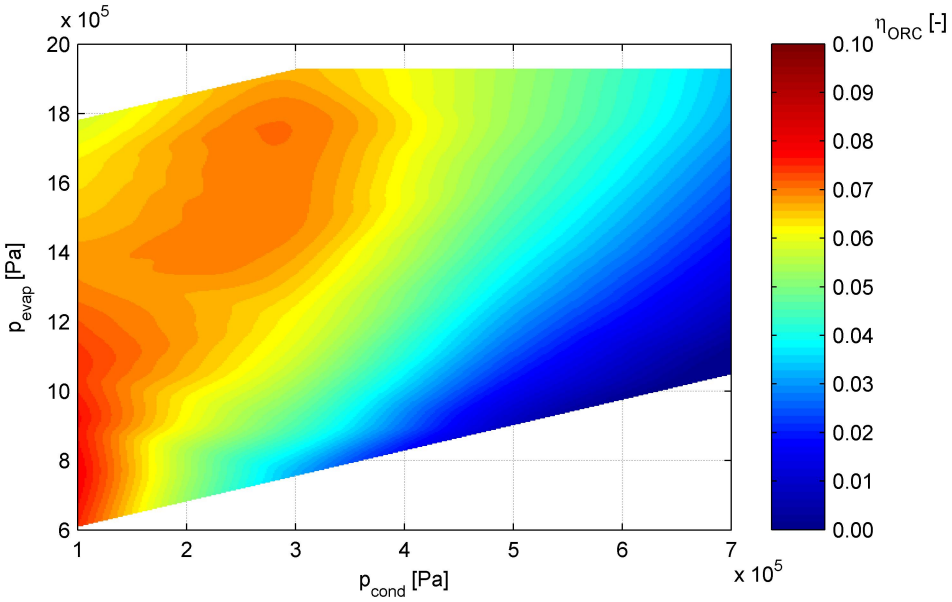

Fig. 4.28: Electrical efficiency of an ORC system in simple configuration

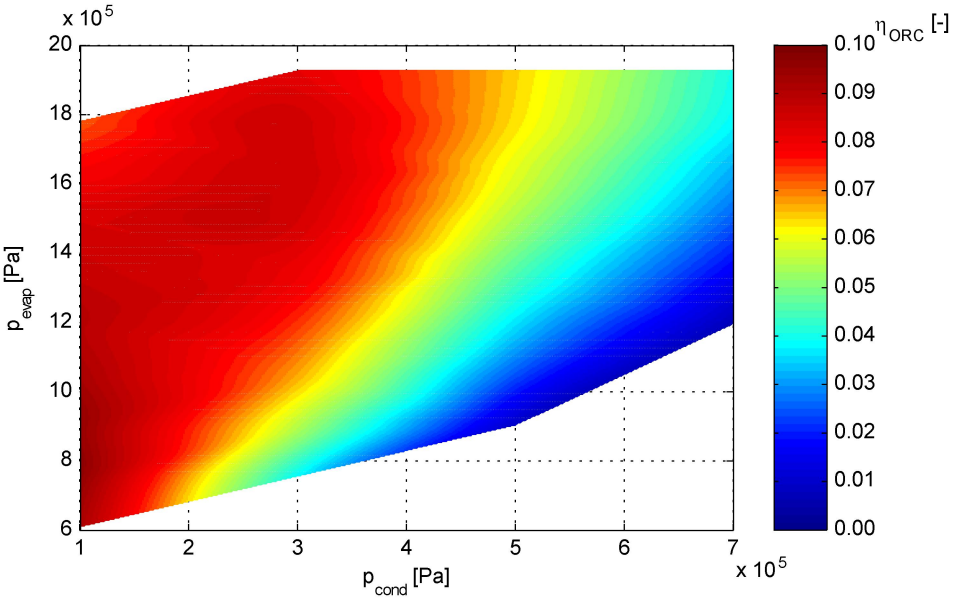

Fig. 4.29: Electrical efficiency of an ORC system in regenerative configuration

and regenerative configurations respectively, always with R245fa taken into account as working fluid. The best performances are achieved by the system at intermediate values of evaporation pressure and, obviously, at the lowest condensation conditions. However, mainly because of the good skill of a scroll expander to operate satisfactorily even in off-design conditions, acceptable performances are achieved by the system in a quite large operational range, in particular also at higher condensation pressures, if the evaporation pressure is sufficiently high. This behavior is interesting especially for cogenerative applications, where the condensation pressure should be set on the basis of the needed temperature for the cogenerated heat. Finally, the comparison of Figs. 4.28 and 4.29 allows to quantify the gain in terms of electrical efficiency of a regenerative configuration with respect to the simple system: in most of the operating conditions, the difference between these two cases can be assumed with a good approximation equal to 2 percentage points, with the internal recuperator capable to reach an average efficiency equal to 0.70.

The effect of the internal recuperator is reported also in Fig. 4.30, in which a comparison is conducted between the thermal power needed from the boiler in a simple ORC system and in a regenerative one: it is interesting to note that the difference between the two curves (i.e. the saved thermal input) grows with the imposed pressure ratio, starting, in the particular prototype analyzed with the Aspen Plus® model, from 2.5 kW for $p_{evap}/p_{cond} = 3$, to 7.6 kW at the highest ratios, where a regenerative configuration is even more convenient.

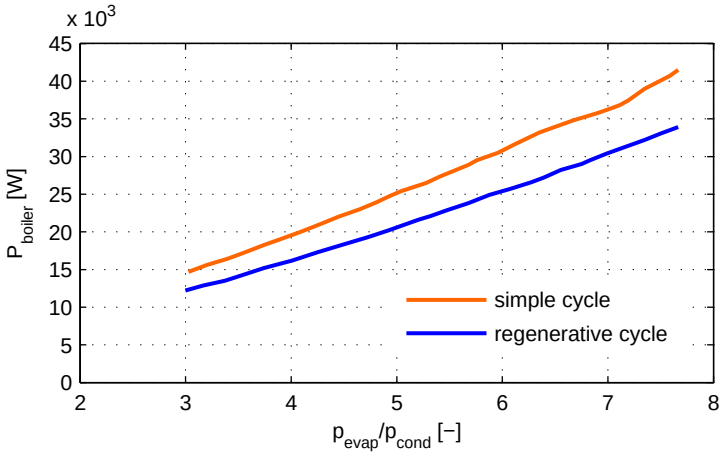

Fig. 4.30: Thermal power needed by the boiler in simple and regenerative cases

Another fundamental parameter to predict with the numerical model is the net electric power delivered by the system. In Fig. 4.31 this quantity is reported as a function of the imposed pressure ratio: obviously the delivered power increases with p_{evap}/p_{cond}, but it

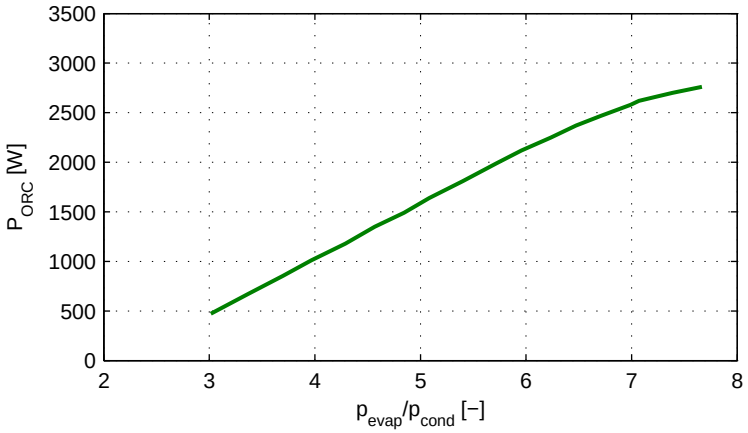

Fig. 4.31: Net electric power delivered by the ORC system

is interesting to note that, beyond a certain threshold, the gain in power becomes less than proportional.

4.3.1.3 Exergy analysis of the system

The data available after the simulation of the system with the Aspen Plus® model have been used to conduct an exergy analysis of the prototype, aimed to detect the components in which the major exergy destructions occur. Figs. 4.32 and 4.33 report, for a reference working condition, two pie charts (for the simple and the regenerative system respectively) which display how the exergy input is shared among useful outputs (mechanical and thermal power) and destructions. As observable, the biggest exergy destruction occurs, in both cases, in the boiler: this is due mainly to the large temperature difference between the two streams inside this heat exchanger (the working fluid and the thermal oil, assumed as heat source for the considered prototype). Other important exergy amounts are destroyed in the expander and in the condenser, while the contributions of the destructions in the pump and in the pipes are limited to 1% and 2.5% respectively.

The sum of the shares of the electric power and the exergy content of the hot water produced shown in Figs. 4.32 and 4.33 represents the overall exergy efficiency of the system η_{II}: since the regenerative system utilizes a lower exergy input than the simple configuration (in the considered working conditions 10.3 kW instead of 12.1 kW) to generate the same amount of electric power (2.6 kW), the former exhibits a higher exergy efficiency (0.298 instead of 0.264), even if the latter is capable to a larger production of low-temperature (and low-exergy) heat (33.2 kW instead of 26.1 kW). The values of η_{II} are reported, together with the exergy efficiencies of the single components, in form of histograms in Fig. 4.34, for a simple system, and in Fig. 4.35, for a prototype equipped

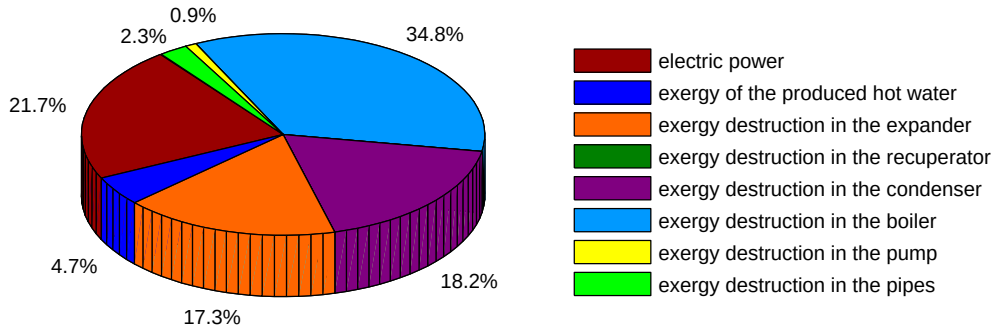

Fig. 4.32: Shares of exergy input, simple case

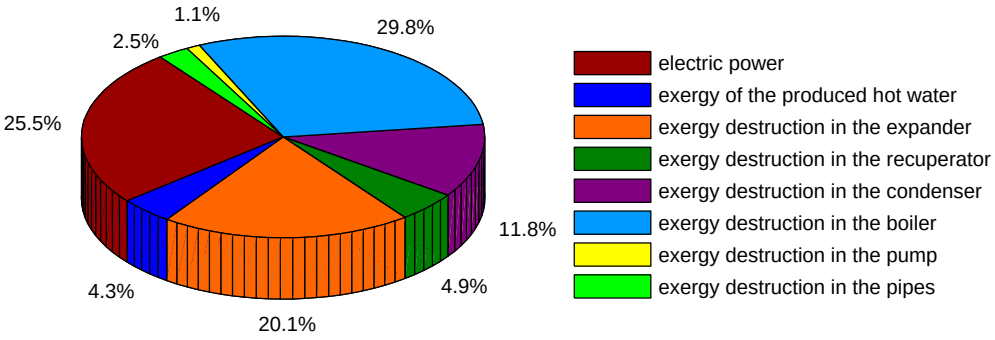

Fig. 4.33: Shares of exergy input, regenerative case

with an internal recuperator. The general expression used in this analysis to describe the exergy efficiency of a component is the ratio between the benefit delivered and the exergy input depleted to obtain the latter. This definition cannot be applied to the pipes, since these are merely dissipative elements: in this case, the values reported in Figs. 4.34 and 4.35 are referred to an exergy conservation factor, defined as the ratio between the exergy output and the exergy input of the component.

Among the other values, the condenser shows a particularly low exergy efficiency (in the considered conditions, 0.206 for the simple configuration and 0.268 for the regenerative one): this is due both to the high temperature difference between the two streams inside the exchanger and to the very low temperature of the hot water produced (only few degrees above the ambient temperature).

The results of this exergy analysis are useful to take some considerations on the possibility of future enhancements of the system performances. In particular, two ways

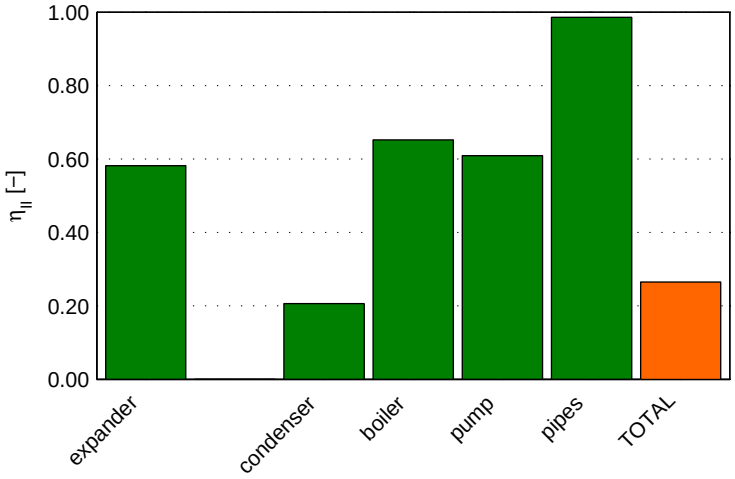

Fig. 4.34: Exergy efficiencies in a simple ORC system

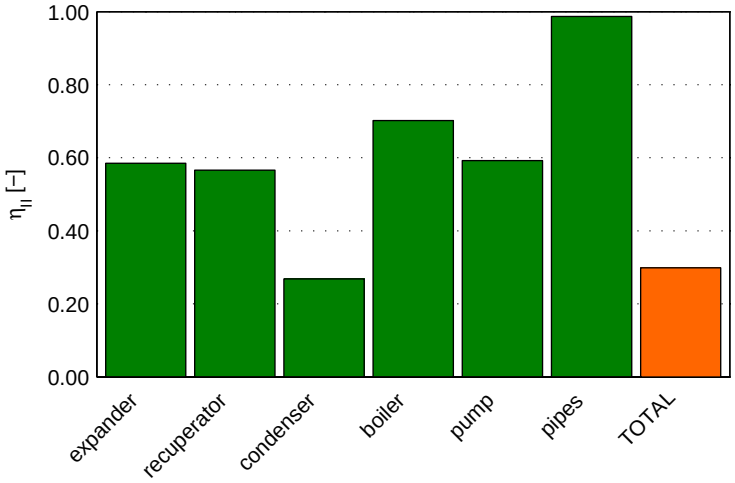

Fig. 4.35: Exergy efficiencies in a recuperative ORC system

can be followed to improve the overall efficiency:

- the reduction of the exergy destruction in the two largest heat exchangers (the boiler and the condenser);
- the reduction of the exergy destruction in the expander.

The first task can be addressed, for example, with the adoption of a mixture, instead of a pure substance, as working fluid. In this case, the isobaric evaporation would take place with a progressive temperature increment, resulting in a reduction of the mean temperature difference between the two streams inside the boiler. It must be noted, however, that effective benefits in terms of overall efficiency can be obtained only if the mixture composition is properly defined and optimized. Other solutions suggested in literature to lower the mean temperature difference in the heat exchangers are supercritical cycles, pressure-staged cycles and water-ammonia cycles, but these technologies appear to be too complex to be applied in domestic scale systems. The goal of the enhancement of the expander efficiency, on the other hand, can be chased firstly with the reduction of the leakages and of the mechanical losses inside the scroll device, since these are the phenomena with the largest influences on the machine behavior, as already stated in Subsection 4.1.4 and reported in Fig. 4.9.

4.3.2 AMESim® model

Another model of a small scale ORC cogenerator has been realized using the commercial simulation software LMS Imagine.Lab AMESim®. In particular, the studied system has been a prototype already built and tested (the experimental activity conducted on this facility is described in Section 5.2): the modelization in this case was aimed to develop a tool capable to simulate the behavior of the real prototype in both stationary and transient conditions, the latter being potentially dangerous for the proper operation and particularly important in the definition of the best suited control strategies. For this reason, the simulation environment AMESim® has been chosen, since it is devoted in particular to the development of dynamic models of one-dimensional systems [110].

4.3.2.1 Description of the model

The experimental prototype considered for this modelization is made up of a diaphragm pump, an electric boiler (with direct evaporation of the working fluid), a hermetic scroll expander and a plate condenser, other than a power conditioning system used to generate a DC voltage starting from the three-phase, variable-frequency voltage generated by the alternator (a complete and detailed description of the test bench is reported in Section 5.2). A sketch of the simulation model is reported in Fig. 4.36. It includes the schemes of the ORC circuit assembly, slightly simplified with respect to the real one, and of the electric section of the bench (made up of alternator, power conditioning system and electronic load). The working fluid flowing in the prototype is a mixture of R245fa and lubricating oil. The properties of the refrigerant are available in the software libraries, among the standard two-phase fluids, while the effects of the oil concentration on the thermo-physical properties of the mixture have been neglected in this first phase. The expander submodel requires the values of the displacement and of three characteristic efficiencies (isentropic, mechanical and volumetric) of the machine: these data have been obtained on the basis of the technical information provided by the scroll manufacturer and of the combined use of some experimental results and of the scroll simulation tool described in Section 4.1.

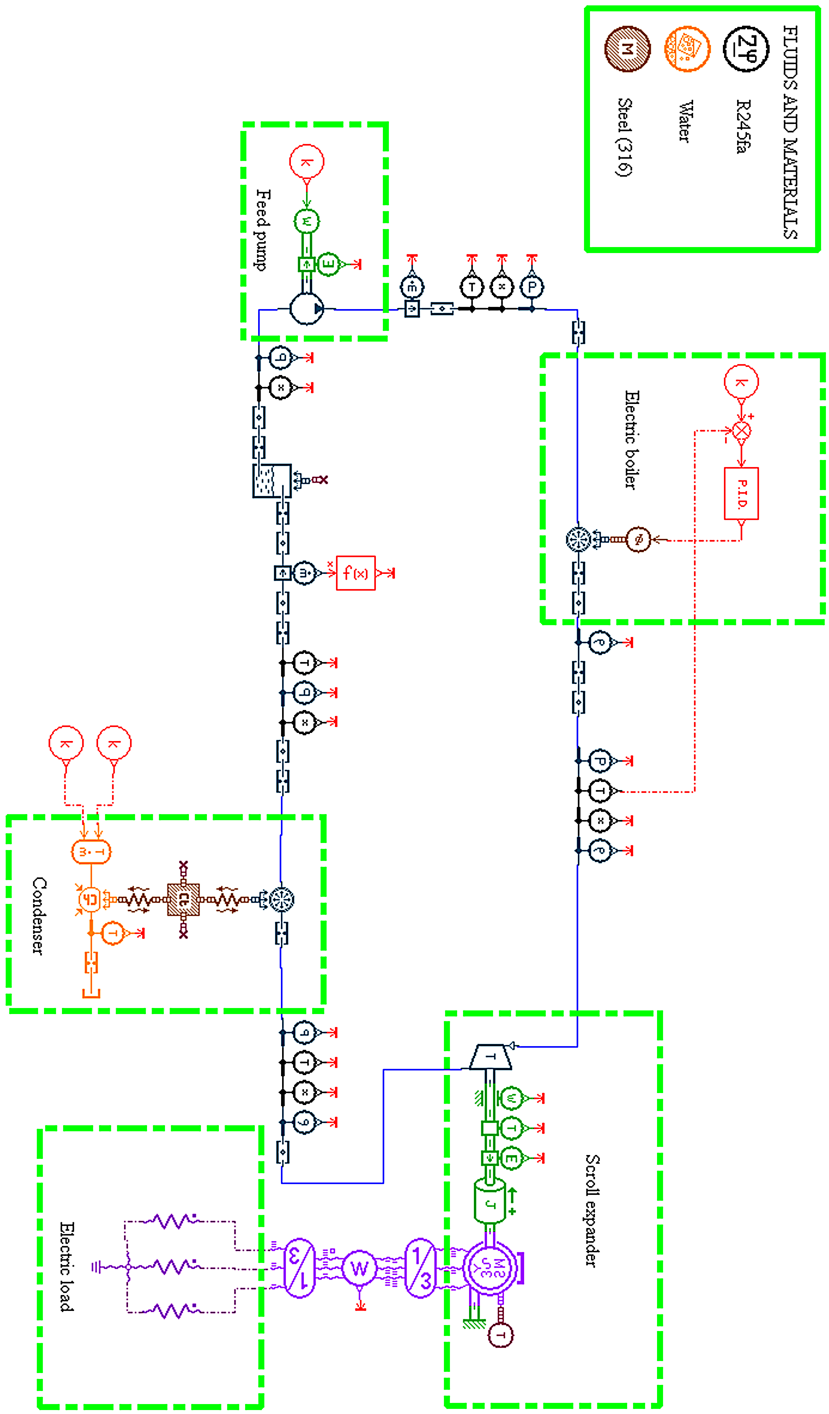

Fig. 4.36: AMESim® flowchart

The efficiencies values have been considered constant and the expansion process has been assumed to be adiabatic: these hypotheses are quite far from the actual phenomena taking place in the machine and then they will be removed with the planned development of an improved expander submodel, but at the moment the accuracy of these assumptions appears to be sufficient for the aim of the work, i.e. the simulation of the performances of a real system in conditions different from the ones in which it has been tested. The pump is modeled as a standard fixed displacement hydraulic unit with given volumetric and mechanical efficiencies, which values have been estimated on the basis of the performance curves reported in a technical data sheet. The condenser is modeled with a small number of standard components, as shown in Fig. 4.36. Its internal volumes and heat capacities have been obtained on the basis of technical data sheets and direct measurements on the prototype. The mass of the refrigerant introduced in the system has been measured on the experimental bench, but the effective amount of fluid running in the system was only approximately known, due to some leakages towards ambient, so it has been considered a free validation parameter, within a range of reasonable values, together with the internal volume of the vaporizer circuits and the coefficients of the friction losses in the connecting pipes. An optimization has been carried out with the minimization of the error on the expander shaft speed at a given working point as objective. The considered reference conditions were a pump shaft speed of 300 rpm, a vapor production temperature of 130 °C and an electric resistance of the electronic load set to 70 Ω.

4.3.2.2 Comparison between numerical and experimental results

Once the model had been calibrated, its outputs at different working conditions have been compared with the experimental measurements conducted during the field tests fully described in Section 5.2, in order to verify its accuracy. In Figs. 4.37 to 4.43 several diagrams are reported, with the aim to show the correlation between experimental and numerical results: a perfect correspondence between the two sources of data would result in a point placed on the bisector of the planes.

The first diagram, shown in Fig. 4.37, displays the expander shaft speed: a satisfactory correspondence between the two series of data can be noted even if, in some particular working conditions, the model over-estimates the real values. The diagram in Fig. 4.38 reports the voltage supplied by the system after rectification, as representative of all the electrical parameters simulated by the model: in this case, the correlation between numerical and experimental data could certainly be considered good, confirming the accuracy in the modelization of the electric devices.

The model exhibits larger difficulties in the calculation of the fluid properties, in particular of the pressures on few characteristic sections of the system: for example, in the diagram reporting the pressure at the boiler outlet in Fig. 4.39, a general underestimation by the model is highlighted. The poor correlation can be due to an inadequate model calibration, but also to a scarce correspondence between the actual fluid mixture properties and the ones calculated by the chosen submodel, or even to the simplified modelization of some plant components. In fact, as already stated in Paragraph 4.3.2.1,

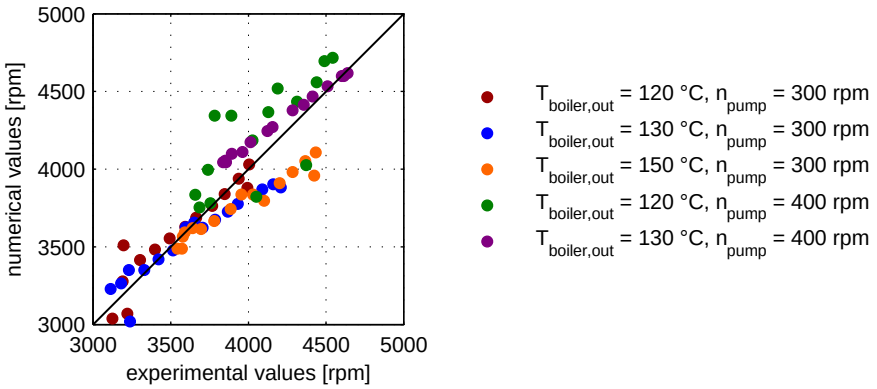

Fig. 4.37: Numerical-experimental comparison - Expander shaft speed

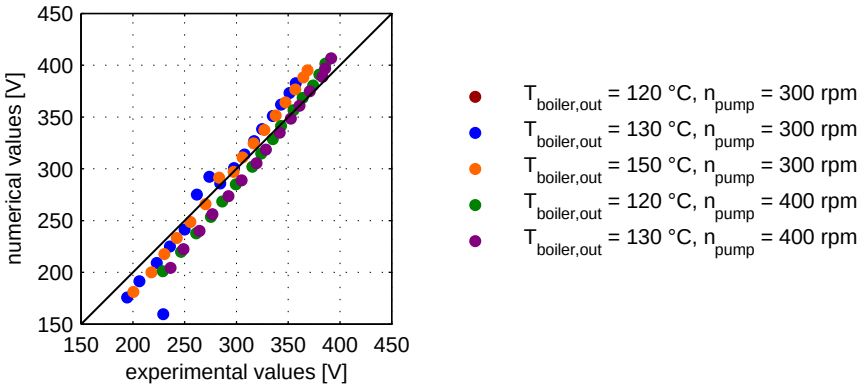

Fig. 4.38: Numerical-experimental comparison - Voltage

the real system is filled by a mixture of R245fa and lubricant, while the simulation is carried out taking into account only the refrigerant as a pure substance. Besides, the expander is modeled as an adiabatic machine with a constant efficiency while, in a real scroll device, the heat transfer is not negligible and the efficiency varies with the working conditions. In this first phase of utilization of the simulation model, the approximation given by these assumptions is considered sufficient, but the accuracy in calculating the thermodynamic properties of the fluid is surely affected by the cited factors. Another cause of the poor correlation can be, in particular when the temperature imposed at the boiler exit is low, the presence of fluid with an unknown vapor quality at the expander inlet: this problem in the system control strategy, which will be carefully described in Subsection 5.2.2, results in measurement errors and therefore in difficulties in calculating the actual fluid properties.

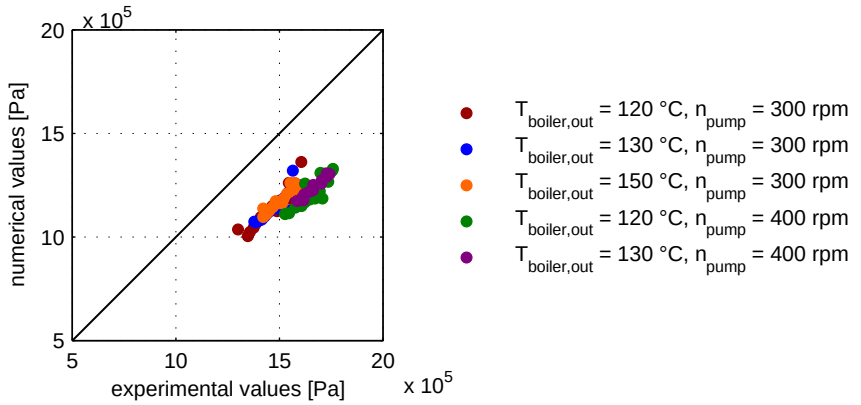

Fig. 4.39: Numerical-experimental comparison - Boiler outlet pressure

The simulation model achieves a greater accuracy in the calculation of the pressure at the condenser outlet, as reported in the corresponding graph in Fig. 4.40: in this section, the thermodynamic state is strongly influenced by the temperature of the cooling water, which is a direct calibration parameter for the model, so a better correspondence between experimental and numerical results is reached.

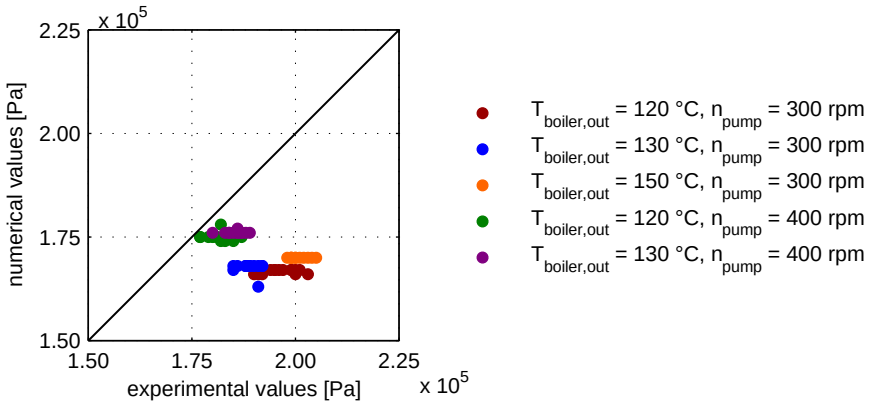

Fig. 4.40: Numerical-experimental comparison - Condenser outlet pressure

Obviously, due to the problems highlighted in the definition of the thermodynamic states of the fluid, even the calculation of the working parameters of the system based on these states is affected by a relatively low accuracy. For instance, as shown in the corresponding diagram in Fig. 4.41, the calculated values of the enthalpy drop across the expander lie in a quite large region around the plane bisector. In particular, an underestimation occurs when the vapor production temperature is set on high values,

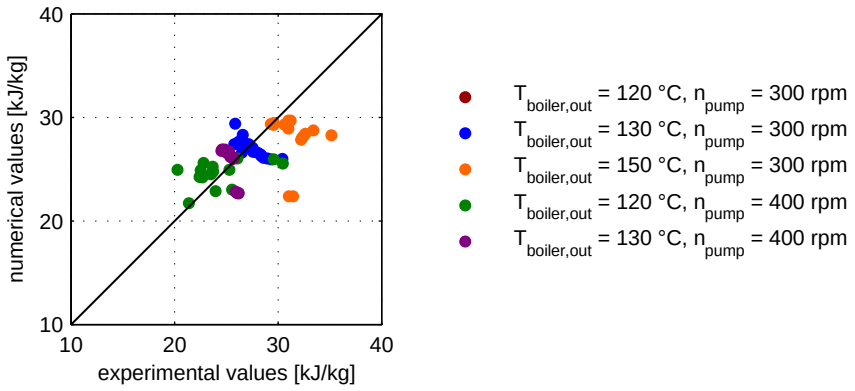

Fig. 4.41: Numerical-experimental comparison - Expander enthalpy drop

i.e. 150 °C. On the other hand, the global working parameters of the system, i.e. the delivered power and the electrical efficiency of the cycle, are only slightly overestimated, as shown in Figs. 4.42 and 4.43 respectively: in these cases the accuracy is satisfactory, since the scarce precision revealed in the estimation of the thermodynamic properties is counterbalanced by the good skill of the model to calculate other data such as the fluid flow rate or the electric output. In particular, the mean relative error detected in the numerical estimations of the delivered power (reported in Fig. 4.42) is lower than 5% , while the global efficiency (shown in Fig. 4.43) is overestimated, on the average, by only one percentage point.

In summary, the comparison between numerical and experimental data highlighted a surely improvable accuracy for the simulation model but, at the moment, the achieved

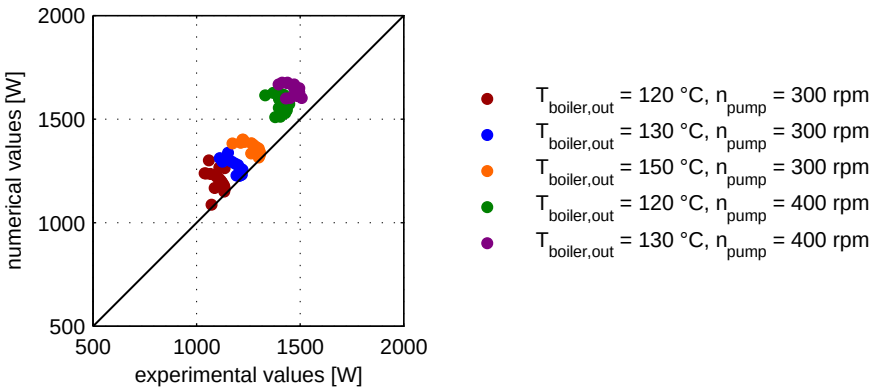

Fig. 4.42: Numerical-experimental comparison - Expander delivered power

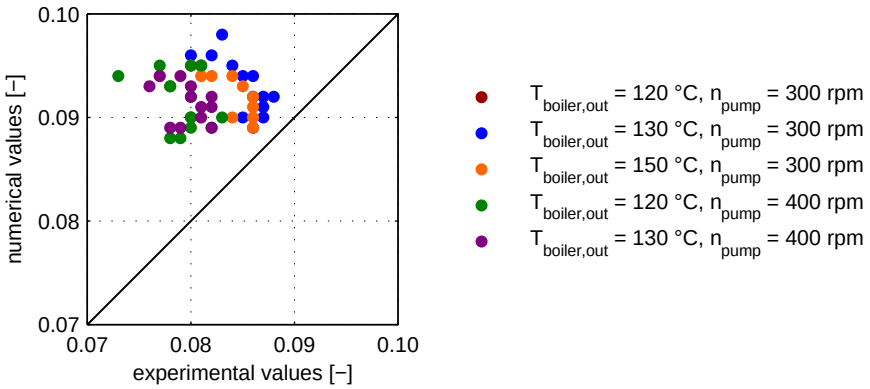

Fig. 4.43: Numerical-experimental comparison - Cycle electrical efficiency

precision can be considered sufficient for the goal of the tool, i.e. to carry out dynamic simulations aimed to predict the behavior of the system in not tested conditions and to define a suitable control strategy.

5

Experimental facilities and tests

Beside the theoretical and the numerical studies on small scale ORC applications, described in the previous Chapters 2, 3 and 4, an experimental activity has been scheduled and conducted, with the aim of achieving a direct knowledge of the problems related with these system, of testing the studied solutions and of confirming the results obtained from the numerical models. In particular, the work has been carried out on two different facilities. The first one is a bench designed in particular for the conduction of tests on feed pumps working with an organic fluid (the refrigerant R245fa), while the second is an experimental prototype of a complete ORC system.

5.1 Pump test bench

As already discussed in Section 2.5, the feed pump is a critical component of an ORC system, due to the difficulties connected with the handling of the organic fluids suitable for these installations. Moreover, only few studies can be found in literature concerning in particular the problems related to the feed pumps in ORC applications of small scale, as the object of the present thesis.

For these reasons, it has been decided to design and build a test rig aimed specifically to the study of pumps operating on a mixture of R245fa and oil. In particular, the bench has been utilized to measure the performances of a commercial gear pump, originally designed to operate with light oils in industrial burners.

5.1.1 Description of the bench

A comprehensive view of the test rig is reported in the picture of Fig. 5.1, while the piping and instrumentation diagram is shown in Fig. 5.2.

The bench, derived from an experimental facility developed by Riello SpA for the test of industrial boiler pumps, is set up in a closed loop, which main components are a regulation valve, an air heat exchanger and an expansion tank, other than the analyzed pump. The valve, used to dissipate the energy of the pumped fluid and to lower the pressure down to suction conditions, is a manually driven diaphragm unit. The membrane

Fig. 5.1: Comprehensive view of the pump test bench

technology is required to ensure a perfect sealing of the circuit and to avoid any fluid leakage towards ambient.

The exchanger is a fin-and-tube cooler used to dissipate the excess of heat of the fluid and to maintain the thermal equilibrium in the circuit. A centrifugal fan is also installed on the exchanger, useful to force the air through the fins and to increase the heat dissipation when required.

The expansion tank is a device required in each system filled purely by a liquid substance, aimed to absorb every possible fluid expansion (for example due to thermal dilatation), avoiding the dramatic pressure increments which would occur in a circuit without any elastic component. In the considered experimental facility, a membrane hydro-pneumatic accumulator has been chosen to this task and installed. This device is made up of a steel tank subdivided in two volumes by an elastic diaphragm: one ambient is filled by the liquid mixture of R245fa and oil, while the second is loaded with nitrogen at a controlled value of pressure. In this way, other than compensate any thermal dilatation or also any leakage of working fluid towards ambient, the accumulator can be used to the system preload (i.e. the setting of a proper suction pressure in the circuit), by changing the nitrogen pressure.

The electric motor installed on the test rig to drive the studied pump is a brushless DC motor, characterized by a nominal shaft speed of 4000 rpm and a nominal driving torque

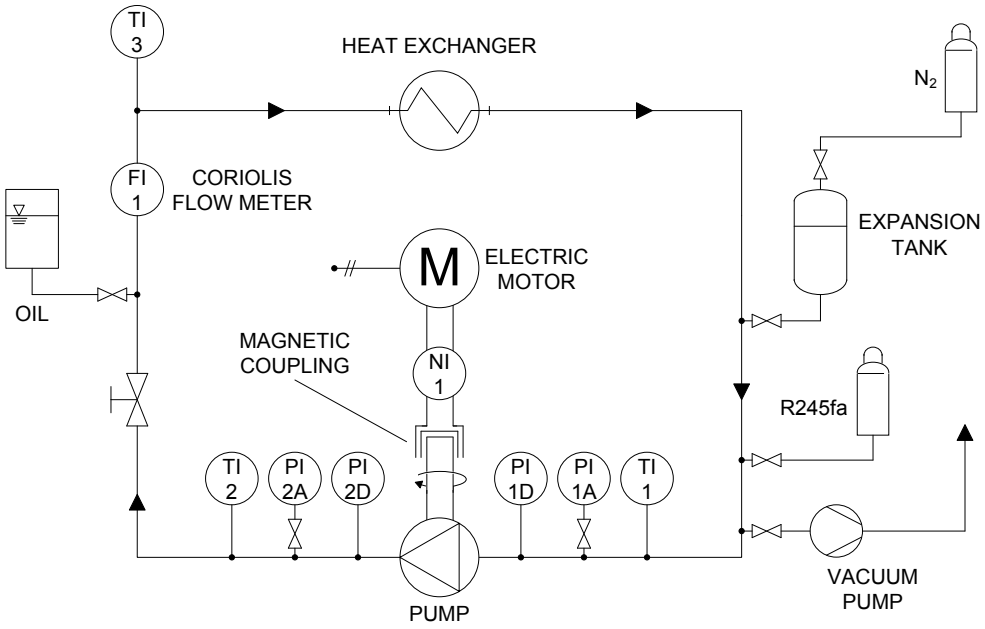

Fig. 5.2: Piping and instrumentation diagram of the pump test bench

of 1.65 Nm, but capable to operate at any exactly set velocity in the range from 0 rpm to 4000 rpm. The connection between the motor and the pump is made up by means of a magnetic coupling, capable to transmit the entire torque generate by the electric motor without slip. The main components of this device are an internal magnetic rotor, mounted on the pump shaft and covered with a thin enclosure fixed on the pump main body, and an outer rotor, mounted on the motor shaft. This choice allows a hermetic insulation of the circuit towards ambient, since the dynamic sealing on the pump shaft cannot avoid perfectly the leakage. A pressure sensor has been connected to the ambient of the pump shaft enclosed by the coupling shell, in order to allow, in future, measurements useful for a quantification of the fluid leaked from the pump main body. A detail of the magnetic coupling is depicted in Fig. 5.3. The power transmission of the test rig is completed by a torque meter (marked by NI 1 in Fig. 5.2 and visible also in Fig. 5.3), interposed between the motor and the magnetic coupling.

A series of sensors for the measurements on the various circuit streams completes the test bench. In particular, the pressure is acquired on both the suction and the discharge lines by means of two piezo-resistive pressure transducers (indicated respectively with PI 1D and PI 2D in the piping and instrumentation diagram of Fig. 5.2), while two analogical manometers (PI 1A and PI 2A) have been installed on the same pipes, in order to allow the pressure monitoring even without electricity supply, for safety reasons. The suction and the discharge temperatures are measured with two Resistance Temperature

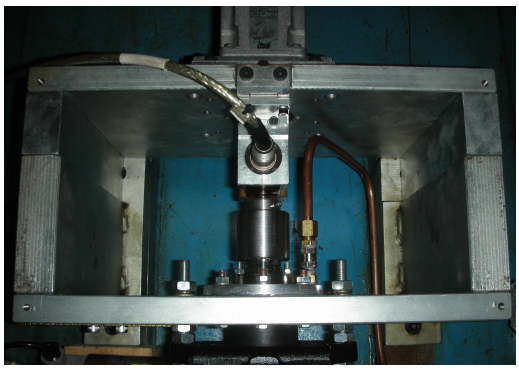

Fig. 5.3: Detail of the magnetic coupling

Detectors (RTDs) (marked by TI 1 and TI 2 in Fig. 5.2) in three-wire configuration. A third RTD (TI 3) is mounted at the heat exchanger inlet, with the aim of monitoring the thermal dissipation process. The last sensor installed on the system is a Coriolis flow meter, placed between the regulation valve and the heat exchanger (as visible in Fig. 5.2, where it is indicated by FI 1) and used to acquire data on the mass flow rate flowing in the circuit and on the fluid density. The picture of Fig. 5.4 reports a view of the just described instruments (arranged in the configuration shown in Fig. 5.2), together with the tested pump.

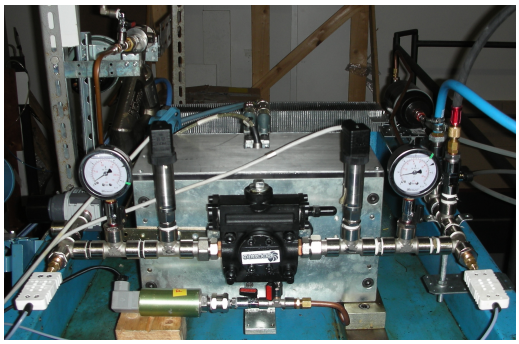

Fig. 5.4: Detail of the pump and of the sensors

The circuit is equipped with three ports for the external connection, used during the charging of the test bench, which is not a trivial operation. In fact, due to the particular fluid used, any presence of air or humidity inside the system should be avoided. For this reason, after a preliminary flushing with nitrogen, every time when a new charging is required, a vacuum pump is connected to the first port (on the right bottom side of Fig. 5.2) and it is run for several minutes, in order to reach a high and stable vacuum degree in the circuit. After this operation, the lubricant is loaded through the second

port: this is connected to a deformable tank, the latter being previously fully filled by the needed amount of oil, so that no air is trapped in the volume. Once the valve interposed between the tank and the circuit is opened, the oil flows in the system, driven by two forces: the difference between the ambient pressure and the vacuum created in the loop and the manual compression of the deformable tank during the charging process. The last operation is obviously the introduction of the refrigerant R245fa in the circuit: the fluid is provided in a tank in thermal equilibrium with ambient, so there is the concurrent presence of liquid and vapor at the evaporation pressure corresponding to the ambient temperature (e.g. the evaporation pressure of R245fa at a temperature of 20 °C is 1.238 bar). In order to increase this pressure, the bottle is heated up in a thermostatic bath before each filling process: in particular, the fluid is warmed up to a temperature of 40 °C, which entails a tank pressure of 2.518 bar. Once the needed temperature is reached, the bottle is installed above the test bench and connected to the latter through the third port, and the fluid is drawn from the bottom of the tank: in this way, only liquid enters the test bench, since, at equilibrium, all the vapor is concentrated on the highest zone of the available volume, i.e. the bottle. After the disconnection of the refrigerant tank, the circuit is finally pressurized at the needed level, acting on the nitrogen volume of the expansion tank. The charging system of the test rig is reported in the picture of Fig. 5.5: on the bottom, the vacuum pump, the thermostatic bath and the nitrogen bottle are placed from left to right, while the green tank of R245fa is visible on the top.

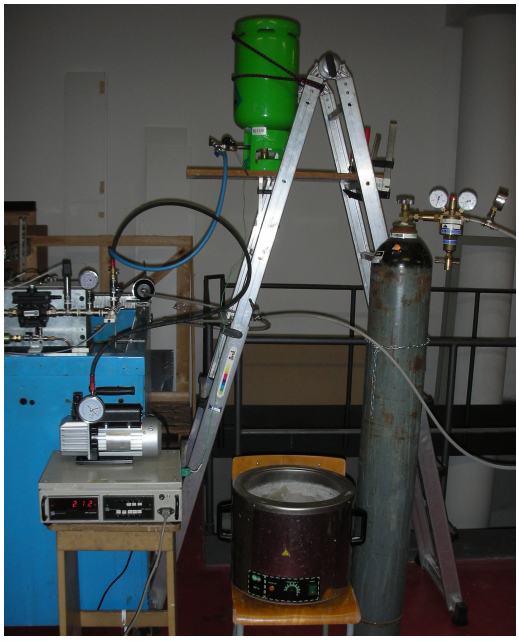

Fig. 5.5: Detail of the charging system

5.1.2 Description of the tested pump

The first machine studied on the test rig is a gear pump from the French manufacturer SUNTEC, in particular the model identified by the code TA2C-4010_7, which scheme is reported in Fig. 5.6 [111] and which is visible in detail in Fig. 5.4. This pump is specially designed for industrial heating applications using light or heavy oils and kerosene, and its main features, derived from technical data sheets, are reported in Tab. 5.1. Among the other data, the most critical parameter for the usage of this pump with R245fa is the operating range of viscosity. In fact, in the normal working conditions considered for the studied small scale ORC applications, the pump operates on R245fa at a temperature included in a range from 15 °C to 50 °C and with a suction pressure from 1 bar to 5 bar: in this field, the kinematic viscosity of the selected fluid is approximately equal to 0.3 mm^2/s. This value is about 10 times lower than the minimum limit indicated by the manufacturer for proper operations (3 mm^2/s, as reported in Tab. 5.1). For this reason, one of the objectives of the laboratory tests on the pump is the check of the performances with the particular fluid, actually a mixture of R245fa and lubricant.

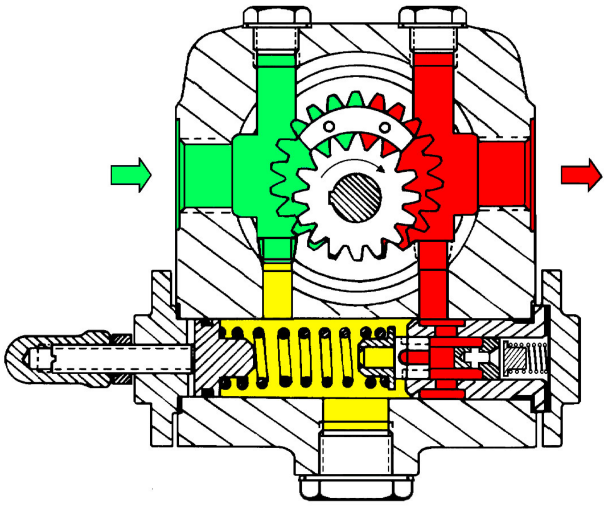

Fig. 5.6: SUNTEC TA2C-4010_7 pump scheme [111]

Tab. 5.1: SUNTEC TA2C-4010_7 pump technical data [111]

Weight [kg]	5.4
Max discharge pressure [bar]	40
Operating temperatures [°C]	0–150
Operating kinematic viscosities [mm^2/s]	3–75
Max shaft speed [rpm]	3600
Rated torque (@ 40 rpm) [Nm]	0.3

The performances of the analyzed pump, when operating with light oils of different viscosity and at a rated speed of 2850 rpm, are reported, as declared by the manufacturer, in Fig. 5.7: in particular, the curves show the delivered flow rate and the absorbed power as functions of the imposed discharge pressure. It can be noted that, if the viscosity of the pumped liquid is low (5 mm^2/s in Fig. 5.7, anyway more than 15 times larger than the mean viscosity of R245fa at the considered conditions), the delivered flow rate decreases with a quite large slope with the discharge pressure: this is due to the backward leakage of the low-viscosity fluid across the pump gears. Therefore, the tests are aimed also to verify the actual capacity of the pump to reach a sufficient discharge pressure: after the previous numerical work, this level has been calculated in the range of 15 bar, as reported in Section 4.3.

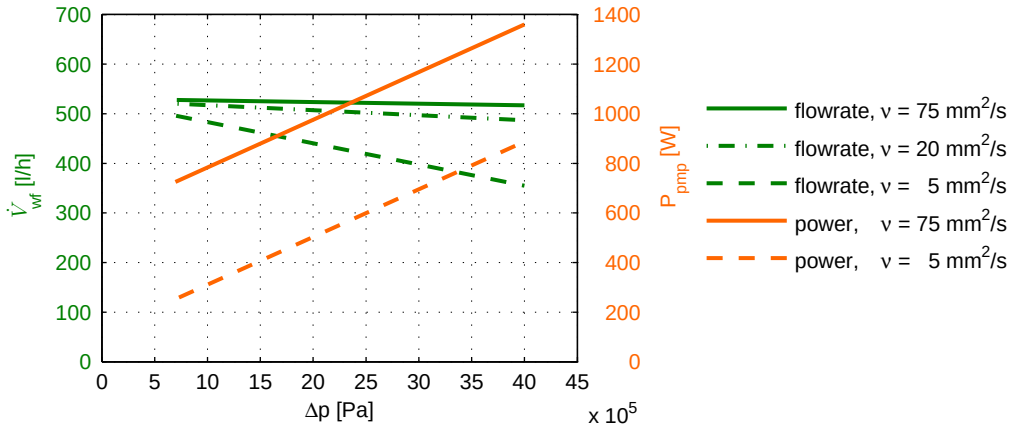

Fig. 5.7: Declared performances of the pump at $n = 2850$ rpm

5.1.3 Tests and results

The experimental work on the pump described in this Subsection has been aimed to verify the general performances of the machine when operating on a mixture of R245fa and lubricant in the conditions normally found in a small scale ORC application. In these first tests the composition of the mixture has not been exactly controlled, but an abundant amount of oil (between 15% and 20% in mass) has been charged in the system, in order to avoid any possible problem related to the absence of any lubricating capacity of R245fa. In any case, the exact percentage of oil in the mixture has to be set properly not only with respect to the pump, but also according to the expander requirements: for example, in normal conditions, a scroll expander (not of oil-free type) needs a lubricant content of at least 5% . The performances of the pump have been registered varying the imposed discharge pressure (by means of the control valve installed on the circuit) and for six different shaft speeds, in a range from 1000 rpm to 3450 rpm.

The diagram in Fig. 5.8 reports the volumetric flow rate delivered by the pump as a function of the difference of pressure between suction and discharge. As observable, the flow rate does not collapse even at the highest values of Δp, despite the very low viscosity of R245fa. This behavior is probably due to the presence of a sufficient amount of oil, which reduces the impact of the backward leakage across the pump gears: the influence of the fluid viscosity on the delivered flow rate is reported in Fig. 5.9, where performances surely poorer, but still acceptable for the pump operating on the R245fa-oil mixture are highlighted. Therefore, from this stand point, the machine can be considered suitable for the application in an ORC prototype. In particular, from previously developed studies on the performances achievable by a small system capable to deliver a power of about 3 kW recovering low-temperature heat (below 150 °C), a flow rate of about 400 l/h has been calculated to be needed, while the numerical simulations described in Subsection 4.3.2 found that an approximate Δp of 12–13 bar is required at the best working conditions. It can be concluded from Fig. 5.8 that these performances can be achieved by the pump when operating at a shaft speed of 2850 rpm, i.e. its rated velocity.

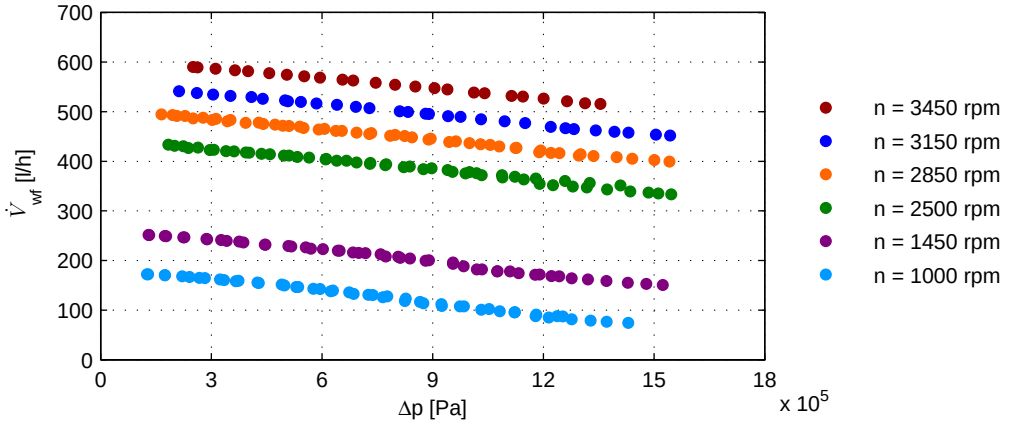

Fig. 5.8: Pump delivered flow rate as a function of the imposed differential pressure

From the trends shown in Fig. 5.10 it can be noted that the power absorbed by the pump varies in a range from 150 W to 300 W during normal operations: in particular, at the conditions already cited in the description of Fig. 5.8 ($n = 2850$ rpm and $\Delta p = 12-13$ bar), the pump absorbs a power of about 250 W. This represents a share of about 8–10% of the power delivered by the expander, a part surely remarkable, but acceptable for systems of this range of power.

The last performance of the pump analyzed during the first tests has been its global efficiency, defined by Eq. 5.1 as the ratio between the power given to the fluid (i.e. the product of the volumetric flow rate and the differential pressure) and the absorbed power:

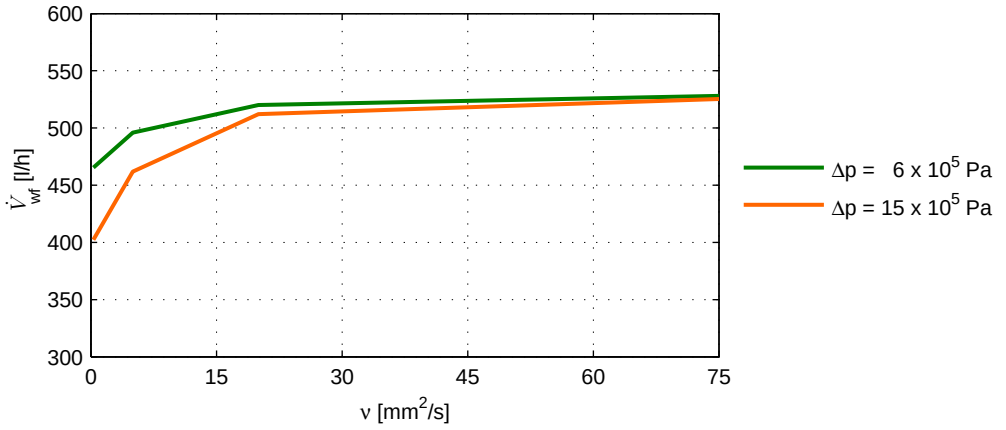

Fig. 5.9: Pump delivered flow rate as a function of the fluid viscosity

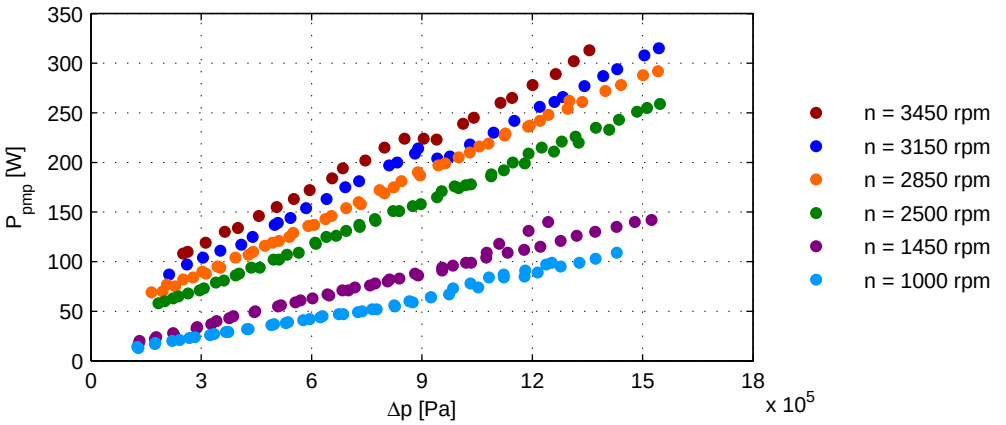

Fig. 5.10: Pump absorbed power as a function of the imposed differential pressure

$$\eta_{pmp} = \frac{\dot{V}_{wf}\Delta p}{P_{pmp}} \tag{5.1}$$

where $\dot{V}_{wf}$, in this case, is obviously expressed in m^3/s. The trends of η_{pmp} are reported in Fig. 5.11 as functions of Δp and for different values of shaft speed. As observable, except for the lowest velocities, when the relative influence of the leakage across the gears is larger, η_{pmp} is increasing with Δp, with a stabilization around a value of 0.60 for differential pressures larger than 6 bar (below this threshold the power given to the fluid is low, but the absorbed mechanical power does not decrease with the same pace, due to

the larger relative contribution of the mechanical losses). These efficiencies appear to be very interesting, in particular if compared with the values typically found in literature for the feed pumps installed in small scale ORC systems, already reported in Section 2.5.

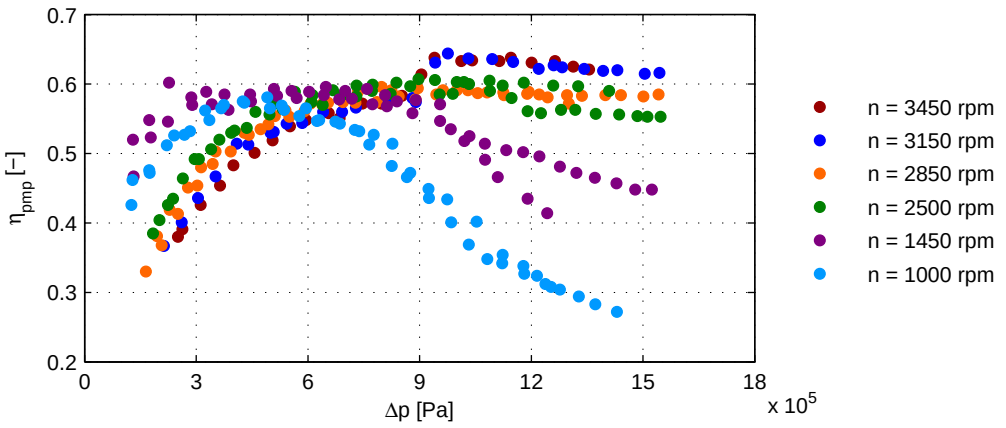

Fig. 5.11: Pump efficiency as a function of the imposed differential pressure

5.1.4 Final remarks

The test bench described in Subsection 5.1.1 has been used to conduct an experimental activity on a gear pump operating on a mixture of R245fa and oil, with the aim of evaluating its suitability for the application in an ORC system. The first measurements revealed that the pump is capable to reach the performances (flow rate and discharge pressure) needed for a proper operation of the power cycle, and also to work with a very good global efficiency.

However, the first tests have been conducted with a mixture very rich in lubricant (about 15-20% in mass), and this can mitigate excessively the bad influence of the low viscosity of R245fa on the pumpability of the fluid and on the pump efficiency. Moreover, in this phase the pump has been connected to the electric motor with the interposition of a magnetic coupling, in order to avoid any possible leakage of fluid towards ambient. This solution, in any case, appears to be quite expensive, so further measurements are required to quantify the influence of the fluid leakage through the sealings on the pump shaft and to study different technologies to lower this phenomenon below acceptable limits (e.g. using different materials for the dynamic sealings) or to avoid completely any leakage by means of lower cost systems (for example installing the pump and the relative motor together in a hermetic vessel).

For these reasons, the experimental activity on the pump has to be continued and new tests have to be concluded before a definitive statement on the actual suitability for ORC

applications can be drawn. These performance measurements will be conducted both on the specifically designed bench described in Subsection 5.1.1 (a series of tests is scheduled, aiming to evaluate the influence of the oil amount in the mixture and some modifications on the bench layout are planned in order to allow the detection of the leakage through the shaft sealings) and on a future version (currently under development) of the experimental prototype of ORC system described in the next Section 5.2.

5.2 ORC experimental prototype

After the literature and numerical studies reported in the previous Chapters, a first experimental prototype of a domestic size ORC system has been designed, built and tested, with the aim of creating a test bench useful to achieve a better knowledge of the system behavior, in both stationary and transient operating conditions. In particular, the experimental activity has been conducted together with the development of the numerical model of the prototype, carried out in AMESim® environment and described in Subsection 4.3.2.

5.2.1 Description of the prototype

The experimental facility, developed and installed in the Thermal System Laboratory at Centro Ricerche FIAT in Orbassano (Turin), Italy, is shown in the scheme of Fig. 5.12 and in the picture of Fig. 5.13. This Subsection reports a brief description of the prototype, focusing on the peculiar features of its main components. The first design choice has been the selection of the working fluid: on the basis of the considerations already reported in the previous Chapters, R245fa has been taken into account, for its thermo-physical, environmental and safety features. Since the goals of the first experimental work on the system are to achieve a general knowledge of all its components and to learn how the controllable variables could affect its performances, a simple cycle (without regeneration) has been chosen, according to the scheme reported in Fig. 5.12.

The chosen pump is an inverter-driven diaphragm unit, since this represent the most usual solution in small-sized systems, as already discussed in Section 2.5: it has been decided to start the experimental activity with this proven technology, and then, in case, to install a new machine (for example the gear pump cited in the previous Section 5.1), in order to carry on a comparative analysis among different options.

An electric boiler has been chosen to evaporate the fluid: this seemed to be the best solution for an experimental prototype, since it allows the direct setup of the superheating temperature and reduces the thermal inertia with respect to other boiling systems, therefore decreasing the time needed to reach an imposed steady state condition. Moreover, an electric boiler features a great flexibility in control strategies, allowing also the simulation of the dynamic behavior of different real heat sources, such as a condensing boiler or a solar panel system.

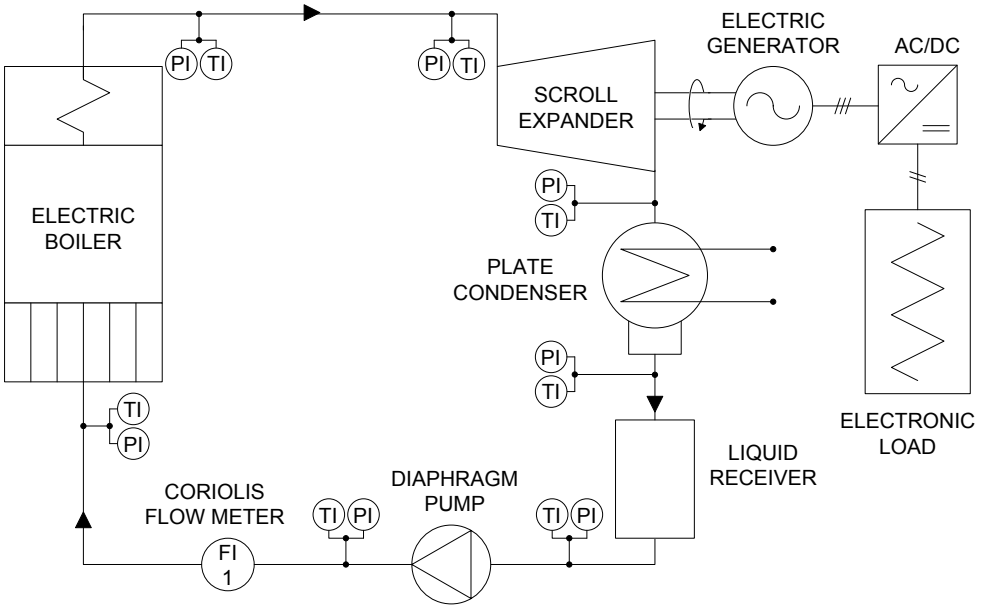

Fig. 5.12: Piping and instrumentation diagram of the ORC test bench

Following the detailed studies on the expanders described in Sections 2.4, 4.1 and 4.2, it has been decided to use a scroll machine, due to its demonstrated high isentropic efficiency and its diffusion on the market as HVAC compressor (a comprehensive analysis on the peculiar features of scroll devices is reported in Section 2.4). In particular, a small-size (about 1 kWe) unit slightly modified by the manufacturer has been installed in the system. The three-phase voltage, generated by the alternator at variable frequency (since the shaft speed of the group is free), is converted in a DC voltage by a power conditioning system. Finally, the power is dissipated on a programmable electronic load, capable to measure all the electric variables related to the DC power, while the AC frequency, measured to detect the expander shaft speed, is recorded upstream of the rectifier unit.

A commercial plate heat exchanger has been selected as the cycle condenser. Here the fluid is de-superheated, condensed and slightly subcooled by industrial water, then it flows into the liquid receiver interposed between the condenser and the feed pump.

All the hot parts of the facility have been thermal insulated, then the test bench has been completed with the auxiliaries required to fill and empty the circuit and with the measurement devices, in particular thermocouples (marked by TI in Fig. 5.12), pressure sensors (PI) and a Coriolis flow meter at the pump outlet (FI 1). The scroll expander, the condenser and the thermal insulation of the circuit are visible in detail in Fig. 5.14.

Fig. 5.13: Comprehensive view of the ORC test bench

After the circuit has been carefully purged with nitrogen and evacuated with a vacuum pump, it has been filled by a mixture of R245fa and lubricant, at the concentration required by the expander for proper operation. Since the selected oil ensures the solubility in the refrigerant and since the circuit was designed in order to reach sufficiently high velocities in all its components, the circulation of the mixture through the system is acceptable, avoiding the need of an oil separator downstream of the expander.

5.2.2 Experimental tests

The first tests conducted on the system had the aim of achieving a general knowledge of the prototype, of verifying the rough correspondence between measured and expected performances and of obtaining the set of data needed to calibrate, in stationary conditions, the ORC simulation model realized in AMESim® environment and described in Subsection 4.3.2.

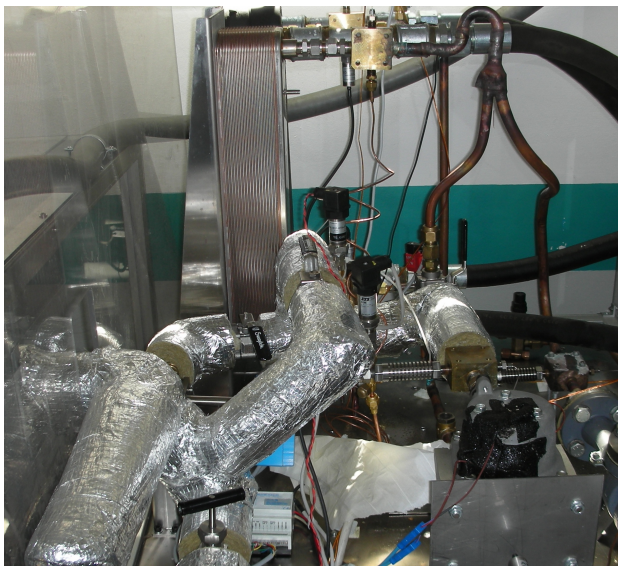

Fig. 5.14: Details of the ORC test bench

Further experimental work will be required to define properly the potentialities of the system, to optimize its efficiency and to find the best working conditions: these tests will be carried out after the definition of a suitable control strategy for the cogenerator. This task will be achieved using the already cited dynamic simulation skill of the model, that can be validated also on the basis of the actual performance of the prototype, although in this phase it is not optimized yet.

The data acquired on the system are the pressures and the temperatures of the fluid measured along the circuit, its mass flow rate and the values of the electric variables of the generated power. Two global performance indexes are taken into account: the expander isentropic efficiency, η_{is}, and the cycle electrical efficiency, η_{ORC}.

The first one has been already cited when describing the scroll expander model in Subsection 4.1.4, but the definition used in this case is slightly different, as reported in Eq. 5.2:

$$\eta_{is} = \frac{P_{exp}}{\dot{m}_{wf}(h_{inlet} - h_{dis,is})} \tag{5.2}$$

where P_{exp} is the electric power delivered by the expander (actually measured as the power dissipated on the electronic load), $\dot{m}_{wf}$ is the working fluid mass flow rate, h_{inlet} is the specific enthalpy of the fluid at the expander inlet and $h_{dis,is}$ is the specific enthalpy of the fluid after an isentropic expansion from the inlet conditions to the discharge pressure. It must be noted that this is not the classical definition of isentropic efficiency, usually adopted for the analysis of turbomachinery performances: at the numerator there is the

net delivered power (i.e. purged of mechanical and electric losses) instead of the enthalpy drop of the actual expansion (that in a turbomachinery, but not in a scroll expander, can be considered an adiabatic process, so that the enthalpy drop corresponds to the specific work). The net power is then compared to the work rate of the fluid in an ideal adiabatic expansion, within the hypothesis that kinetic energies in the expander inlet and discharge measurement sections were negligible.

The cycle electrical efficiency is defined by Eq. 5.3 as the ratio between the net electric power generated by the system and the heat rate absorbed by the fluid in the boiler:

$$\eta_{ORC} = \frac{P_{exp} - P_{pmp}}{\dot{m}_{wf}(h_{boiler,out} - h_{boiler,in})} \tag{5.3}$$

where P_{pmp} is the power absorbed by the pump and $h_{boiler,out}$ and $h_{boiler,in}$ are the specific enthalpies of the fluid at the boiler outlet and inlet respectively.

In the preliminary tests reported in this thesis, the system has been controlled adjusting three variables: the shaft speed of the pump (and therefore the volumetric flow rate flowing through the pump), the temperature of the fluid at the boiler outlet and the resistance of the electronic load (and therefore the braking torque applied on the expander). As a result of the variation of one or more of these control parameters the system reacts and, after a brief transient, it reaches a new equilibrium state, characterized by different values of the free parameters, such as the working pressures and the expander rotational speed.

The superheating degree of the fluid at the expander inlet is reported as a function of the expansion ratio (i.e. the ratio between evaporation and condensation pressures) for all the considered temperatures of vapor production, $h_{boiler,out}$, and for two pump speeds, $n_{pump} = 300\,\text{rpm}$ and $n_{pump} = 400\,\text{rpm}$, in Figs. 5.15 and 5.16 respectively. This parameter, defined as the difference between the actual fluid temperature and the saturation temperature at the actual pressure, has been used to carry out some considerations on the ORC performances and on the control system effectiveness.

As shown in the diagrams, when the temperature imposed at the boiler outlet is higher or equal to 120 °C, the superheating degree is always larger than 10 K and the quality of the vapor is known. At lower temperatures, the degree of superheating is always very close or equal to 0 K, i.e. the vapor is produced at saturated or partially saturated conditions. In this situation, in fact, the quality of the vapor cannot be controlled, since with the actual regulation system only one parameter of the fluid, the temperature, can be set and the electric heaters could be shut down when the fluid has reached only a low and unknown degree of vapor saturation. This uncertainty is increased by the inaccuracy of temperature measurements linked to thermocouples precision. So, in order to broaden the test range towards lower temperatures of the thermal source, a new control strategy will be implemented in the system regulation software, allowing the operator to set the superheating degree instead of the absolute vapor production temperature.

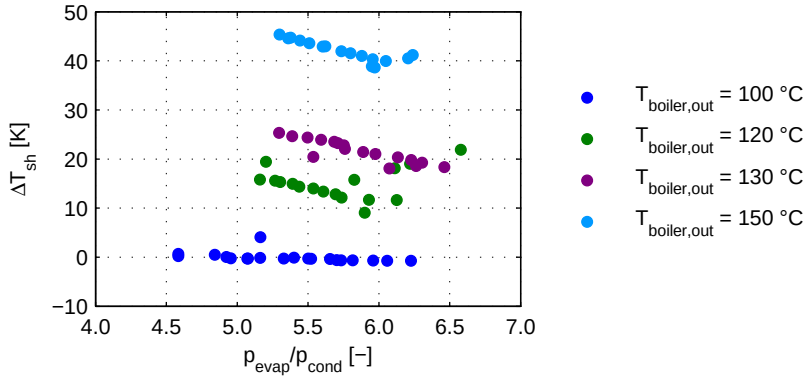

Fig. 5.15: Superheating degree at the expander inlet, $n_{pump} = 300\,\text{rpm}$

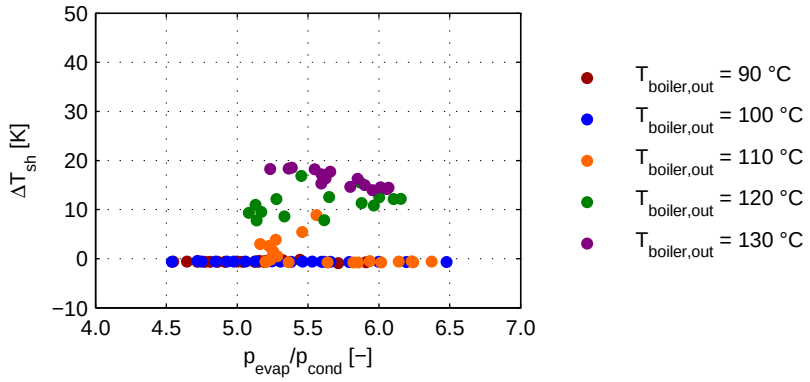

Fig. 5.16: Superheating degree at the expander inlet, $n_{pump} = 400\,\text{rpm}$

For the just explained reason, the measurement points with a degree of superheating near to 0 K have been excluded from the successive performance analysis. The isentropic efficiency of the expander, defined by Eq. 5.2, is reported in Figs. 5.17 and 5.18 as a function of the pressure ratio. The trends, slightly decreasing with the expansion ratio, show that the machine is operated in under-expansion (i.e. with a pressure ratio higher than the one defined by the geometry), which is a condition much more preferable than over-expansion, since the latter causes a quick drop of efficiency (this phenomenon has been deeply treated in Subsection 4.1.4).

The literature review carried out in Section 2.4 indicated that the average values reported for scroll expander isentropic efficiency are usually in the range from 0.60 to 0.65 [73–76], with peaks between 0.68 and 0.70 [40, 75, 77, 78]. The efficiency achieved by the tested scroll is in a good agreement with these values, as shown in Figs. 5.17 and 5.18,

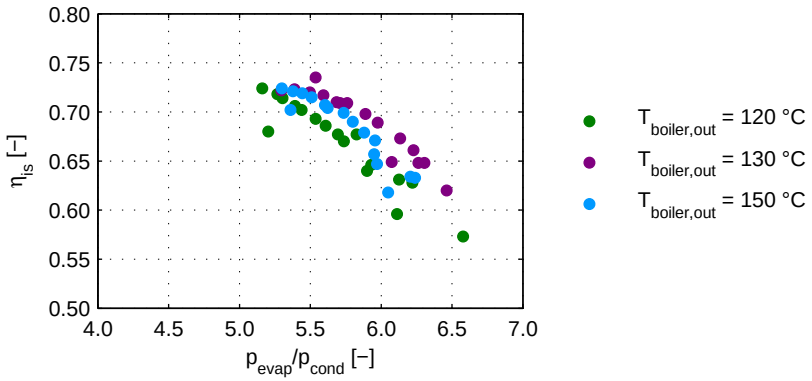

Fig. 5.17: Expander isentropic efficiency, $n_{pump} = 300\,\text{rpm}$

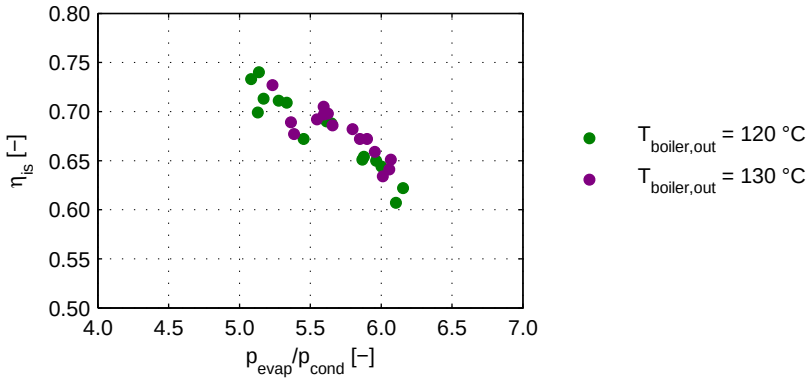

Fig. 5.18: Expander isentropic efficiency, $n_{pump} = 400\,\text{rpm}$

and this confirms that both the displacement and the built-in volumetric ratio of the machine are suitable for the cycle size, and also that the few modifications made by the manufacturer on the scroll compressor are sufficient to obtain good performances from the machine operated in expansion mode.

The electrical efficiency of the cycle, defined by Eq. 5.3, is reported in Figs. 5.19 and 5.20 at the same conditions of the previous diagrams (the error bars shown in the charts are the results of the calculations described in Subsection 5.2.3). It can be noted that the efficiency measured on the system, in all the considered working points, is always around 0.08, with only limited variations with the expansion ratio.

This last behavior is due to the combination of the scroll efficiency, slightly decreasing with the expansion ratio, as just reported in Figs. 5.17 and 5.18, and the theoretical cycle

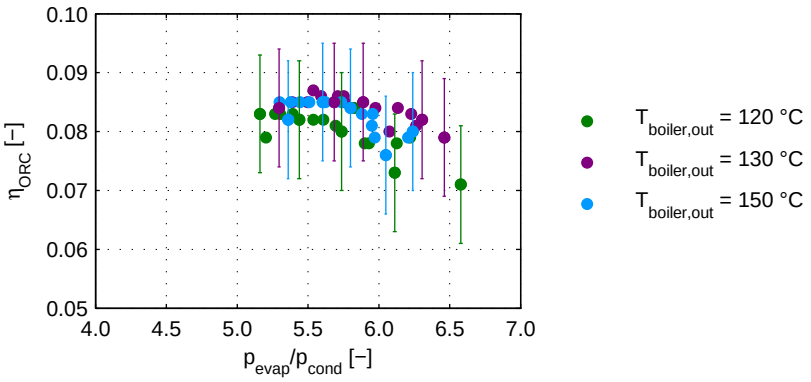

Fig. 5.19: ORC electrical efficiency, $n_{pump} = 300\,\mathrm{rpm}$

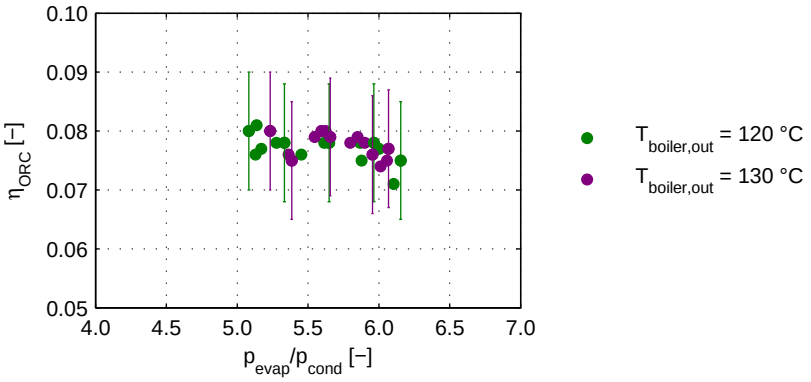

Fig. 5.20: ORC electrical efficiency, $n_{pump} = 400\,\mathrm{rpm}$

efficiency, which increases with the evaporation pressure. The mean calculated value, 0.08, appears to be in good agreement with the literature data related to not regenerative ORC systems of the same size. It must be underlined once again, however, that these are the performances of a system during its very first tests: after the optimization of the cycle, the improvement of some features such as the thermal insulation and the control system, and the possible installation of an internal recuperator (even if the choice between simple and regenerative cycles must be evaluated in each single case, as already discussed in Subsection 2.3.6 [53]), electrical efficiencies higher than 0.10 are expected, meaning very good performances, in consideration of the low maximum temperatures of the cycle.

In Figs. 5.21 and 5.22 the expander shaft speed is reported as a function of the expansion ratio, for different maximum temperatures and feed pump velocities. As already

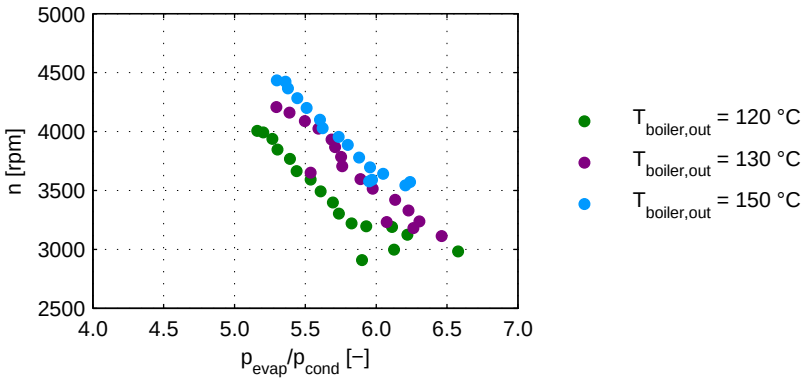

Fig. 5.21: Expander shaft speed, $n_{pump} = 300\,\text{rpm}$

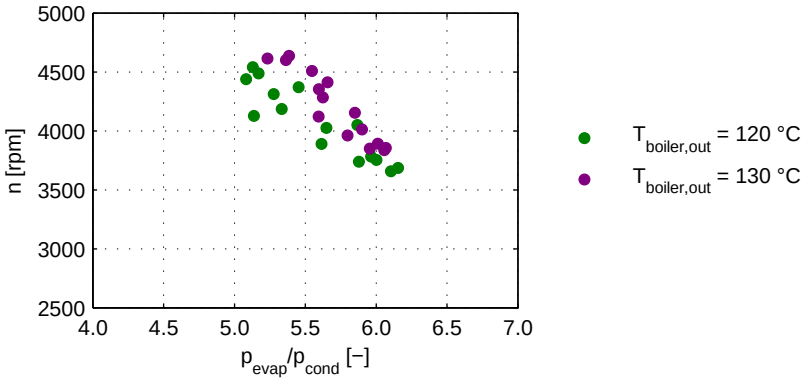

Fig. 5.22: Expander shaft speed, $n_{pump} = 400\,\text{rpm}$

written, in this prototype the scroll speed is free, being governed by the equilibrium between driving and braking torque: when a higher load is applied, the expander slows down, causing a larger chocking effect for the fluid. In this way, a higher pressure ratio is created across the machine, so finally a larger driving torque is delivered by the expander, equilibrating the braking one. The described dependence between shaft speed and expansion ratio is clearly shown in Figs. 5.21 and 5.22, where the speed assumed by the expander varies in a range from 4500 rpm to 3000 rpm against an increase of the expansion ratio from 5 to 6.5.

The velocity variations approximately counterbalance the different torque regulations so that, as reported in Figs. 5.23 and 5.24, the delivered power at given values of pump speed and vapor temperature is more or less constant with the expansion ratio, and it varies from 1100 W at the lower pump speed and minimum vapor temperature to

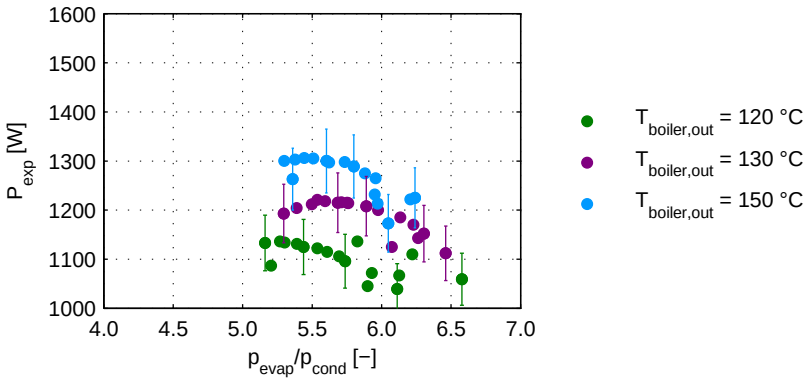

Fig. 5.23: Expander delivered power, $n_{pump} = 300\,\text{rpm}$

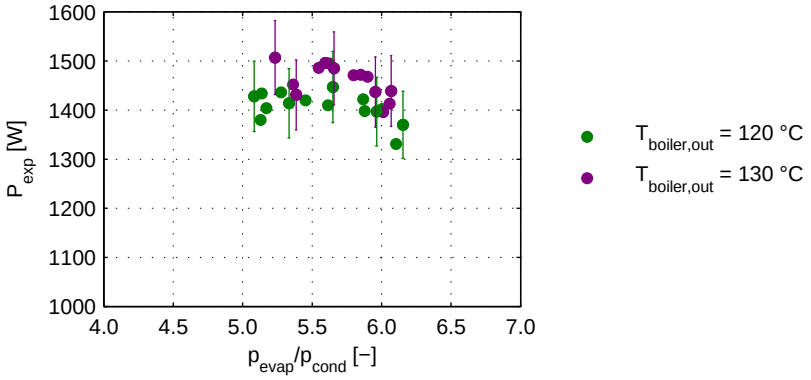

Fig. 5.24: Expander delivered power, $n_{pump} = 400\,\text{rpm}$

1500 W at the highest ones (the error bars shown in the diagrams are the results of the calculations described in Subsection 5.2.3).

It is interesting to note, in Figs. 5.15 to 5.24, that the pump speed and thus the R245fa flow rate do not influence significantly the performances of the system, with the obvious exception of delivered power, which increases with the mass flow rate.

5.2.3 Analysis of the errors in the experimental measurements

The theory of error propagation has been applied on the data measured on the test facility, in order to define the uncertainty ranges of the two main global working parameters, i.e. the delivered electric power and the cycle efficiency. This analysis appears to be fundamental, since, in case of important measurement errors, the actual system

efficiency could be very low, far from the promising values calculated in the previous Subsection 5.2.2 (around 0.08).

The electric power has been calculated, in Eq. 5.4, as the product of the direct voltage U and current I measured on the electronic load:

$$P_{el} = UI \tag{5.4}$$

The absolute uncertainty in the evaluation of the delivered power, expressed by Eq. 5.5, can therefore be obtained applying the formula of errors propagation on Eq. 5.4, which is a function of two not correlated variables, U and I:

$$\Delta P_{el} = \sqrt{\left(\frac{\partial P_{el}}{\partial U}\Delta U\right)^2 + \left(\frac{\partial P_{el}}{\partial I}\Delta I\right)^2} \tag{5.5}$$

where ΔU and ΔI are the absolute uncertainties in the measurements of voltage and current, respectively.

The voltmeter used during the tests features a declared accuracy equal to 0.7% of the read value, so ΔU varies for each different measurement point, while the ammeter accuracy is reported as a fraction of the instrument full scale range, then ΔI is considered constant and equal to 0.2 A. Starting from Eq. 5.5, the expression of the relative error in the definition of the power delivered by the expander is given by Eq. 5.6:

$$e_P = \sqrt{(e_U)^2 + (e_I)^2} \tag{5.6}$$

where e_U and e_I represent the relative uncertainties in the measurements of voltage and current respectively. The results achieved from Eq. 5.6, when applied on the data obtained from the different measurement points, vary in a narrow range, so a constant value can be assumed for e_P, equal to 5%. The uncertainties on the delivered power, calculated according to the just described procedure, have been reported, in form of bars, in Figs. 5.23 and 5.24.

The expression of the cycle electrical efficiency, defined by Eq. 5.3, is quite more complex, since it involves, among the other variables, the specific enthalpy of the fluid at the boiler inlet and outlet. The enthalpy values have been calculated, as reported in Eq. 5.7, as functions of temperature and pressure, two directly measured, so uncorrelated, variables:

$$h = (T, p) \tag{5.7}$$

Therefore the expression of the absolute uncertainty in the enthalpy estimation is given by Eq. 5.8:

$$\Delta h = \sqrt{\left(\frac{\partial h}{\partial T}\Delta T\right)^2 + \left(\frac{\partial h}{\partial p}\Delta p\right)^2} \tag{5.8}$$

where ΔT and Δp are the absolute uncertainties in the measurements of temperature and pressure respectively.

The analysis of the temperature measurement chain (from the thermocouples to the data acquisition system) installed on the prototype led to the conclusion that ΔT can be considered, to a good approximation, equal to 0.63 K when the measured value is lower than 90 °C and equal to 0.90 K beyond this threshold. Furthermore, the calibration of the pressure sensors revealed that the uncertainty is linearly dependent (on first approximation) from the measured value, so Δp is defined by Eq. 5.9:

$$\Delta p = 0.0266 \cdot p + 0.2318 \cdot 10^5 \tag{5.9}$$

where p is the measured value for the pressure.

The equation of state used to calculate the thermodynamic properties of the refrigerant R245fa, and thus to express explicitly the relationship defined in Eq. 5.7, is the equation derived by Lemmon and Span [107]: for R245fa, this equation introduces an uncertainty in the properties calculation equal to 1.18%, when the refrigerant is in the gaseous state, or to 0.10%, when in the liquid state. The final expression of the relative uncertainty in the calculation of the fluid specific enthalpy is then reported in Eq. 5.10:

$$e_h = \sqrt{\left(\frac{\Delta h}{h}\right)^2 + {e_{LS}}^2} \tag{5.10}$$

where e_{LS} is the relative error introduced with the equation by Lemmon and Span.

As written in Eq. 5.3, another contribution in the efficiency formula is given by the refrigerant flow rate. The error introduced by the flow rate measurement chain, made up of a Coriolis flow meter and of its data acquisition system, is equal to 0.23%.

The application of all the equations described above, together with other simple calculations, led to determine the relative uncertainty on the cycle electrical efficiency, e_η, referred to each measurement point. It resulted to be practically constant, as in the case of the delivered power error, and equal to 13% of the calculated values, corresponding to one efficiency point when η_{ORC} is 0.08. A representation of these errors is given by the bars reported in Figs. 5.19 and 5.20.

5.2.4 Final remarks

The tests conducted on the ORC prototype described in this Section revealed promising performances, with a global electric efficiency of about 0.08, even if these have been the very first tests and all the components of the cycle need an optimization. However, some operating limits have been detected, mainly related to an unsuitable control of the vapor quality at the boiler output when the maximum temperature of the cycle is set to low values: this problem has to be overcome in a future, improved version of the prototype. For this reason, further field tests on the system are scheduled, aimed to the development of a new, more performing prototype, using also the numerical model described in Subsection 4.3.2.

6 Conclusions

In the field of energy sustainability, one of the most important opportunities is represented by the exploitation of low temperature heat to generate electricity. The literature review conducted in the present thesis revealed that the number of possible sources is very large: among the others, the examples with the highest potential have been recognized in renewable energies such as solar, geothermal or biomass and in heat recovery from industrial processes and internal combustion engines.

The ORCs represent today one of the most studied solutions in this framework, due in particular to their suitability for low temperature and small size sources. An extensive bibliographic analysis has been carried out in Chapter 2, where the great potentiality of the ORCs has been confirmed, as well as their current relatively limited exploitation, particularly in the smallest scales. For this reason, domestic size systems have been chosen as the main subject of the research. Besides the general study of the cycle, particular attention has been reserved for the elements most influencing the system performances, i.e. the working fluid, the expander and the feed pump.

A fluid screening has been conducted by means of a multi-objective optimization based on the Process Integration, referring to the case-study of an ORC system coupled with a biomass boiler sized to satisfy the heat demand of a residential building. The results of the calculations, reported in Chapter 3, detected a refrigerant, R245fa, and two hydrocarbons, isopentane and isobutane, as the best performing fluids in small systems operating at limited pressures. Among these, R245fa is favorite by the possibility to work satisfactorily at lower temperatures of the heat source, by its null ODP and by its very low toxicity. For these reasons, R245fa has been finally selected and used in the experimental facilities built and tested during this work, confirming the choice widely adopted and reported in literature by researchers on small scale ORC systems.

Dedicated numerical codes have been developed for the modelization of two different expanders, as described in Chapter 4. The analysis of the first machine, a scroll expander derived from a commercial compressor, revealed the suitability of the device for the installation on a domestic sized ORC cogenerator: the best achievable isentropic efficiency is around 0.65, in good agreement with the values reported in literature, and

the simulations predicted also an acceptable behavior of the machine in working conditions quite different from the rated ones. Besides, the possibility to realize an expander starting from a commercial scroll compressor, with only minor revisions, leads to a great reduction in the costs, an unavoidable condition for small scale systems. A second model has been realized for a reciprocating expander: even in this case very good performances have been predicted (with a maximum isentropic efficiency in the order of 0.65), but the transformation of a commercial piston-type compressor for this purpose appeared to be unfeasible, leading to the need for a dedicated, completely new design and to a not negligible increasing of the costs. For this reason, the scroll machine has been finally designated as the expander for all the further system models and for the experimental prototypes.

The numerical study of the system has been conducted with two different models, described in Chapter 4. The first of them, implemented in Aspen Plus® environment, has been aimed to the preliminary simulations of a system currently under construction in the Department of Engineering and Architecture at University of Trieste, while the second, realized with the commercial software AMESim®, concerned a prototype already built and tested in the Thermal System Laboratory at Centro Ricerche FIAT in Orbassano (Turin), Italy. Both models, besides confirming the achievability of the performances reported in literature for a small scale ORC cogenerator exploiting a low temperature thermal source, exhibited a good accuracy in the prediction of the system performances, so they can be considered very useful tools for the investigation of the cogenerator behavior in a wide range of operating conditions and working parameters.

The experimental work conducted on a gear pump originally designed for light oils highlighted, as reported in Chapter 5, that the machine is suitable for operations with a mixture of R245fa and oil, achieving acceptable performances despite the very low viscosity of the refrigerant fluid. In particular, it has been demonstrated that the pump is capable to deliver the flow rate needed by a domestic scale ORC system at the requested pressure, with an overall efficiency around 0.60 and at its rated rotational speed, avoiding the need for an inverter. However, the tests completed up to now featured only a mixture very rich in oil, and the influence of the lubricant on the pump performances has not been quantified yet. Moreover, the usage of a magnetic coupling on the pump shaft completely avoided the problem of leakage, but this solution features a relatively high cost: a quantification of the fluid leaking through the shaft sealings is then needed, in order to evaluate the importance of the phenomenon and to verify the feasibility of different and cheaper solutions.

Finally, the experimental prototype of a complete, small size ORC unit has been developed, built and tested. The measurements conducted on the facility, reported in Chapter 5, allowed to conclude the great potentiality of a such designed system in the production of electric power from a low temperature heat source. In particular, an electrical efficiency in the order of 0.08 has been detected for the system, even if the internal regeneration has not been implemented yet and an optimization has still to be completed for both the single components and the global configuration. After these

improvements, a global electrical efficiency around 0.12 is expected from the prototype, this representing a very good value, in consideration of the small scale and of the low working temperatures. On the other hand, some problems have been detected in the system operations, in particular due to a bad control strategy currently adopted for the setting of the vapor production temperature: this has to be modified, in order to ensure a widening of the operational range of the unit towards low temperatures, the most interesting conditions in this field. All these considerations finally demonstrated the need for further work on the system, with the aim of developing a cogenerator with good performances and economically feasible.

In conclusion, this thesis contributed to demonstrate the great potentiality of ORC technology even in smaller scale systems and for domestic applications. However, the researches described in the previous Chapters have to be completed in order to confirm the already achieved results and to obtain the information needed for the realization of a commercial prototype of domestic ORC cogenerator.

Nomenclature

Notation	Description
A_{d-dd}	flow area of the discharge ports, [m^2]
A_{suct}	flow area of the suction ports, [m^2]
b	availability, [J/kg]
$b_{hs,in}$	availability of the heating system water at the heat exchanger inlet, [J/kg]
$b_{hs,out}$	availability of the heating system water at the heat exchanger outlet, [J/kg]
$b_{hw,in}$	availability of the fresh water at the heat exchanger inlet, [J/kg]
$b_{hw,out}$	availability of the produced hot water at the heat exchanger outlet, [J/kg]
c_v	isochoric specific heat, [J/(kg K)]
e_h	relative error in the enthalpy evaluation, [-]
e_I	relative error in the current measurement, [-]
e_{LS}	relative error introduced with the equation by Lemmon and Span, [-]
e_P	relative error in the power evaluation, [-]
e_U	relative error in the voltage measurement, [-]
e_η	relative error in the evaluation of the cycle electrical efficiency, [-]
h	enthalpy, [J/kg]
$h_{boiler,in}$	enthalpy of the fluid at the boiler inlet, [J/kg]
$h_{boiler,out}$	enthalpy of the fluid at the boiler outlet, [J/kg]
$h_{dis,is}$	enthalpy of the fluid at discharge after an isentropic process, [J/kg]
h_{in}	enthalpy of the fluid when entering the control volume, [J/kg]
h_{inlet}	enthalpy of the fluid at inlet, [J/kg]
h_s	scroll height, [m]
$h_{scr,in}$	enthalpy of the fluid at the inlet of the scroll zone, [J/kg]

Notation	Description
$h_{scr,out}$	enthalpy of the fluid at the outlet of the scroll zone, [J/kg]
$h_{suction}$	enthalpy of the fluid at suction, [J/kg]
I	current, [A]
K	level of the scroll chambers, [-]
K_{max}	maximum level of the scroll chambers, [-]
LHV_{bm}	biomass lower heating value, [J/kg]
m	mass, [kg]
$\dot{m}_{bm}$	biomass flow rate, [kg/s]
$\dot{m}_{hs}$	flow rate of the heating system water, [kg/s]
$\dot{m}_{hw}$	flow rate of the produced hot water, [kg/s]
$\dot{m}_{in}$	flow rate entering the control volume, [kg/s]
$\dot{m}_{out}$	flow rate exiting from the control volume, [kg/s]
$\dot{m}_{wf}$	working fluid flow rate, [kg/s]
n	shaft speed, [rev./s]
n_{pump}	pump shaft speed, [rev./s]
P_{el}	electric power, [W]
P_{exp}	power delivered by the expander, [W]
P_{pmp}	power absorbed by the pump, [W]
p	pressure, [Pa]
p_{cond}	condensation pressure, [Pa]
$p_{discharge}$	discharge pressure, [Pa]
p_{evap}	evaporation pressure, [Pa]
$p_{scr,out}$	pressure of the fluid at the outlet of the scroll zone, [Pa]
$p_{suction}$	suction pressure, [Pa]
$\dot{Q}$	heat, [W]
$\dot{Q}_{hs}$	power of the floor heating system, [W]
$\dot{Q}_{hw}$	power of the hot water production system, [W]
r_b	radius of the basic circumference, [m]
r_c	radius of the circular arc forming the inner portion of the scrolls, [m]
r_o	radius of the orbiting circular path, [m]

Notation	Description
s	entropy, [J/(kg K)]
T	temperature, [K]
T_{amb}	ambient temperature, [K]
$T_{discharge}$	discharge temperature, [K]
$T_{exp,in}$	expander inlet temperature, [K]
U	voltage, [V]
V	volume, [m^3]
$V_{c,K}$	volume of a compression chamber in the K-th level, [m^3]
V_{cl}	clearance volume, [m^3]
$V_{cut-off}$	cylinder internal volume at cut-off, [m^3]
V_d	volume of a lateral discharge chamber, [m^3]
V_{dd}	volume of the inner discharge chamber, [m^3]
V_{d-dd}	volume of the unique discharge zone, [m^3]
V_{displ}	displacement of the machine, [m^3]
V_s	volume of a suction chamber, [m^3]
V_{UDC}	cylinder internal volume at UDC, [m^3]
$\dot{V}_{wf}$	working fluid volumetric flow rate, [l/h]
v	specific volume, [m^3/kg]
$v_{scr,out}$	specific volume of the fluid at the outlet of the scroll zone, [m^3/kg]
$\dot{W}_f$	power of a real transformation of the fluid, [W]
$\dot{W}_{loss}$	power dissipated in mechanical losses, [W]
w_{d-dd}	width of the opening between scrolls, [m]
(x_i, y_i)	coordinates of the inner profile, [m]
(x_o, y_o)	coordinates of the outer profile, [m]

Greek symbols

α_i	starting angle of the inner involute, [rad]
α_o	starting angle of the outer involute, [rad]
β	coefficient for scroll geometry definition, [rad]
γ_{speed}	corrective factor for the radial gap size with the shaft speed, [-]

Notation	Description
Δh	absolute uncertainty in the evaluation of the enthalpy, [J/kg]
ΔI	absolute uncertainty in the measurement of the current, [A]
Δp	differential pressure, [Pa]
Δp	absolute uncertainty in the measurement of the pressure, [Pa]
ΔP_{el}	absolute uncertainty in the evaluation of the power, [W]
ΔT	absolute uncertainty in the measurement of the temperature, [K]
ΔT_{sh}	superheating degree, [K]
ΔU	absolute uncertainty in the measurement of the voltage, [V]
δ_f	flank gap between scrolls, [mm]
δ_r	radial gap between scrolls, [mm]
$\varepsilon_{ch,bm}$	biomass chemical exergy, [J/kg]
ε_v	volumetric expansion ratio, [-]
η_I	first law efficiency, [-]
η_{II}	exergy efficiency, [-]
η_{is}	isentropic efficiency, [-]
η_{ORC}	efficiency of the organic Rankine cycle, [-]
η_{pmp}	efficiency of the pump, [-]
η_{vol}	volumetric efficiency, [-]
θ	shaft angle, [rad]
θ_d	scroll shaft angle at discharge position, [rad]
Φ	cut-off ratio, [-]
φ	involute angle, [rad]
φ_e	ending angle of the involutes, [rad]
φ_{is}	initial angle of the inner spiral, [rad]
φ_K	involute angle of the innermost contact point between scrolls, [rad]
φ_{os}	initial angle of the outer spiral, [rad]
ρ	density, [kg/m^3]
ω	rotational speed, [rad/s]

Acronyms

Notation	Description
ALT	Atmospheric Lifetime
BDC	Bottom Dead Center
CFCs	Chlorofluorocarbons
CHP	Combined Heat and Power
COP	Coefficient of Performance
CSP	Concentrating Solar Power
DHC	District Heating and Cooling
GHG	Greenhouse Gas
GWP	Global Warming Potential
HCFCs	Hydrochlorofluorocarbons
HFCs	Hydrofluorocarbons
HFEs	Hydrofluoroethers
HVAC	Heating, Ventilation and Air Conditioning
ICE	Internal Combustion Engine
LNG	Liquefied Natural Gas
ODP	Ozone Depletion Potential
ORC	Organic Rankine Cycle
ORV	Open Rack Vaporizer
OTEC	Ocean Thermal Energy Conversion
RO	Reverse Osmosis
RTD	Resistance Temperature Detector
UDC	Upper Dead Center
WHR	Waste Heat Recovery

Bibliography

[1] U. S. Energy Information Administration. International Energy Outlook 2011. *Technical Report*, 2011.

[2] Eni S.p.A. World oil and gas review 2011. *Technical Report*, 2011.

[3] International Energy Agency. Combined heat and power - Evaluating the benefits of greater global investment. *Technical Report*, 2008.

[4] V. M. Nguyen, P. S. Doherty, and S. B. Riffat. Development of a prototype low-temperature Rankine cycle electricity generation system. *Applied Thermal Engineering*, 21:169–181, 2001.

[5] F. A. Al-Sulaiman, F. Hamdullahpur, and I. Dincer. Trigeneration: a comprehensive review based on prime movers. *International Journal of Energy Research*, 35:233–258, 2011.

[6] T. C. Hung, T. Y. Shai, and S. K. Wang. A review of organic Rankine cycles (ORCs) for the recovery of low-grade waste heat. *Energy*, 22:661–667, 1997.

[7] D. Wei, X. Lu, Z. Lu, and J. Gu. Performance analysis and optimization of organic Rankine cycle (ORC) for waste heat recovery. *Energy Conversion and Management*, 48:1113–1119, 2007.

[8] L. Wei, Y. Zhang, Y. Mu, X. Yang, and X. Chen. Efficiency improving strategies of low-temperature heat conversion systems using organic Rankine cycles: an overview. *Energy Sources, Part A: Recovery, Utilization, and Environmental Effects*, 33:869–878, 2011.

[9] U. Desideri and G. Bidini. Study of possible optimisation criteria for geothermal power plants. *Energy Conversion and Management*, 38:1681–1691, 1997.

[10] A. M. Delgado-Torres and L. Garcia-Rodriguez. Analysis and optimization of the low-temperature solar organic Rankine cycle (ORC). *Energy Conversion and Management*, 51:2846–2856, 2010.

[11] D. Gewald, A. Schuster, H. Spliethoff, and N. König. Comparative study of water-steam- and organic-Rankine-cycles as bottoming cycles for heavy-duty Diesel engines by means of exergetic and economic analysis. In *Proceedings of the 23rd International Conference on Efficiency, Cost, Optimization, Simulation and Environmental Impact of Energy Systems - ECOS2010, Lausanne, Switzerland*, 2010.

[12] B. F. Tchanche, G. Lambrinos, A. Frangoudakis, and G. Papadakis. Low-grade heat conversion into power using organic Rankine cycles - A review of various applications. *Renewable and Sustainable Energy Reviews*, 15:3963–3979, 2011.

[13] E. Wali. Optimum working fluids for solar powered Rankine cycle cooling of buildings. *Solar Energy*, 25:235–241, 1980.

[14] H. H. Dow. Diphenyl oxide bi-fluid power plants. *Journal of the American Society for Naval Engineers*, 38:940–950, 1926.

[15] S. K. Ray and G. Moss. Fluorochemicals as working fluids for small Rankine cycle power units. *Advanced Energy Conversion*, 6:89–102, 1966.

[16] R. H. Sawyer and S. Ichikawa. The organic Rankine cycle system, its application to extract energy from low temperature waste heat. In *Proceedings of the 2nd Industrial Energy Technology Conference, Houston, TX, USA*, 1980.

[17] T. A. Davidson. Design and analysis of a 1 kW Rankine power cycle, employing a multi-vane expander, for use with a low temperature solar collector. *Bachelor's Thesis, Massachusetts Institute of Technology*, 1977.

[18] H. M. Curran. Use of organic working fluids in Rankine engines. *Journal of Energy*, 5:218–223, 1981.

[19] O. Badr, P. W. O'Callaghan, M. Hussein, and S. D. Probert. Multi-vane expanders as prime movers for low-grade energy organic Rankine-cycle engines. *Applied Energy*, 16:129–146, 1984.

[20] K. K. Srinivasan, P. J. Mago, and S. R. Krishnan. Analysis of exhaust waste heat recovery from a dual fuel low temperature combustion engine using an organic Rankine cycle. *Energy*, 35:2387–2399, 2010.

[21] ORC 2011. First International Seminar on ORC Power Systems, 22-23 September 2011, TU Delft, The Netherlands. `http://www.orc2011.nl/`, Last accessed: February 2013.

[22] S. Quoilin and V. Lemort. Technological and economical survey of organic Rankine cycle systems. In *Proceedings of the 5th European Conference Economics and Management of Energy in Industry - ECEMEI2009, Vilamoura, Portugal*, 2009.

[23] H. Chen, D. Y. Goswami, and E. K. Stefanakos. A review of thermodynamic cycles and working fluids for the conversion of low-grade heat. *Renewable and Sustainable Energy Reviews*, 14:3059–3067, 2010.

[24] M. Z. Stijepovic, P. Linke, A. I. Papadopoulos, and A. S. Grujic. On the role of working fluid properties in organic Rankine cycle performance. *Applied Thermal Engineering*, 36:406–413, 2012.

[25] G. Manfrida. Clean energy from the ground: new technologies for a sustainable use of geothermal resources. In *Proceedings of the 3rd International Conference on Contemporary Problems of Thermal Engineering - CPOTE2012, Gliwice, Poland*, 2012.

[26] W. W. Husband and A. Beyene. Low-grade heat-driven Rankine cycle, a feasibility study. *International Journal of Energy Research*, 32:1373–1382, 2008.

[27] United Nations Environment Programme. The Montreal protocol on substances that deplete the ozone layer. *International Protocol*, 1987.

[28] P. J. Mago, L. M. Chamra, and C. Somayaji. Performance analysis of different working fluids for use in organic Rankine cycles. *Proceedings of the Institution of Mechanical Engineers, Part A: Journal of Power and Energy*, 221:255–264, 2007.

[29] A. Schuster, S. Karellas, E. Kakaras, and H. Spliethoff. Energetic and economic investigation of organic Rankine cycle applications. *Applied Thermal Engineering*, 29:1809–1817, 2009.

[30] E. Barbier. Geothermal energy technology and current status: an overview. *Renewable and Sustainable Energy Reviews*, 6:3–65, 2002.

[31] A. Franco and M. Villani. Optimal design of binary cycle power plants for water-dominated, medium-temperature geothermal fields. *Geothermics*, 38:379–391, 2009.

[32] R. DiPippo. Second law assessment of binary plants generating power from low-temperature geothermal fluids. *Geothermics*, 33:565–586, 2004.

[33] A. Borsukiewicz-Gozdur and W. Nowak. Comparative analysis of natural and synthetic refrigerants in application to low temperature Clausius-Rankine cycle. *Energy*, 32:344–352, 2007.

[34] F. Heberle and D. Bruggemann. Exergy based fluid selection for a geothermal organic Rankine cycle for combined heat and power generation. *Applied Thermal Engineering*, 30:1326–1332, 2010.

[35] S. Canada, G. Cohen, R. Cable, D. Brosseau, and H. Price. Parabolic Trough organic Rankine cycle solar power plant. In *Proceedings of the 2004 DOE Solar Energy Technologies, Denver, CO, USA*, 2004.

[36] A. M. Delgado-Torres and L. Garcia-Rodriguez. Preliminary assessment of solar organic Rankine cycles for driving a desalination system. *Desalination*, 216:252–275, 2007.

[37] X. D. Wang, L. Zhao, J. L. Wang, W. Z. Zhang, X. Z. Zhao, and W. Wu. Performance evaluation of a low-temperature solar Rankine cycle system utilizing R245fa. *Solar Energy*, 84:353–364, 2010.

[38] J. L. Wang, L. Zhao, and X. D. Wang. A comparative study of pure and zeotropic mixtures in low-temperature solar Rankine cycle. *Applied Energy*, 87:3366–3373, 2010.

[39] L. Jing, P. Gang, and J. Jie. Optimization of low temperature solar thermal electric generation with organic Rankine cycle in different areas. *Applied Energy*, 87:3355–3365, 2010.

[40] M. Kane, D. Larrain, D. Favrat, and Y. Allani. Small hybrid solar power system. *Energy*, 28:1427–1443, 2003.

[41] F. Trieb, O. Langniss, and H. Klaiss. Solar electricity generation - a comparative view of technologies, costs and environmental impact. *Solar Energy*, 59:89–99, 1997.

[42] G. Raluy, L. Serra, and J. Uche. Life cycle assessment of MSF, MED and RO desalination technologies. *Energy*, 31:2361–2372, 2006.

[43] D. Manolakos, S. Kyritsis, J. Karagiannis, and P. Soldatos. Cost analysis of an autonomous low-temperature solar Rankine cycle system for reverse osmosis desalination. In *Proceedings of the 2005 International Conference on Environment, Ecosystems and Development - WSEAS , Venice, Italy*, 2005.

[44] D. Manolakos, G. Kosmadakis, S. Kyritsis, and G. Papadakis. Identification of behaviour and evaluation of performance of small scale, low-temperature organic Rankine cycle system coupled with a RO desalination unit. *Energy*, 34:767–774, 2009.

[45] I. W. Eames, S. Aphornratana, and H. Haider. A theoretical and experimental study of a small-scale steam jet refrigerator. *International Journal of Refrigeration*, 18:378–386, 1995.

[46] J. Demierre and D. Favrat. Low power ORC-ORC systems for heat pump applications. In *Proceedings of the 9th International International Energy Agency Heat Pump Conference, Zurich, Switzerland*, 2008.

[47] J. Demierre, S. Henchoz, and D. Favrat. Prototype of a thermally driven heat pump based on integrated organic Rankine cycles (ORC). In *Proceedings of the 23rd International Conference on Efficiency, Cost, Optimization, Simulation and Environmental Impact of Energy Systems - ECOS2010, Lausanne, Switzerland*, 2010.

[48] L. Dong, H. Liu, and S. Riffat. Development of small-scale and micro-scale biomass-fuelled CHP systems - a literature review. *Applied Thermal Engineering*, 29:2119–2126, 2009.

[49] U. Drescher and D. Bruggermann. Fluid selection for the organic Rankine cycle (ORC) in biomass power and heat plants. *Applied Thermal Engineering*, 27:223–228, 2007.

[50] R. Bini and E. Manciana. Organic Rankine cycle turbogenerators for combined heat and power production from biomass. In *Proceedings of the 3rd Munich Discussion Meeting "Energy Conversion from Biomass Fuels Current Trends and Future Systems", Munich, Germany*, 1996.

[51] L. Lombardi, A. Corti, and E. Carnevale. Energy recovery from biogas: internal combustion engines coupled with organic Rankine cycle. In *Proceedings of the 23rd International Conference on Efficiency, Cost, Optimization, Simulation and Environmental Impact of Energy Systems - ECOS2010, Lausanne, Switzerland*, 2010.

[52] G. Ast, H. Kopecek, J. Gomez, P. Huck, T. Frey, B. Wilmsen, and F. Gruber. Experimental investigation of an organic Rankine cycle prototype plant being developed to boost the electric output of gas engine power stations. In *Proceedings of the ASME International Combustion Engine Division 2009 Fall Technical Conference - ICEF2009, Lucerne, Switzerland*, 2009.

[53] I. Vaja and A. Gambarotta. Internal combustion engine (ICE) bottoming with organic Rankine cycles (ORCs). *Energy*, 35:1084–1093, 2010.

[54] J. Bonafin, P. Pinamonti, M. Reini, and P. Tremuli. Performance improving of an internal combustion engine for ship propulsion with a bottom ORC. In *Proceedings of the 23rd International Conference on Efficiency, Cost, Optimization, Simulation and Environmental Impact of Energy Systems - ECOS2010, Lausanne, Switzerland*, 2010.

[55] Y. Durmusoglu, T. Satir, C. Deniz, and A. Kilic. A novel energy saving and power production system performance analysis in marine power plant using waste heat. In *Proceedings of the 8th International Conference on Machine Learning and Applications - ICMLA2009, Miami Beach, FL, USA*, 2009.

[56] R. Aumann, A. Grill, A. Schuster, and H. Spliethoff. Evaluation of fuel saving and economics for an organic Rankine cycle as bottoming cycle in utility vehicles. In *Proceedings of the 23rd International Conference on Efficiency, Cost, Optimization, Simulation and Environmental Impact of Energy Systems - ECOS2010, Lausanne, Switzerland*, 2010.

[57] M. Yari and S. M. S. Mahmoudi. Utilization of waste heat from GT-MHR for power generation in organic Rankine cycles. *Applied Thermal Engineering*, 30:366–375, 2010.

[58] R. Chawla. Nuclear power plants - Lecture notes. *Laboratory for reactor physics and systems behaviour, EPFL*, 2011.

[59] W. Qiang, L. Yanzhong, and W. Jiang. Analysis of power cycle based on cold energy of liquefied natural gas and low-grade heat source. *Applied Thermal Engineering*, 24:539–548, 2004.

[60] J. Maertens. Design of Rankine cycles for power generation from evaporating LNG. *International Journal of Refrigeration*, 9:137–143, 1986.

[61] Y. Hisazumi, Y. Yamasaki, and S. Sugiyama. Proposal for a high efficiency LNG power generation syste, utilizing waste heat from the combined cycle. *Applied Energy*, 60:169–182, 1998.

[62] C. Invernizzi, P. Iora, and P. Silva. Bottoming micro-Rankine cycles for micro-gas turbines. *Applied Thermal Engineering*, 27:100–110, 2007.

[63] M. Yari. Thermodynamic analysis of a combined micro turbine with a micro ORC. In *Proceedings of the ASME Turbo Expo 2008, Berlin, Germany*, 2008.

[64] O. Badr, S. Naik, P. W. O'Callaghan, and S. D. Probert. Expansion machine for a low power-output steam Rankine-cycle engine. *Applied Energy*, 39:93–116, 1991.

[65] G. Haiqing, M. Yitai, and L. Minxia. Some design features of CO2 swing piston expander. *Applied Thermal Engineering*, 26:237–243, 2006.

[66] G. Manfrida and S. Padula. Model of a steam Wankel expander. In *Proceedings of the 23rd International Conference on Efficiency, Cost, Optimization, Simulation and Environmental Impact of Energy Systems - ECOS2010, Lausanne, Switzerland*, 2010.

[67] L. Creux. Rotary engine. *U.S. Patent no. 801,182*, Oct. 3rd 1905.

[68] N. O. Young. Scroll-type positive fluid displacement apparatus. *U.S. Patent no. 3,884,599*, May 20th 1975.

[69] J. E. McCullough and F. Hirschfeld. The scroll machine - an old principle with a new twist. *Mechanical Engineering*, 101(12):46–51, 1979.

[70] K. T. Ooi and J. Zhu. Convective heat transfer in a scroll compressor chamber: a 2-D simulation. *International Journal of Thermal Sciences*, 43:677688, 2004.

[71] Copeland Corporation. Scroll compressor technology and air conditioning, heat pump and refrigeration applications. In *Proceedings of the 6th Ibero-American Congress of Air Conditioning and Refrigeration - CIAR2001, Buenos Aires, Argentina*, 2001.

[72] J. J. Brasz, B. P. Biederman, and G. Holdmann. Power production from a moderate-temperature geothermal resource. In *Proceedings of the Geothermal Resources Council Annual Meeting 2005, Reno, NV, USA*, 2005.

[73] R. Zanelli and D. Favrat. Experimental investigation of a hermetic scroll expander-generator. In *Proceedings of the International Compressor Engineering Conference at Purdue 1994, West Lafayette, IN, USA*, 1994.

[74] T. Yanagisawa, M. Fukuta, Y. Ogi, and T. Hikichi. Performance of an oil-free scroll-type air expander. In *Proceedings of the IMechE International Conference on Compressors and Their Systems 2001, London, UK*, 2001.

[75] V. Lemort, I. V. Teodorese, and J. Lebrun. Experimental study of the integration of a scroll expander into a heat recovery Rankine cycle. In *Proceedings of the International Compressor Engineering Conference at Purdue 2006, West Lafayette, IN, USA*, 2006.

[76] T. Saitoh, N. Yamada, and S. Wakashima. Solar Rankine cycle system using scroll expander. *Journal of Environment and Engineering*, 2(4):708–719, 2007.

[77] J. Hugenroth, J. Braun, E. Groll, and G. King. Experimental investigation of a liquid-flooded Ericsson cycle cooler. *International Journal of Refrigeration*, 31:1241–1252, 2008.

[78] V. Lemort, S. Quoilin, C. Cuevas, and J. Lebrun. Testing and modeling a scroll expander integrated into an organic Rankine cycle. *Applied Thermal Engineering*, 29:3094–3102, 2009.

[79] H. J. Kim, J. M. Ahn, I. Park, and P. C. Rha. Scroll expander for power generation from a low-grade steam source. *Proceedings of the IMechE, Part A: Journal of Power and Energy*, 221:705–712, 2007.

[80] R. B. Peterson, H. Wang, and T. Herron. Performance of a small-scale regenerative Rankine power cycle employing a scroll expander. *Proceedings of the IMechE, Part A: Journal of Power and Energy*, 222:271–282, 2008.

[81] G. Manfrida and L. Marraccini. Model of a steam/organic vapour volumetric reciprocating expander. In *Proceedings of the 23rd International Conference on Efficiency, Cost, Optimization, Simulation and Environmental Impact of Energy Systems - ECOS2010, Lausanne, Switzerland*, 2010.

[82] M. Badami, M. Mura, P. Campanile, and F. Anzioso. Design and performance evaluation of an innovative small scale combined cycle cogeneration system. *Energy*, 33:1264–1276, 2008.

[83] M. Badami and M. Mura. Preliminary design and controlling strategies of a small-scale wood waste Rankine cycle (RC) with a reciprocating steam engine (SE). *Energy*, 34:1315–1324, 2009.

[84] J.S. Baek, E.A. Groll, and P.B. Lawless. Piston-cylinder work producing expansion device in a transcritical carbon dioxide cycle. Part I: experimental investigation. *International Journal of Refrigeration*, 28:141–151, 2005.

[85] J.S. Baek, E.A. Groll, and P.B. Lawless. Piston-cylinder work producing expansion device in a transcritical carbon dioxide cycle. Part II: theoretical model. *International Journal of Refrigeration*, 28:152–164, 2005.

[86] B. Aoun. Micro combined heat and power operating on renewable energy for residential building. *PhD Thesis, École Nationale Supérieure des Mines de Paris*, 2008.

[87] E. J. Bala, P. W. O'Callaghan, and S. D. Probert. Influence of organic working fluids on the performance of a positive-displacement pump with sliding vanes. *Applied Energy*, 20:153–159, 1985.

[88] S. Declaye. Design, optimization and modeling of an organic Rankine cycle for waste heat recovery. *Master's Thesis, Université de Liège*, 2009.

[89] S. Quoilin. Sustainable energy conversion through the use of organic Rankine cycles for waste heat recovery and solar applications. *PhD Thesis, Université de Liège*, 2011.

[90] Natural Resources Canada. Pinch analysis: for the efficient use of energy, water and hydrogen. *Technical Report*, 2003.

[91] I. C. Kemp. *Pinch analysis and process integration.* 2nd edition. Butterworth-Heinemann, Boston, 2007.

[92] European Commission Joint Research Centre. Monthly ambient temperature data. `http://re.jrc.ec.europa.eu/pvgis/`, Last accessed: February 2013.

[93] International Energy Agency. Statistics and balances for electricity and heat. *Technical Report*, 2008.

[94] M. Gassner. Process design methodology for thermochemical production of fuels from biomass. Application to the production of synthetic natural gas from lignocellulosic resources. *PhD Thesis, École Polytechnique Fédérale de Lausanne*, 2010.

[95] M. Gassner and F. Maréchal. Thermo-economic process model for thermochemical production of synthetic natural gas (SNG) from lignocellulosic biomass. *Biomass and Bioenergy*, 33:1587–1604, 2009.

[96] Belsim S.A. Belsim - Your performance wizard - Process data validation and reconciliation experts. `http://www.belsim.com/`, Last accessed: February 2013.

[97] D. R. Morris and J. Szargut. Standard chemical exergy of some elements and compounds on the planet Earth. *Energy*, 11:733–755, 1986.

[98] K. J. Ptasinski, M. J. Prins, and A. Pierik. Exergetic evaluation of biomass gasification. *Energy*, 32:568–574, 2007.

[99] L. Borel and D. Favrat. *Thermodynamics and energy systems analysis: from energy to exergy.* 1st edition. EPFL Press, Lausanne, 2010.

[100] A. Bejan, G. Tsatsaronis, and M. Moran. *Thermal design and optimization.* 1st edition. Wiley-Interscience, New York, 1996.

[101] E. Winandy, C. Saavedra, and J. Lebrun. Experimental analysis and simplified modeling of a hermetic scroll refrigeration compressor. *Applied Thermal Engineering*, 22:107–120, 2002.

[102] C. Cuevas, J. Lebrun, V. Lemort, and E. Winandy. Characterization of a scroll compressor under extended operating conditions. *Applied Thermal Engineering*, 30:605–615, 2010.

[103] N. P. Halm. Mathematical modeling of scroll compressors. *Master's Thesis, Purdue University*, 1997.

[104] Y. Chen, N. P. Halm, E. A. Groll, and J. E. Braun. Mathematical modeling of scroll compressors - part I: compression process modeling. *International Journal of Refrigeration*, 25:731–750, 2002.

[105] Y. Chen, N. P. Halm, J. E. Braun, and E. A. Groll. Mathematical modeling of scroll compressors - part II: overall scroll compressor modeling. *International Journal of Refrigeration*, 25:751–764, 2002.

[106] B. Wang, X. Li, and W. Shi. A general geometrical model of scroll compressors based on discretional initial angles of involute. *International Journal Refrigeration*, 28:958–966, 2005.

[107] E. W. Lemmon and R. Span. Short fundamental equations of state for 20 industrial fluids. *Journal of Chemical and Engineering Data*, 51:785–850, 2006.

[108] S. Kakac, R. Shah, and W. Aung. *Handbook of single-phase convective heat transfer*. 1st edition. Wiley-Interscience, New York, 1987.

[109] J. B. Heywood. *Internal combustion engine fundamentals*. 1st edition. McGraw-Hill, New York, 1988.

[110] LMS International NV. LMS Imagine.Lab AMESim - The integrated platform. `http://www.lmsintl.com/LMS-Imagine-Lab-AMESim/`, Last accessed: February 2013.

[111] SUNTEC Industries France. SUNTEC gear pumps. `http://www.suntec.fr`, Last accessed: February 2013.

List of publications

This thesis is based on the following original publications:

- S. Clemente, D. Micheli, M. Reini, and R. Taccani. Bottoming organic Rankine cycle for a small scale gas turbine: a comparison of different solutions. *Applied Energy*, 106:355-364, 2013.
- R. Bracco, S. Clemente, D. Micheli, and M. Reini. Experimental tests and modelization of a domestic-scale ORC (Organic Rankine Cycle). *Energy*, in press, DOI: *10.1016/j.energy.2012.12.016*, 2013.
- S. Clemente, D. Micheli, M. Reini, and R. Taccani. Energy efficiency analysis of organic Rankine cycles with scroll expanders for cogenerative applications. *Applied Energy*, 97:792-801, 2012.
- S. Clemente, D. Micheli, R. Radu, G. Toniato. Experimental tests on a gear pump for organic Rankine cycle applications. In *Proceedings of the 3rd International Conference on Microgeneration and Related Technologies - MicrogenIII, Naples, Italy*, 2013.
- R. Bracco, S. Clemente, D. Micheli, and M. Reini. Experimental tests and modelization of a domestic-scale organic Rankine cycle. In *Proceedings of the 25th International Conference on Efficiency, Cost, Optimization, Simulation and Environmental Impact of Energy Systems - ECOS2012, Perugia, Italy*, 2012.
- S. Clemente, D. Micheli, M. Reini, and R. Taccani. Simulation model of an experimental small scale ORC cogenerator. Poster presented at the *First International Seminar on ORC Power Systems - ORC2011, Delft, The Netherlands*, 2011.
- S. Clemente, J. Demierre, and D. Favrat. Multi-objective optimization of an ORC-based biomass cogenerator for residential applications. Presented at the *First International Seminar on ORC Power Systems - ORC2011, Delft, The Netherlands*, 2011.
- S. Clemente, D. Micheli, M. Reini, and R. Taccani. Performance analysis and modeling of different volumetric expanders for small-scale organic Rankine cycles. In *Proceedings of the ASME 5th International Conference on Energy Sustainability and 9th Cell Science, Engineering and Technology Conference - ESFuelCell2011, Washington, DC, USA*, 2011.
- S. Clemente, D. Micheli, M. Reini, and R. Taccani. Preliminary design of organic Rankine cycles with scroll expanders. In *Proceedings of the 3rd International Conference on Applied Energy - ICAE2011, Perugia, Italy*, 2011.

- S. Clemente, D. Micheli, M. Reini, and R. Taccani. Numerical model and performance analysis of a scroll machine for ORC applications. In *Proceedings of the 23rd International Conference on Efficiency, Cost, Optimization, Simulation and Environmental Impact of Energy Systems - ECOS2010, Lausanne, Switzerland*, 2010.
- S. Clemente, D. Micheli, M. Reini, and R. Bracco. Prime prove del prototipo di un gruppo ORC di piccola taglia (First tests on a small-scale ORC prototype). In *Atti del* 67° *Congresso Nazionale ATI - ATI2012, Trieste, Italy*, 2012 (in Italian).
- S. Clemente, D. Micheli, M. Reini, and R. Taccani. Modello numerico ed analisi delle prestazioni di cicli ORC con espansore scroll (Numerical model and performance analysis of organic Rankine cycles with scroll expander). In *Atti del* 65° *Congresso Nazionale ATI - ATI2010, Domus de Maria (Cagliari), Italy*, 2010 (in Italian).